TRANSPORTATION RESEARCH RECORD 694

Railroad Track and Electrification Studies

TRANSPORTATION RESEARCH BOARD

COMMISSION ON SOCIOTECHNICAL SYSTEMS
NATIONAL RESEARCH COUNCIL

NATIONAL ACADEMY OF SCIENCES
WASHINGTON, D.C. 1978

Transportation Research Record 694
Price $4.00

modes
2 public transit
3 rail transportation

subject area
21 facilities design

Transportation Research Board publications are available by ordering directly from the board. They may also be obtained on a regular basis through organizational or individual supporting membership in the board; members or library subscribers are eligible for substantial discounts. For further information, write to the Transportation Research Board, National Academy of Sciences, 2101 Constitution Avenue, N.W., Washington, DC 20418.

Library of Congress Cataloging in Publication Data
National Research Council. Transportation Research Board.
Railroad track and electrification studies.

(Transportation research record; 694)

1. Railroads–Track–Addresses, essays, lectures. 2. Railroads–Electrification–Addresses, essays, lectures. I. Title. II. Series.
TE7.H5 no. 694 [TF240] 380.5'08s [625.1'4] 79-9508
ISBN 0-309-02840-X

Sponsorship of the Papers in This Transportation Research Record

GROUP 2–DESIGN AND CONSTRUCTION OF TRANSPORTATION FACILITIES
Eldon J. Yoder, Purdue University, chairman

Railway Systems Section
Thomas B. Hutcheson, Seaboard Coast Line Railroad Company, chairman

Committee on Track Structure System Design
M. E. Harr, Purdue University, chairman
Gilbert L. Butler, John S. Collins, Harold D. Decker, C. Page Fisher, Amir N. Hanna, John B. Heagler, Jr., William P. Hofmann, James D. Jardine, Ben J. Johnson, C. R. Kaelin, Arnold D. Kerr, W. S. Lovelace, R. Michael McCafferty, Francis G. McLean, John T. O'Neill, A. C. Parker, Jr., Gerald P. Raymond, Robert N. Schmidt, Paul S. Settle, Donald A. Shoff, Marshall R. Thompson, George H. Way, Jr.

Edward J. Ward and Lawrence F. Spaine, Transportation Research Board staff

The organizational units and officers and members are as of December 31, 1977.

Contents

Part 1. Track

PREDICTION OF FATIGUE CRACK GROWTH IN RAILROAD RAILS
David Broek, Richard C. Rice, and Roger K. Steele 2

INTRODUCTION TO STRESSES IN RAILS: STRESSES IN MIDRAIL REGIONS
Thomas G. Johns, Kent B. Davies, and Donald P. McConnell 10

ANALYTICAL AND EXPERIMENTAL STUDY OF RESIDUAL STRESSES IN RAILS
Kent B. Davies and Thomas G. Johns 19

MATHEMATICAL MODEL FOR LATERAL THERMAL BUCKLING AND DISPLACEMENT OF CURVED TRACK
W. So and W. W. Yang 24

STATISTICAL DESCRIPTION OF SERVICE LOADS FOR CONCRETE CROSSTIE TRACK
Robert H. Prause and Andrew Kish 30

DEVELOPMENT OF MULTILAYER ANALYSIS MODEL FOR TIE-BALLAST TRACK STRUCTURES
James C. Kennedy, Jr., and Robert H. Prause 39

PERMANENT-DEFORMATION BEHAVIOR OF RAILWAY BALLAST
Reid M. Knutson and Marshall R. Thompson 47

BALLAST AND SUBGRADE RESPONSE TO TRAIN LOADS
Ernest T. Selig and Andrew Sluz. 53

TECHNIQUES FOR EVALUATING EFFECTS OF TRACK AND VEHICLE WEAR ON FREIGHT-CAR PERFORMANCE
C. Thomas Jones and Donald E. Gray 60

Part 2. Electrification

EFFECTS OF ENERGY-COST VARIATION ON FEASIBILITY OF ELECTRIFYING THE CINCINNATI-ATLANTA MAIN LINE OF THE SOUTHERN RAILWAY SYSTEM
K. L. Lawson, J. H. Wujek, and K. J. Ingram 68

Part 1
Track

Prediction of Fatigue Crack Growth in Railroad Rails

David Broek and Richard C. Rice, Battelle Columbus Laboratories, Columbus, Ohio
Roger K. Steele, Transportation Systems Center, Cambridge, Massachusetts

The objective of this study was the development of a computational model for the prediction of fatigue-crack propagation in rails under train-service loading. Constant-amplitude fatigue-crack-growth properties were determined for 66 rail steels. The effects of mean stress, temperature, and crack orientation were investigated. Variable-amplitude tests showed almost no load-interaction effects in fatigue crack growth in rail steels. Thus a linear integration scheme could be used for crack-growth prediction. Service-simulation tests were performed on the basis of four measured load spectra. The specimens were subjected to random loading, train-by-train loading, loading that used a sequence associated with 170 trains of six different types, and unit-train loading. The load sequence represented 0.9 million gross metric tons (1 million gross tons) of traffic and was repeated until failure of the specimens. Crack growth in the service-simulation tests could be reproduced by using the computational prediction model within a factor of 2 and within a factor of 1.5 in most cases. Discrepancies between predictions and tests results are partially due to the variability of crack-growth properties of rail steels. The way in which the prediction model can be used in a reliability analysis for failure-rate prediction is discussed. Such an analysis would allow management decisions with regard to the most cost-effective means to reduce failure rates of a given track. This is possible because the relative accuracy of the crack-growth prediction is expected to be better than its absolute accuracy.

Fatigue failure of railroad rails is a common cause of derailment accidents. The reduction of fatigue failures can be achieved by more intensive track maintenance, reduction of traffic (loads), or replacement of rails. In addition, timely detection of fatigue cracks through periodic inspection might prevent most cracks from causing failures.

However, measures to reduce fatigue failures will be effective only if there are adequate methods for the prediction of the time to crack initiation and the subsequent rate of crack growth. Such prediction methods require rather accurate information about service loads, rail stresses, and fatigue and crack-growth properties of rail material. Moreover, a computational scheme is required that can use this information to predict behavior under service circumstances.

One portion of the track performance improvement program sponsored by the Federal Railroad Administration is the development of a predictive rail-failure model that can be used for the determination of optimal inspection periods through a calculation of fatigue-crack-propagation behavior. The research reported here concerns a program to develop a computational rail-failure model.

The laboratory fatigue-crack-growth data used as input to the predictive model should be obtained from a sufficiently large sample of rails to manifest the statistical variability. Such data did not exist in the first phase of the program. Data were generated for 66 rail samples of various ages and masses and from various suppliers (1, 2). The samples were taken from existing track in all sections of the United States. Fatigue-crack-growth tests were performed under constant-amplitude loading and zero minimum load.

Actual cracks in rails develop under more complex conditions than constant-amplitude tension loading and zero minimum load. They are subjected to stress histories in which there are varying amplitudes of combined tension and shear that cover a wide range of mean stresses. Cracks can initiate in different sections of the rail and have different orientations; they are internal flaws of predominantly quasi-elliptical shape. Moreover, the rail is subjected to varying temperatures, which may affect the behavior of cracks. A predictive failure model should be cognizant of these complex circumstances. Therefore, data are required on the influences of the various parameters on crack growth. Such data were generated during the second phase of the program.

In the third phase of the program, the predictive failure model was developed. For this purpose, experiments were performed under service-simulation loading. On the basis of these experiments, a crack-growth integration model was established that gives predictions of sufficient accuracy to be within the normal variability of crack growth as observed in the first and second phases of the program.

CRACK-GROWTH PROPERTIES OF RAIL STEELS (PHASES 1 AND 2)

Experiments

A total of 66 rail samples were collected from track all over the United States. The samples were characterized with regard to mass, year of production, chemical composition, and mechanical properties. A brief summary of the variability of the data is given below (1 mm = 0.04 in and 1 MPa = 145 lbf/in^2).

Variable	Value			SD	
	Low	High	Mean	Value	Percent of Mean
Carbon, %	0.57	0.85	0.76	0.06	8
Manganese, %	0.61	1.48	0.88	0.17	20
Sulfur, %	0.014	0.052	0.229	0.010	34
Grain diameter, mm	0.066	0.0120	0.087	0.021	25
Pearlite interlamellar spacing	2470	4160	3211	632	20
Tensile ultimate strength, MPa	766	980	918	5.5	4
Tensile yield strength, MPa	414	566	504	5	7
Crack-growth life, log cycles	5.18	6.22	5.68	0.30	5

In phase 1, one crack-propagation specimen was cut from each rail sample. All specimens were subjected to the same cyclic loads at R = 0 where R = ratio between minimum and maximum load in a cycle. This allowed a judgment of the variability of crack-growth properties of the various rail steels.

In phase 2, more detailed tests were performed on a number of rail samples. These experiments included the following:

1. Tests at positive and negative R-ratios;
2. Tests at -40, 21, and 60°C (-40, 70, and 140°F);
3. Tests on cracks of different orientations;
4. Threshold tests (determination of threshold conditions below which fatigue cracks do not propagate);
5. Tests on semielliptical cracks; and

6. Tests under combined tension and shear.

The majority of the specimens were of the compact-tension type. Where such specimens were not suitable (e.g., in the case of negative R-ratio), different types of specimens were used. Figure 1 shows the specimens and the way in which they were taken from the rail. All specimens were machined to 1.25 cm (0.5 in) thick. The planar dimensions of the compact-tension specimens were determined according to ASTM E 399, with W = 7.6 cm (3.0 in). In the following discussion, the coding of specimens as defined in Figure 1 will be used for identification. Rail samples were numbered 001 to 066.

Crack-growth experiments were performed in servo-controlled fatigue machines. Records were made of the crack size (a) as a function of the number of load cycles (N). The rate of crack growth (da/dN) can be calculated easily from these records.

Data Presentation

The crack-growth records of the various types of specimens are not directly comparable, nor are they directly applicable to the case of a crack in a rail. The correlation between cracks of different types can be made only if their crack-growth data can be expressed in a unique way that is independent of the crack size and specimen geometry.

Cracks of different types can be correlated on the basis of the stress-intensity factor (K), which for any crack loaded in tension can be expressed as

$$K = \beta\sigma(\pi a)^{1/2} \quad (1)$$

where σ = remote stress and β = factor that depends on sample geometry (3). If we consider a case for which $\beta = 1$, it follows that two cracks (a_1) and (a_2) that have $a_1 = 4a_2$ will have the same stress intensity if a_2 is subjected to twice as high a stress as a_1. The geometric factors (β) are known for all specimen types used in this program. Geometric factors for actual rail cracks were computed in a parallel program on stress analysis of rails.

The K-value fully describes the entire stress field at the tip of a crack. Thus, if two cracks have the same K-value, they will have equal stress fields at their tips, regardless of σ, β, or a. If two cracks have the same tip stress field, their behavior will be the same. Hence, two cracks that have the same K-value will exhibit equal rates of crack growth:

$$da/dN = f(\Delta K) \quad (2)$$

where ΔK = range of stress intensity during one cycle of loading (minimum load to maximum load).

Equation 2 provides the ability to correlate data about different types of specimens, provided β is known for the rail crack. Therefore, the crack-growth data of the rail steels will be presented in accordance with Equation 2; i.e., the measured crack-growth rates will be presented as a function of ΔK.

Variability of Crack-Growth (Phase 1)

In phase 1 of this program, one constant-amplitude fatigue-crack propagation (FCP) test was completed on each of the 66 samples. Data on some individual samples and the scatter band of all 66 are shown in Figure 2.

The cracking behavior from one specimen to the next was rather variable—the number of cycles required to grow a crack from 25 mm (1.00 in) to failure ranged from 150 000 to more than 2 000 000. These crack-growth lives were statistically analyzed.

The entire collection of data can be described by a single normal distribution. Figure 3 shows the ranking of fatigue lives versus the predicted failure percentages for a log-normal distribution. The ratio of the logarithmic SD of the 66 data points to the logarithmic mean value of the population (commonly called the coefficient of variation) is about 0.053 (5.3 percent).

An attempt to correlate crack-growth behavior with other mechanical properties, chemical composition, and microstructural parameters was made, but no correlations were found, apart from a weak correlation with hardness.

The variability of all parameters for the 66 rail samples is given above. Despite the large variations in chemical composition, the bulk properties (tensile strength and yield stress) do not vary much. The coefficient of variation of the chemical composition is on the order of 10 percent or more. This number is only a few percent for the mechanical properties and, more important, also for the log life. Apparently, the large variations in chemical and structural parameters are not reflected in the variability of the crack-growth life.

Chemical composition and mechanical properties are bulk properties; i.e., they are averages for a large conglomerate of grains, pearlite colonies, and inclusions. Fatigue-crack growth is a very local phenomenon. In each cycle, the crack propagates over a small distance that may vary from 10^{-3} to 10^{-2} mm (10^{-7} to 10^{-4} in), so that only an extremely small amount of material is affected at a given time. Therefore, the variability in crack growth is more a function of local variations in structural and chemical composition. As a consequence, correlations with bulk material properties are not obvious or easily assessable. Another consequence is that the variability of crack-growth properties within a material can be almost as large as the variability among materials of the same type (i.e., variability within one rail as opposed to variability among rails).

Results of Detail Tests (Phase 2)

The overall data trends for the room-temperature crack-growth experiments on LT orientation specimens are shown in Figure 4. Three distinct bands are formed for each stress ratio when the data are plotted against ΔK. Trend lines for the effects of orientation and temperature are shown in Figures 5 and 6. There appeared to be no discernable effect of cycling frequency on crack growth.

Threshold experiments were done at three stress ratios (R = -1.0, 0.0, and 0.50) to develop estimates of threshold stress-intensity levels below which crack-growth rates would asymptotically approach zero. The results of these tests are reflected in the trend lines in Figures 4, 5, and 6, which show that the crack-growth rates become extremely low at a given ΔK level. If the crack becomes long, the conditions for final failure are approached. Therefore, the crack-growth rate tends to infinity at high ΔK levels. This results in the typical sigmoidal shape of the rate curves shown in Figures 4, 5, and 6.

If the data are to be used for predictive purposes, it is beneficial to use an equation that fits the data. Data sets for a limited range of ΔK values (such as those in Figure 2) often can be described by a straight line on a double-log plot. This leads to the simple relationship

$$da/dN = C\Delta K^m \quad (3)$$

Obviously, this equation is inadequate if the complete sigmoidal curve must be represented.

Many theoretical and empirical relationships have been proposed for the rate curve. Because none of these equations has a sound physical basis, it is often more useful to determine an empirical equation that fits the data for a particular application. This provides the best guarantee of technically adequate predictions.

It was found that a further development of some existing equations was the best suited to the rail-steel data generated here. The equation reads

$$da/dN = C(1 - R)^2 (K_{max}^2 - K_{th}^2)[K_{max}^n/(K_c - K_{max})] \quad (4)$$

where

K_{max} = maximum stress intensity in a cycle = $\Delta K/(1-R)$,
K_{th} = threshold stress intensity, and
K_c = critical stress intensity that causes final fracture and, if $R < 0$, its value should be taken as zero.

Note that K_{th} and K_c are the asymptotes of the sigmoidal curve.

To show the adequacy of Equation 4, the trend lines for the LT orientation and room temperature and the points predicted by Equation 4 are replotted in Figure 7. The generality of Equation 4 was shown by the similar plots for different orientations and temperatures. The equation was used as a basis for crack-growth predictions as discussed below.

Figure 1. Orientation of specimens.

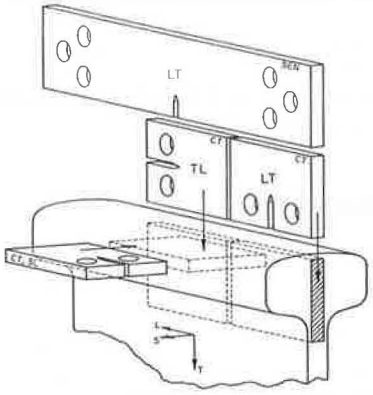

FAILURE MODEL (PHASE 3)

Objective and Scope

The objective of the program was to establish a computational failure model for the prediction of the growth of a flaw in a rail under actual service loading. Flaw growth in a rail is a complex problem; a quasi-elliptical flaw embedded in a nonuniform stress field is growing under a variable-amplitude load history. Probably the most difficult aspect of the problem is the prediction of flaw growth under variable-amplitude loading. This problem was first singled out by the study of a through-the-thickness crack that has a straight front growing under simulated service loading. Once crack growth under these circumstances can be properly predicted, the failure model can be generalized to include the other complexities.

Figure 2. Fatigue-crack-propagation rate behavior: 66 rail samples tested at R = 0.

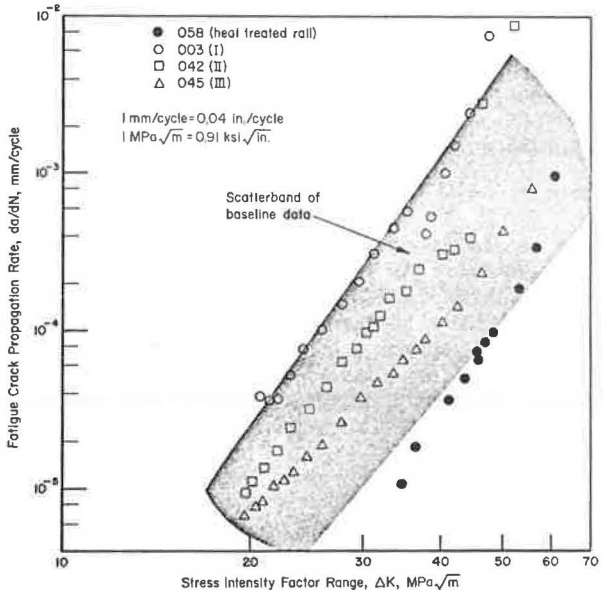

Figure 3. Distribution of baseline FCP lives: 64 rail samples.

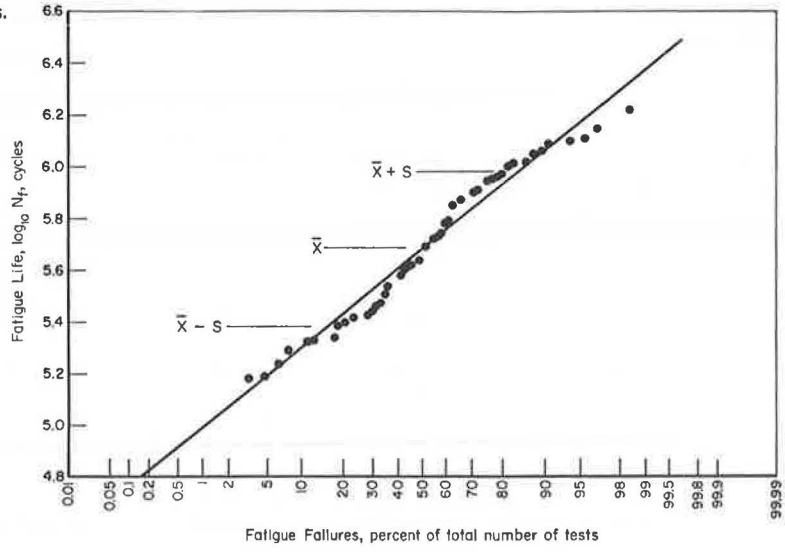

Figure 4. Bands of data variability: LT orientation rail samples at room temperature.

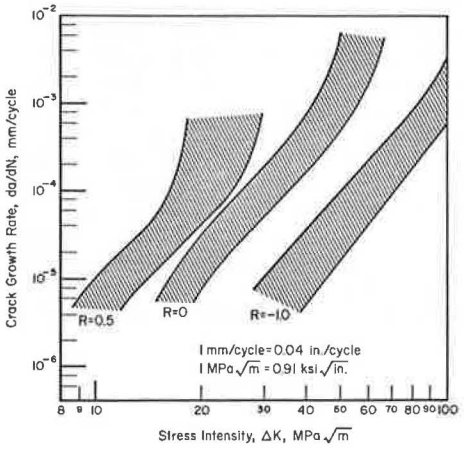

Figure 5. FCP trend lines: rail samples tested at room temperature in three different orientations.

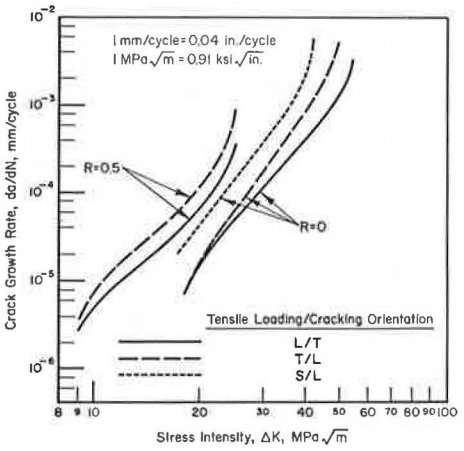

Figure 6. FCP trend lines: LT orientation rail samples at three temperatures and R-ratios.

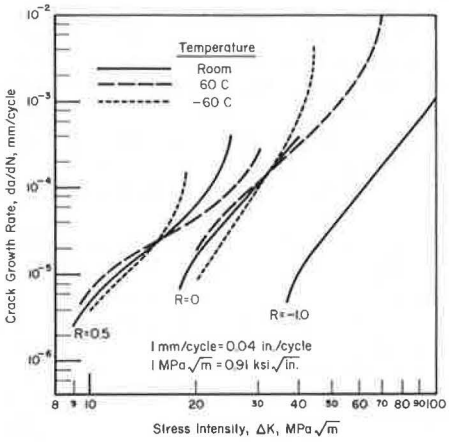

Figure 7. Applicability of crack-growth equations: LT orientation rail samples at room temperature.

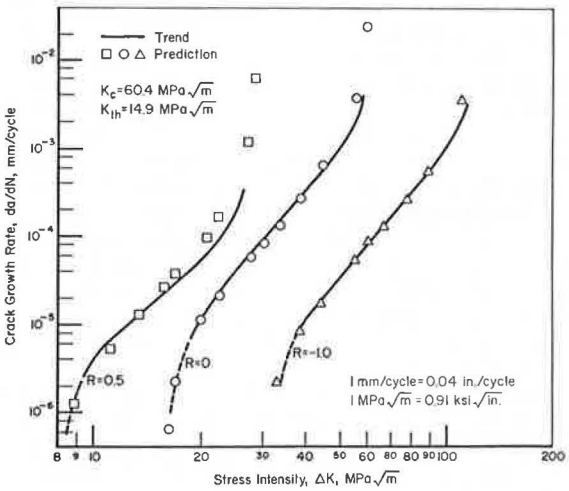

Load Interaction

An important problem in crack-growth prediction is caused by load interaction. In many materials, load interaction will occur if high loads are interspersed among a sequence of low loads. If a high load is followed by a series of loads of lower magnitude, the rate of crack growth can be much lower than if the high load does not occur. This phenomenon is called retardation.

During the application of the high load, a relatively large region of the material around the crack tip is deformed plastically. On unloading, the elastic strains in the surrounding elastic material are reduced to zero. Because the plastic zone at the crack tip is completely contained in elastic material, it has to follow the elastic surroundings during unloading. The plastic strains cannot be (fully) relieved. Thus, a system of residual compressive stresses will develop in the plastic zone at the crack tip when the high load is released and, during subsequent cycling at low loads, the effective stress at the crack tip is reduced because of the presence of the compressive residual stress. As a result, the subsequent loads are less effective in producing crack growth, which means lower crack-growth rates.

Various models have been developed to account for retardation in crack-growth predictions. In the case of random-service loading, crack-growth predictions then have to be based on a cycle-by-cycle integration of growth rates. This is a costly and time-consuming procedure.

A number of rail specimens were subjected to constant-amplitude crack-growth tests in which periodically higher loads of various magnitudes were applied. (The number of high loads was so small that they contributed very little to crack growth.) It was found that rail steels show very little retardation. The crack-growth rates before and after the overloads were virtually the same, and they were no different from the data obtained in experiments that did not have overloads. Therefore, crack-growth prediction in rail steels is not complicated by load interaction effects.

Stresses in the Rail Due to Wheel Passage

In a parallel program, an engineering stress analysis was made of a cracked rail. At the time that the variable-amplitude tests were designed, stress-analysis results were available for an elliptical transverse crack in the rail head. The crack was located approximately in the center of the rail head. The rail was subjected to the passage of a truck that had a wheel load of 84 kN (19 000 lbf). The variation of the mode I stress intensity (K_I) at the lower extremity of the crack is shown in Figure 8.

Initially, when the wheel is still far away, the stress

intensity increases. When the wheel passes over the crack, the rail head is under compressive stress, which causes the stress intensity to decrease. When there is no wheel load on the rail, the only stress in the rail head is the residual stress. It was determined in the rail stress-analysis program that the residual stress at the location of the crack was a tensile stress. Thus, the variation of the stress intensity due to wheel passage is superposed on the positive stress intensity, and the main variation is from the residual stress intensity downward.

A number of load sequences was designed to evaluate the significance of the various small reversals of K_I when a wheel passes. These load sequences are denoted A, B, C, D, E, and F and are shown in Figure 9. The small variations at the top of the cycle have a range that is 15 percent of the total range of the cycle. Because the rate of crack growth is approximately proportional to the fourth power of ΔK, these small variations will contribute 5 percent of the total crack growth. If they are smaller than the threshold, they will not contribute. To evaluate the relative significance of these small load variations, sequences A, B, and C were repeated continuously in a test to simulate the passage of a succession of cars of the same load. Load sequences D, E, and F are self-explanatory.

The most significant results of the sequence tests are shown in Figure 10. Sequences D, E, and F were all run on the same rail sample (025). The results indicate that the small load variations during a wheel pass are insignificant. Therefore, the passage of a truck can be simulated by the two large cycles only (compare sequences D and E). The results for sequence A on rail sample 065 again show the considerable variability of crack growth within one rail sample, even under variable-amplitude loading. This indicates that the results of sequences D, E, and F are equivalent for all practical purposes.

The absence of retardation indicates that a linear integration of crack growth can be sufficient for crack-growth predictions. The results for sequences E and F indicate that it is permissible to combine considerable size blocks of equal cycles, which facilitates the integration procedure.

Rail Service Loading

Actual service-load spectra were obtained from a parallel program on wheel-rail load measurements. Cumulative probability curves are given in Figure 11 for four different railroads (I, II, III, and IV). The spectra are peak counts of measured load histories and show the probability that a certain wheel load is exceeded.

A combination of the I and II spectra was used as the basic spectrum for the service-simulation tests. For this purpose, a load exceedance diagram for 0.9 million gross metric tons (MGMT) (1 million gross tons) of traffic was generated in the following way:

For estimating purposes, 3700 axle passes (peak-load occurrences)/d represent an annual traffic of about 18 MGMT (20 million gross tons). This means that $365 \times 3700 \div 20 = 67\,000$ axles represent 0.9 MGMT. It is assumed that half the traffic is based on spectrum I and half is based on spectrum II, which is 33 500 axles each. The load spectrum was converted into a stress spectrum by taking a stress excursion of 1.45 MPa (210 lbf/in^2) per 4.4-kN (1000-lbf) wheel load. This choice was made to obtain reasonable lives of the test specimens. Because of the generality of the concept of the characterization of crack growth on the basis of ΔK, the selection of an arbitrary stress level for the experiments does not affect the generality of the approach.

For the purposes of analysis and tests, it is necessary to approximate the spectrum by a number of discrete levels. It has been shown for aircraft load histories that 8 to 12 discrete levels are generally adequate (4). The 12 levels selected are shown in Figure 12.

Note that the spectrum was clipped at level 1 at approximately 2 occurrences/MGMT. Higher stress levels may occur; however, they will be rare. One cycle of that level will contribute practically no crack growth as compared with the other 67 000 cycles. Thus, it is impractical to include very high stress levels in experiments. (Of course, these high levels cannot be ignored if the probability of fracture is of concern, but they are unimportant for crack growth if there is little retardation.)

Stress Histories for Predictions and Experiments

The stress history of a rail is extremely complex, and it would be impractical if a prediction of crack growth had to be based on the actual history. In the sequence tests discussed above, it was established that the small load variations occurring during the passage of a wheel can be neglected because they do not contribute to crack growth. One objective of the service-simulation tests discussed below was to investigate whether further simplifications are permissible.

On the basis of the discrete load levels of the spectrum approximation, a stress history was developed that consisted of the six different trains shown in Figure 13. The composition of each of the six trains was selected more or less arbitrarily; however, they resemble actual trains in size and load content. A sequence of two A1 trains, six A2 trains, 12 A3 trains, 120 B-trains, 20 C-trains, and 10 D-trains were mixed in such a way that the heavy and light trains were not clogged together. The mixture of 170 trains was repeated during the tests. Similar procedures were followed by using spectra III and IV in Figure 11. An example of a sequence of trains is shown in Figure 14.

To check whether this simple representation is justified, tests also were run in which the loads of the 170 trains were applied in random order, as will occur in actual service. It was also checked whether further simplifications are possible for prediction purposes, because an efficient prediction scheme requires the simplest possible stress history. On the other hand, the stress history should be realistic in the sense that test results and predictions are representative of actual service conditions.

To evaluate possible simplifications, two other stress histories were developed from the spectrum shown in Figure 12. The first one is based on a reduced number (eight) of stress levels in which stress levels 3 to 10 were combined in pairs to give four new levels, 3 to 6.

Because level 8 (level 12 of the original stress history in Figure 12) has a very small stress range, it will contribute little to crack growth. Therefore, one test case was selected in which the cycles of level 12 were omitted. Obviously, this reduces the number of cycles for 0.9 MGMT from 67 000 to 50 000.

Another simplified stress history for the computational scheme would make use of a hypothetical unit train. This means that all 170 trains constituting the 0.9 MGMT are the same: they contain the same load levels and the same number of cycles at each load level. The highest load level that can be applied is the level that is exceeded at least 170 times (because it must occur in every train). The staircase approximation of

Figure 8. K_I history for passage of 84-kN (19 000-lbf) wheel loads on stiff and soft roadbeds for a particular crack geometry and location.

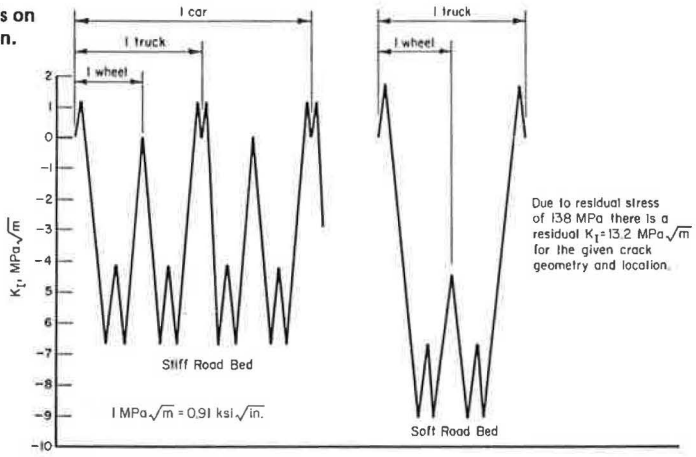

Figure 9. Sequence tests.

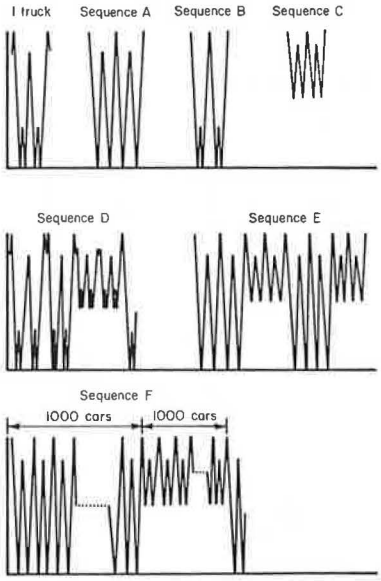

Figure 10. Example of results of sequence tests.

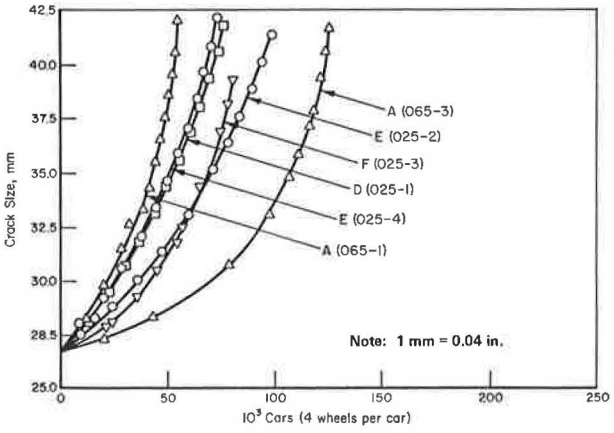

the original spectrum was maintained (Figure 12), but the clipping level was taken at 170 exceedances. The number of cycles at each load level was simply divided by 170 to obtain the number of cycles at each level in the unit train. All loads in the unit train were put in high-low sequence as in Figure 13. Unit trains also were established for spectra III and IV.

Figure 11. Load-probability diagram.

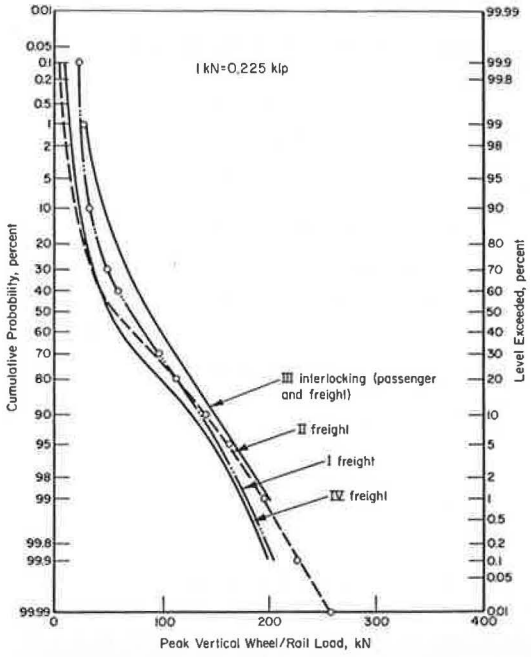

Predictions and Results

Because load interaction did not appear to occur, the service-simulation test data were predicted by integration of the constant-amplitude baseline data without the use of a retardation model. The crack growth (Equation 3) was used as a basis for the integration. Two types of predictions were made. One was based on average crack-growth properties, and the other was based on the constant-amplitude properties of the particular rail sample used for a given service-simulation test.

The integrations were performed numerically. The stress intensity for a certain cycle was calculated, and the crack-growth rate was determined by using Equation 3. If there were k cycles of a given magnitude in a certain train, the total crack growth during those cycles was $\Delta a = \times da/dN$. This crack extension was added to the existing crack. The stress intensity for the next cycle was then calculated, and Δa was determined in the same manner and so on, train after train, until failure.

Predicted curves for the various rail samples and spectra are shown in Figure 15. For a given set of

Figure 12. Stress spectrum for 0.9 MGMT load.

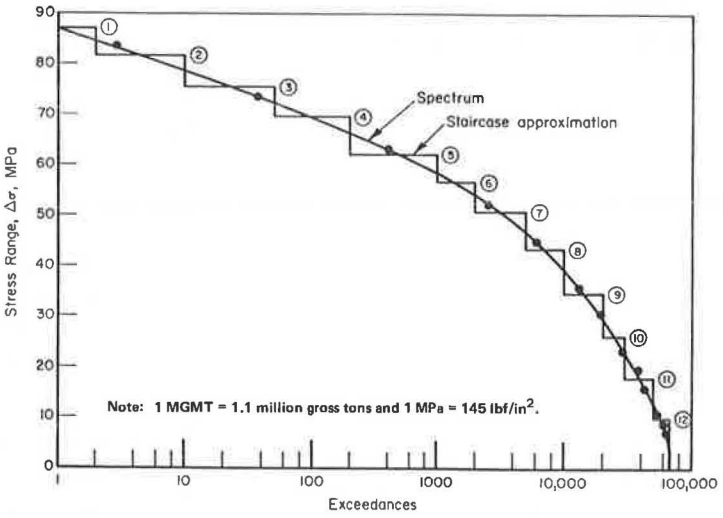

Figure 13. Train compositions for mixed traffic spectrum (all loads included).

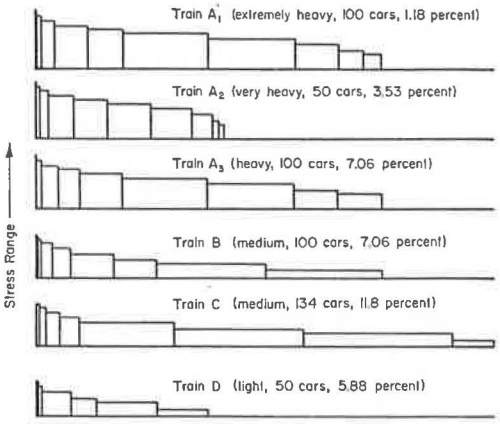

Figure 14. Portion of stress history of 12-level train-by-train service-simulation tests.

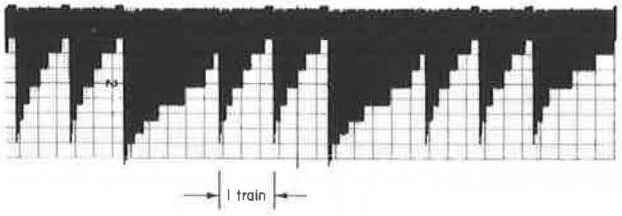

Figure 15. Predicted crack-growth curves.

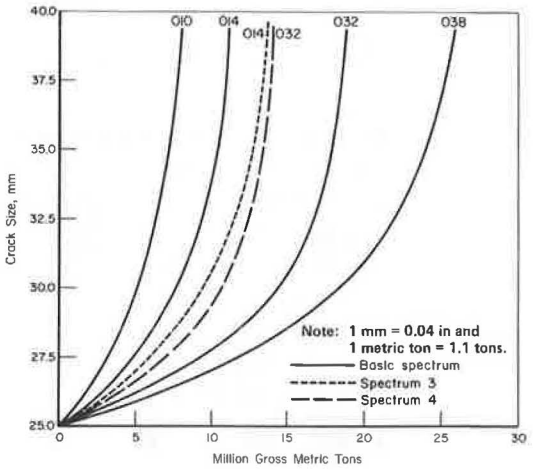

Table 1. Predicted crack-growth life.

Sample No.	Spectrum	Crack-Growth Life (MGMT) 12 Level	8 Level	7 Level	Random	Unit Train
10	Basic	9.1	9.1	9.1	9.1	9.1
14		11.8	10.9	11.8	10.9	11.8
32		19.1	18.2	18.2	18.2	18.2
38		26.4	24.6	25.5	24.6	25.5
14	III	14.6	13.7	13.7	13.7	13.7
18		24.6	22.8	23.7	22.8	23.7
32	IV	14.6	13.7	13.7	13.7	13.7
51		28.2	26.4	27.3	26.4	27.3
20		29.1	27.3	28.2	27.3	28.2
Average data	Basic	11.8	10.9	11.8	11.8	11.8
	III	14.6	13.7	13.7	14.6	13.7
	IV	9.1	9.1	9.1	9.1	9.1

Note: 1 MGMT = 1.1 million gross tons.

data, the computations for 12-level, 8-level, 7-level, and random loading were almost the same, as is shown in Table 1. This indicates that the simplifications are justified for a prediction. Also, the computations for a unit train were almost the same as the others, so that it does not make much difference whether predictions are made by using a random sequence or by using a unit train (which is much simpler).

Of course, it is more important that the predictions agree with the test data. The results of a number of predictions are compared with the actual test data in Figure 16. All predictions and test data are given in Table 2. As can be concluded from these data, the predictions are generally within a multiple of 2, for both the random-loading and the simpler train-by-train simulation tests. This may not be considered very accurate in the light of the more consistent predictions that can be made for aircraft spectra and materials by including the additional complexity of a retardation model (4). However, a look at the actual test data shows that its variability is of the same order of magnitude (compare data that have the same spectrum and the same rail sample), whereas there is no consistent effect of the way the spectrum is approximated. Obviously, if dis-

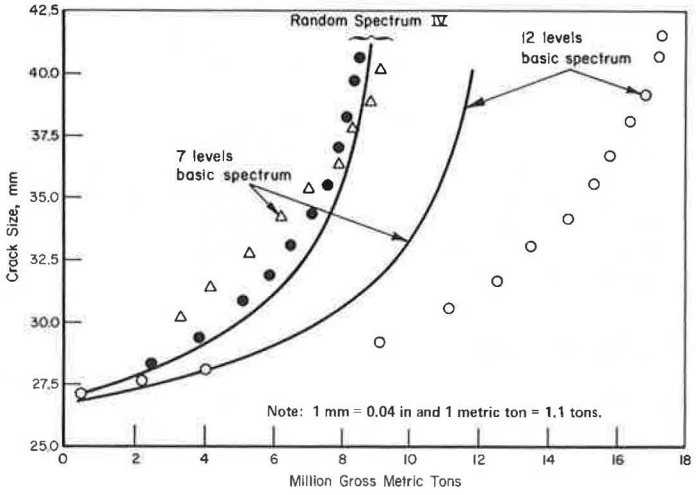

Figure 16. Comparison of predicted and experimental crack-growth curves.

Table 2. Predicted and experimental crack-growth lives.

Sample No.	Spectrum	Type of Loading	Crack-Growth Life[a] (MGMT) Test	Predicted Actual Data	Predicted Avg Data
32	Basic	12 level	18.0	11.8	8.2
	Basic	7 level	10.5	11.8	8.2
38	Basic	8 level	12.0	17.3	8.2
	Basic	Random	12.1	17.3	8.2
14	Basic	8 level	11.7	8.2	8.2
	Basic	Random	17.4	8.2	8.2
14	IV	Random	19.2	9.1	10.9
	IV	Unit train	18.0	9.1	10.0
10	Basic	7 level	12.7	6.4	8.2
32	III	Random	9.2	9.1	7.3
51	III	Random	4.0	15.5	7.3
20	III	Unit train	7.6	15.5	7.3

Note: 1 MGMT = 1.1 million gross tons.
[a] From 27.2 mm (1.07 in) to failure.

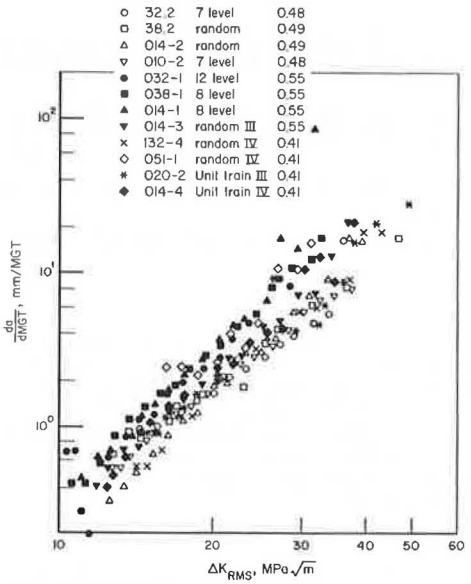

Figure 17. Crack-growth rate per million gross metric tons.

Note: 1 mm/MGT = 0.036 in/million gross tons and 1 MPa$\sqrt{m}$ = 910 (lbf/in^2)$\sqrt{in.}$

crepancies are caused by material variability, they cannot be blamed on the prediction method per se.

As an alternative, it was checked whether the crack-growth rate per 0.9 MGMT of traffic could be expressed uniquely as a function of the root mean square (RMS) value of ΔK. The data for all service-simulation tests are shown in Figure 17. If the data are separated with respect to R-value, a scatter band is found on the order of a factor of 2. This means that predictions within a multiple of 2 also could be obtained by direct integration of data of the type shown in Figure 17.

DISCUSSION AND CONCLUSIONS

These results are a unique and rather complete representation of fatigue-crack-growth properties of rail steels. The effects of R-ratios, orientation, and some other parameters were investigated.

A simple rationale was established to predict behavior under service loading on the basis of constant-amplitude data. This rationale does not give an exact prediction of a particular test result under a particular random sequence of loads, because the variability within a given material cannot be accounted for. However, it does predict the behavior of the family of rail steels to an accuracy within normal material variability. A reliability analysis (or some sort of statistical analysis) then will be required to account for the variability in service.

The combined use of the failure model and a reliability analysis will permit a more rational operation of railroads. For example, consider a railroad in which the number of rail failures is considered unacceptable. The failure model and the reliability analysis are exercised for the particular circumstances of that railroad. The load spectrum is determined for the given traffic and track conditions (a model for spectrum generation is currently being developed). Failure rates are predicted for these circumstances by means of a reliability analysis, which is basically a statistical treatment of the failure model. It is unlikely that the predicted failure rate will be exactly the same as actually experienced.

The question now can be asked: What is the most economical way to reduce this failure rate? To answer this, the reliability analysis is rerun for different conditions [such as (a) reduced speed, (b) reduced traffic, (c) upgraded track, (d) rail replaced, or (e) more frequent inspections]. Each of these measures will reduce the computed failure rate by a certain factor. It then can be decided which measure is the most cost effective.

Because the actual failure rate is known, the reduction factor can be applied to this rate to obtain the actual expected failure rate after one of the measures is carried out.

Thus, the absolute accuracy of the failure model is less important if the trends are predicted properly; i.e., the relative accuracy is more significant. Because all parameters that affect the failure rate (such as material variability and load spectrum) are statistical parameters, a statistical treatment (reliability analysis) is of course necessary.

ACKNOWLEDGMENT

The research described in this paper was performed under contract with the Transportation Systems Center of the Federal Railroad Administration.

REFERENCES

1. C. E. Feddersen, R. D. Buchheit, and D. Broek. Fatigue Crack Propagation in Rail Steels. U.S. Department of Transportation, Rept. DOT-TSC-1076, July 1976.
2. C. E. Feddersen and D. Broek. Fatigue Crack Propagation in Rail Steels. In Standard Testing Procedure 644: Rail Steels—Developments, Processing, and Use (A. H. Stone and G. G. Knupp, eds.), ASTM, May 1978.
3. D. Broek. Elementary Engineering Fracture Mechanics. Nordhoff International Publishing, Leyden, The Netherlands, 1974.
4. D. Broek and S. H. Smith. Spectrum-Loading Fatigue-Crack Growth Predictions and Safety Factors. Naval Air Development Center, Warminster, PA, Rept. No. 76383-30, 1976.

Introduction to Stresses in Rails: Stresses in Midrail Regions

Thomas G. Johns and Kent B. Davies, Battelle Columbus Laboratories, Columbus, Ohio
Donald P. McConnell, Transportation Systems Center, Cambridge, Massachusetts

The results of an extended analysis of the stresses in rails are summarized as an introduction to the mechanisms that drive rail flaws to failure. The mechanics of rail flexural, thermal, contact, and residual stress development are discussed in terms of the distribution of stresses in the rail, the stress cycles that occur with wheel passage, and their relationship to the propagation of typical midrail flaws. These analyses are limited to continuously welded rails and the regions of bolted-joint rails that are outside of the influence of the rail joints.

In recent years, rail failure has ranked as one of the most frequent and costly causes of train derailments (1). Despite substantial programs of inspection and replacement, rail failures remain a significant hazard to the reliability of train operations and a continuing drain on maintenance-of-way budgets. Since the adoption of controlled cooling to prevent hydrogen entrainment by rails and the rail embrittlement that results, a principal concern of railroad engineers has been the stresses induced in the rails by the newest generations of rolling stock. This concern is evident in the writings of Frocht (2) and Code (3) and, most recently, in the report on the problems caused by heavy wheel loads by Way (4) in the Bulletin of the American Railway Engineering Association. This concern is also reflected in the long-standing interest in the analysis of rail stresses that is evident in the literature.

A comprehensive review of approaches to the analysis of the flexural stresses in rails by Kerr (5) has illustrated the historical concern with the complexities of rail behavior under loads. Similarly, the survey by McConnell (6), the recent review of rail stress mechanisms by Johns and Davies (7), and the evaluation of the wheel-rail contact problem by Paul (8) have provided baseline descriptions of the complexities of the stress state in rails that arises from the contact of wheels with the rail and from the residual stresses developed by the yielding of the rail under these severe contact stresses. The interactions between the stresses induced in rails by these mechanisms and the material characteristics of rail steels, which has been discussed by Steele (9), are central to the analysis of the initiation and growth of flaws in rails. Such an analysis is an important part of the evaluation of measures to ensure the reliability of rails in service and to the reduction of the rail failure problem.

In the midrail region (regions between joints), transverse fissures and vertical and horizontal split-head defects (Figure 1) are the principal types of rail fracture. The behavior of these defects when exposed to the railroad load environment is not well understood. However, transverse-fissure defects appear to grow slowly until the defect covers approximately 20 percent of the railhead cross-section area, after which growth becomes rapid and rupture of the entire rail suddenly occurs. A vertical split head may grow to be a meter or so in length before it can be observed on the surface of the rail head. Once an internal crack has reached a free surface, the growth rate normally will increase, but rail fracture will not necessarily immediately occur. A horizontal split-head defect can travel some distance along the rail before turning to run transversely. If both ends of the flaw turn upward, a loss of the running surface results. Alternatively, one end may turn upward and the opposite end turn downward. This results in the type of failure known as a detail fracture. This type of failure is particularly hazardous because it develops rapidly from an embedded horizontal flaw and results in a complete rupture of the rail. As yet, the local stress states that precipitate the branching associated with detail fractures are not well understood.

Figure 1. Models of typical railhead defects.

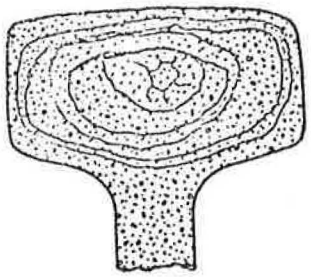

a. Typical Transverse Fissure Defect

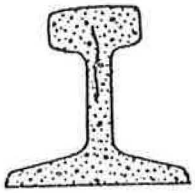

b. Vertical Split Head Defect

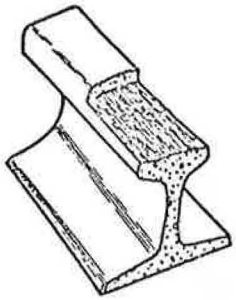

c. Horizontal Split Head

Recently, a comprehensive effort to characterize the stresses in rails encountered in service was initiated under the sponsorship of the Federal Railroad Administration. The results of these analyses, as they apply to the midrail region of unflawed rails, are summarized in this paper as an introduction to the behavior of rail stresses under train loads. [A far more comprehensive discussion of this behavior, including a detailed analysis of stress states at the tips of rail flaws (the so-called stress-intensity factors), is available elsewhere (10).]

In the following sections, the stresses induced by each of the major stress mechanisms are examined in an overview of the stresses in rails. The principal factors that influence rail stresses are described as a guide to those factors that may prove crucial in analyzing the initiation and growth of rail flaws. Finally, a brief discussion of the interactions of these stresses with typical midrail-region flaws is presented as an introduction to the mechanics of flaw propagation in rails.

GENERAL DESCRIPTION OF STRESSES IN RAILS

Stresses Due to Rolling Loads

The rail, a seemingly simple structural member, is, in fact, under the action of very complex stresses that occur during routine operating conditions. Flexural, thermal, contact, and residual stress mechanisms act simultaneously during each passage of load and must be considered in evaluating rail life.

Flexural stresses arise from the bending and twisting of the rail under wheel loads. When a vehicle approaches to a point within 1.8 to 2.6 m (6 to 12 ft) of a particular point in the railhead, that location experiences a tensile bending stress caused by the reversed flexural action of the rail on the elastic foundation of the ties, ballast, and subgrade. As the vehicle approaches closer to the point, the running-surface flexural stress becomes compressive and has a greater absolute value than had the previous tensile stress (as shown in Figure 2). As the first wheel set of a truck passes, interaction of flexural stresses from the adjacent wheel may not permit the flexural stresses to reverse until the second wheel set has passed.

A similar flexural action is caused by the local railhead bending on the elastic foundation of the rail web. As the wheel load approaches to within 7.6 to 3.8 cm (3 to 1.5 in) of a point, this flexural action can become significant, as shown by the dotted and dashed line in Figure 2. The impact of this mode of flexural action on the longitudinal stresses in the railhead is strongly influenced by the relative stiffness of the elastic foundation of the rail web when compared with the stiffness of the ties, ballast, and roadbed (the so-called track modulus). The trace for the railhead (bottom of Figure 3) illustrates that, at extreme values of the track modulus, the head-on-web bending can predominate and the sign of the longitudinal bending stress at the railhead bottom can reverse. This action can result in significant distortions of the bending stresses in the head, as shown by the second distribution of Figure 4. This action may occur locally in the presence of uneven tie support, as would occur in weathered track.

As the discussion above indicates, the flexural stresses in rails are significantly influenced by a range of parameters. In addition to the track moduli, the two other critical factors that affect the distribution of stresses in a rail are the orientation, location, and magnitude of the wheel-load vector and the state of wear of the railhead.

Significant distortions of the distribution of longitudinal stresses across the rail cross section can arise under the action of eccentrically applied vertical loads. As Figure 5 illustrates, the twist of the rail caused by off-centerline loading induces a longitudinal stress due to the warping of the rail cross section. Under moderate loading conditions, this stress reaches levels of 27.6 MPa (4000 lbf/in^2) in the interior region of the head. The detailed stress contours of Figure 6 illustrate how the offset of the vertical wheel load can influence the location of maximum stresses in the head. The location of the maximum longitudinal tensile stress remains within the railhead when the wheel is directly above the web; however, this maximum region occurs on the bottom surface of the head at the gauge corner when the wheel does not load the rail over its centerline (Figure 6b). (Because these contour lines have been developed for U.S. customary units only, SI units are not given in Figures 6, 9, and 10.)

A far more drastic change in longitudinal railhead stresses is that induced by the action of lateral loads such as those caused by the curving or hunting action of railcar suspensions. As Figure 7 indicates, lateral loads induce bending and torsion of the rail and cause substantial stresses that act in consort with the stresses induced by vertical wheel loads. For 65.6-kg/m (132-lb/yd) RE rail, the longitudinal stresses that result from the lateral bending of the rail under a 44.5-kN (10 000-lbf/in^2) lateral load can reach 48.2 MPa (7000 lbf/in^2) in the head. Similarily, simultaneously acting stresses due to bending of the railhead on the web and warping

Figure 2. Railhead flexural stresses.

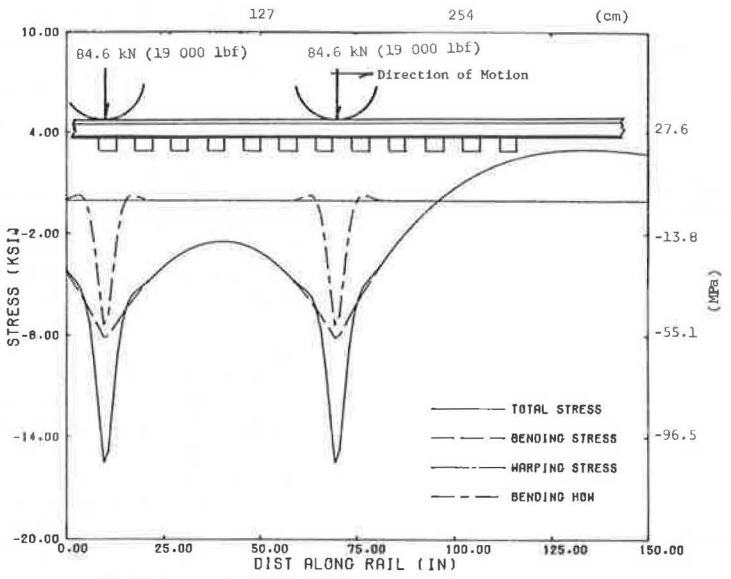

Figure 3. Relationship between longitudinal stresses in the rail and foundation modulus.

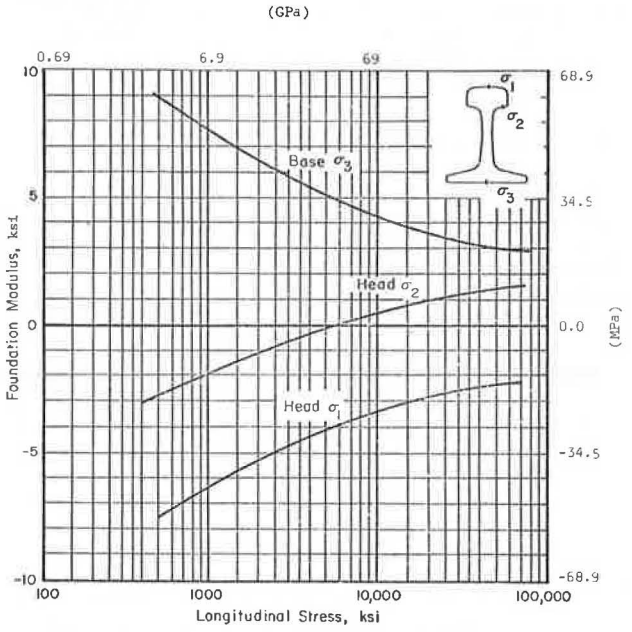

Figure 4. Longitudinal stress contours.

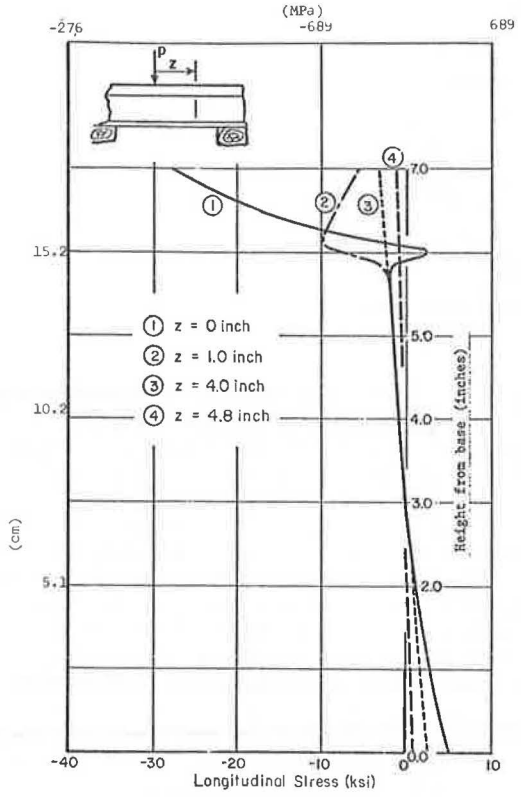

due to twist of the rail can induce stresses of 48.2 MPa and 68.9 MPa (10 000 lbf/in^2) respectively. Total longitudinal stress due to the action of lateral loads can typically reach levels of 165 MPa (24 000 lbf/in^2).

Torsion of the rail also influences stresses in the web. The torsion produced by eccentrically applied vertical loads causes additional stress in the fillet region of 68.9 MPa for an 84.5-kN (19 000-lbf) applied load. When accompanied by high lateral flanging forces, its maximum can exceed 207 MPa (30 000 lbf/in^2) in compression. The vertical stress in the web produced by lateral loads when superimposed on those produced by eccentric vertical loads can be quite significant, as the surface stress distributions of Figure 8 show. For example, the 65.6-kg/m RE rail underwent considerable design changes in the fillet region to correct a fatigue-crack initiation problem in the previous 65.1-kg/m (131-lb/yd) RE rail.

As Figure 8 indicates, rail wear can also significantly influence the flexural stresses in rails. Head wear of 1.9 cm (0.75 in) vertically can increase measured bending stresses due to vertical bending by 100 percent. This wear, however, has a far less dramatic effect on the other modes of flexure.

Thermal Stresses

In addition to the stresses induced by mechanically applied wheel loads, rails are also subjected to stresses induced by the constraint to their thermal expansion and contraction imposed by the fasteners and anchors. In

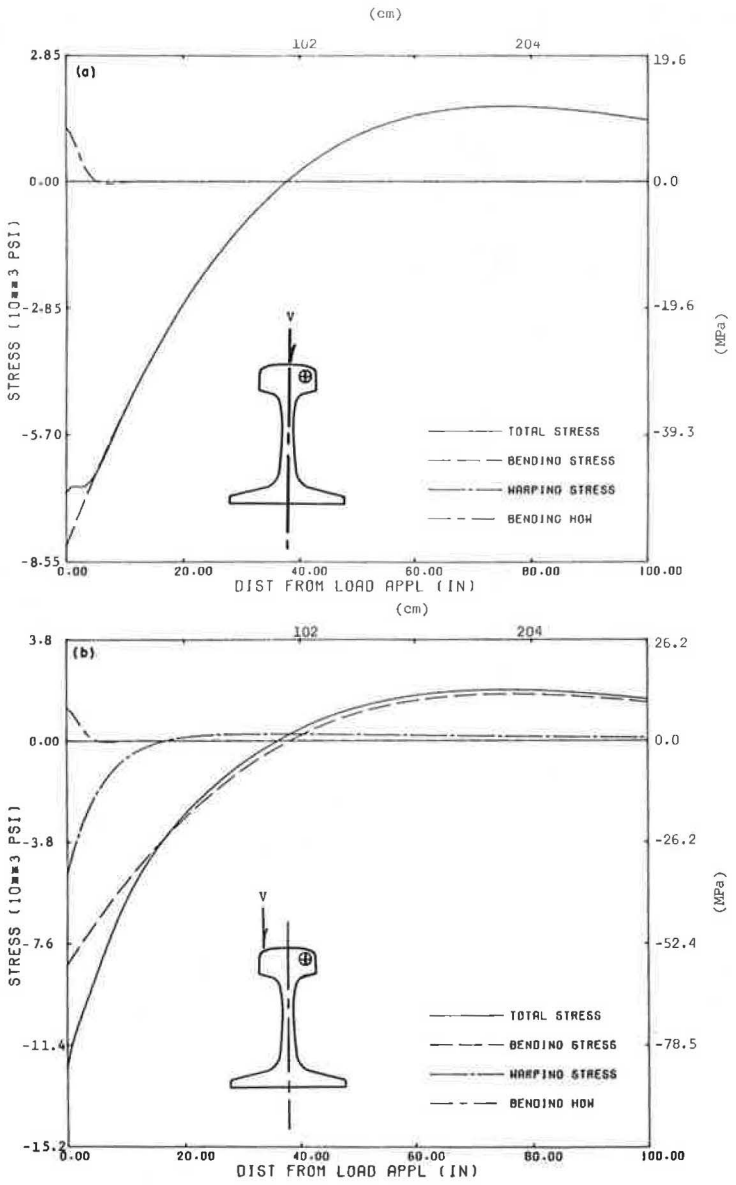

Figure 5. Stresses along rail due to 84.6-kN (19 000-lbf) wheel load: (a) acting on centerline of rail and (b) acting 3.8 cm (1.5 in) from centerline of rail.

continuously welded rail, a change in rail temperature of 38°C (68°F) due to shifts in the ambient environment can induce a stress of 47.5 MPa (6900 lbf/in^2) in the rail. Although this is not severe in comparison with the stresses due to wheel loads, when acting simultaneously with the mechanically induced stresses, thermal stresses prestress the rail before wheel passage. This factor may play an important role in accelerating flaw propagation and in influencing the flow of the railhead during yielding. In addition, this stress component is associated with the failure of rail welds and is instrumental in inducing track instabilities and consequently is critical to an analysis of the reliability of rails.

Contact Stresses

When the point of application of wheel load is within 0.76 to 1.27 cm (0.3 to 0.5 in) of a point in the railhead, large stresses (called contact stresses) are experienced that are the result of local deformation of the railhead near the region of load application (see Figure 9). These stresses are, in general, much larger in absolute magnitude than are the flexural stress components. The stress contours shown in Figure 6 are not sufficiently detailed to accurately show the magnitude of the contact stress components and therefore the contact area must be investigated separately. Figure 10 gives an idea of the magnitudes of the octahedral, longitudinal, and transverse stress respectively on transverse and longitudinal planes through a railhead.

The contact stresses are, in general, compressive [except for a transverse shearing stress that completely reverses as the rolling load passes (see τ_{xz}, Figure 9)]. These stresses are known to be capable of introducing fatigue damage local to the running surface of the rail. The contact stresses developed in the proximity of the wheel-rail contact zone frequently exceed the yield stress of the material and have long been suspected to be an important cause of railhead failures.

Under conditions involving new wheels and rails in normal contact, yielding of the rail will occur at a location 2.54 to 5.1 mm (0.1 to 0.2 in) below the rail surface when the wheel load exceeds approximately 84.5 kN. Under the influence of pure normal wheel loads, the rail surface will tend to flow in the direction of rolling if yielding occurs. If, in this contact situation, the normal wheel load remains lower than 140 kN (31 500 lbf), the plastic deformation occurring with each wheel passage

Figure 6. Contours of longitudinal stress directly beneath point of application of 84.6-kN (19 000-lbf) wheel load: (a) centrally applied load and (b) 1.9-cm (0.75-in) eccentric load.

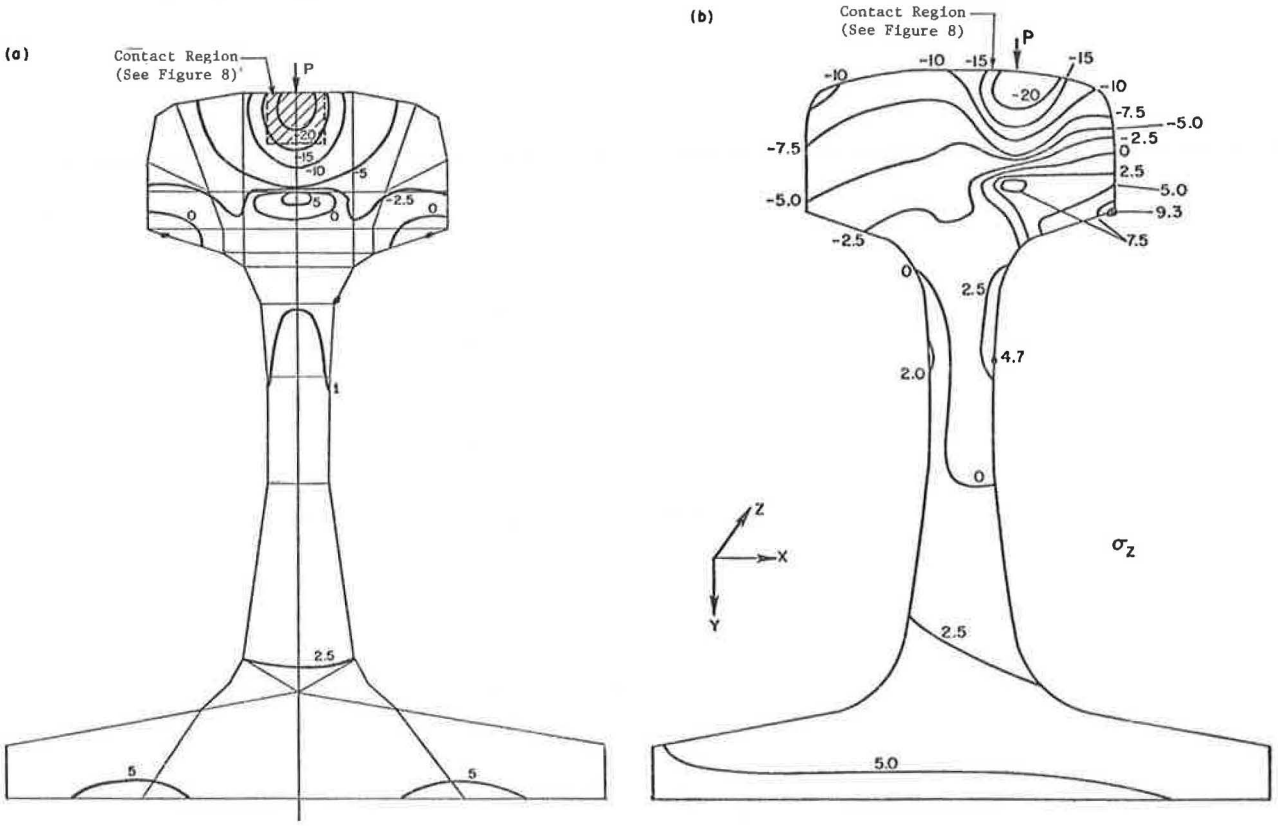

Figure 7. Stresses along rail due to 44.5-kN (10 000-lbf) lateral wheel load.

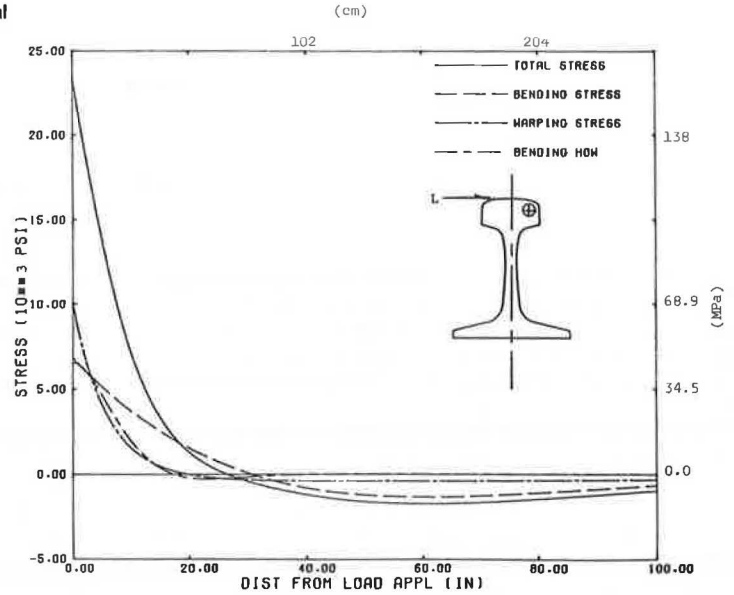

should decrease and eventually stop and the stresses will be thereafter elastic; i.e., shakedown of the post-yield stresses should theoretically occur. However, this situation is complicated by the fact that the rail steel may cyclically work soften, thus reducing its effective yield stress such that yielding will occur for a much longer period of rail life than expected, possibly throughout the entire rail life. Wear also aggravates this phenomenon.

Thus, wear significantly increases the flexural stresses; it is also an important mechanism in determining the combined pressure between wheels and rails. Frequently, the concave and false-flange regions on wheels that result from wear in service result in greater contact pressures between the wheel and rail and, therefore, excessive plastic flow of the rail.

The compressive surface stresses reach levels greater than -1.24 GPa (-180 000 lbf/in^2) for a wheel

Figure 8. Comparison of vertical tangential stress along rail surface for load eccentricities and head wear.

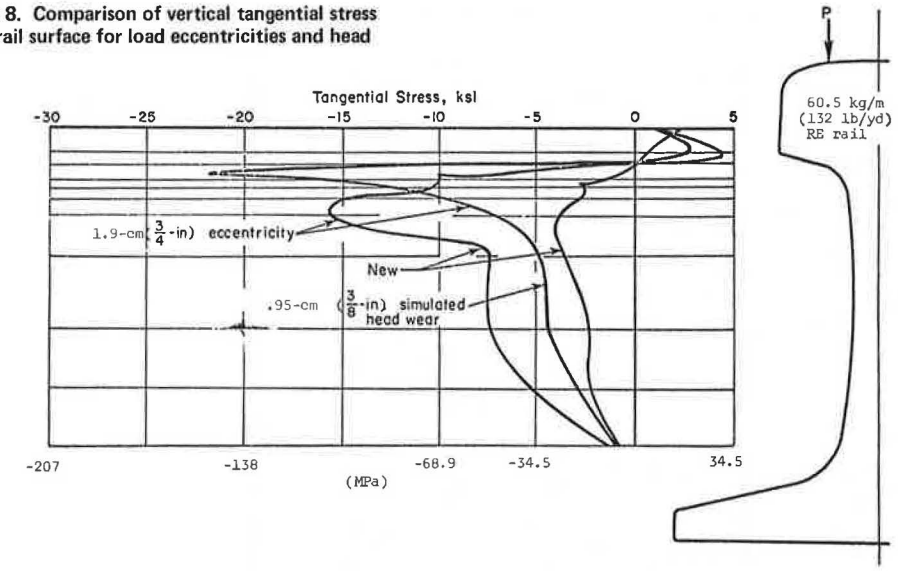

Figure 9. Stresses developed in railhead at depth of 0.37 cm (0.15 in) due to 0.83-m (33-in) diameter wheel and 84.6-kN (19 000-lbf) wheel load.

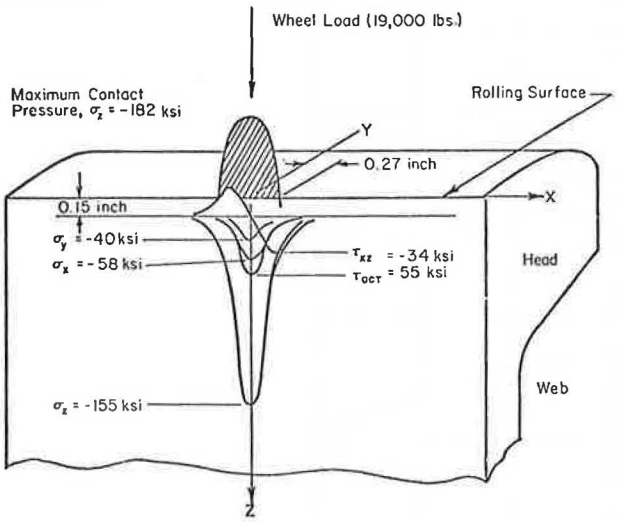

load of 44.5 kN. This same wheel load can create values of octahedral shearing of 372 MPa (54 000 lbf/in^2) and a transverse shearing stress of 234 MPa (34 000 lbf/in^2) that fully reverses during the rolling cycle (Figure 11).

Contact stresses and stresses local to the region of wheel-rail contact are greatly affected by both the lateral and the longitudinal tractions. Lateral forces that result from tracking of the wheel back and forth across the rail or sliding of the wheel laterally can be caused by irregularities or curves. Longitudinal tangential forces result from acceleration and deceleration of the locomotive and the stick-slip of wheels caused by axle windup on curves. In both of the tangential loading conditions, the full slip condition creates the highest shear stresses in the rail. A consequence of tangential traction is that it may be a very important factor in the formation of railhead edge cracks. It is observed (Figure 12) that, under tangential traction, a very high tensile-stress region develops immediately adjacent to the contact area. Clearly, such a stress field would have an opening effect on an edge crack of the type shown.

Residual Stresses

When wheel loads are greater than approximately 84.5 kN, new rails deform plastically on passage of the first vehicle. Under normal freight traffic, residual stresses begin to build up in the railhead in a region adjacent to the tread surface (Figure 13). As the rail experiences more traffic, residual stresses begin to develop deeper within the rail and steadily grow in magnitude. There is evidence of the possibility that this phenomenon is strongly affected by cyclic strain-softening behavior in the rail steel.

When the rail yields, a residual compressive zone is established directly beneath the railhead. Beneath the compressive zone, a tensile stress zone is developed to a depth of 1.27 cm or more. Horizontal cracks and split heads are known to initiate in this area, as indicated in Figure 14. This field may substantially influence the propagation of these flaws. Cracks occurring closer to the surface of the rail are likely to arrest or turn because of the residual compressive fields present in the tread region. Near the tread surface, a maximum range of shear stress occurs, but cracks initiated by this stress may be more likely to result in shelling rather than in such gross defects as horizontal or vertical splits because of the action of the residual stresses.

When longitudinal tangential wheel forces exist in the direction of rolling, more flow occurs. When the force is opposite to the direction of rolling and small, the flow also will be in the direction of rolling. Flow will be opposite to the direction of rolling if this tangential force is greater than approximately 0.13 times the normal wheel load.

When the tangential (longitudinal or lateral) wheel forces exceed approximately 0.35 times the normal wheel load, the onset of plastic deformation occurs on the surface of the rail toward the rear of the contact area. When the tangential wheel forces or tractions exceed approximately 0.37 times the normal wheel load, whether or not plastic flow stops during the life of a rail depends directly on the magnitude of these surface tractions.

ACTION OF MIDRAIL DEFECTS

Although there are a multitude of types of midrail-region defects, those of the greatest importance to rail safety

Figure 10. Stress contours for baseline load: case 1—84.6-kN (19 000-lbf) load, 0.83-m (33-in) diameter wheel, and 0.24-m (10-in) crown radius.

(a) Octahedral Stress

(b) Longitudinal Stress

(c) Transverse Stress

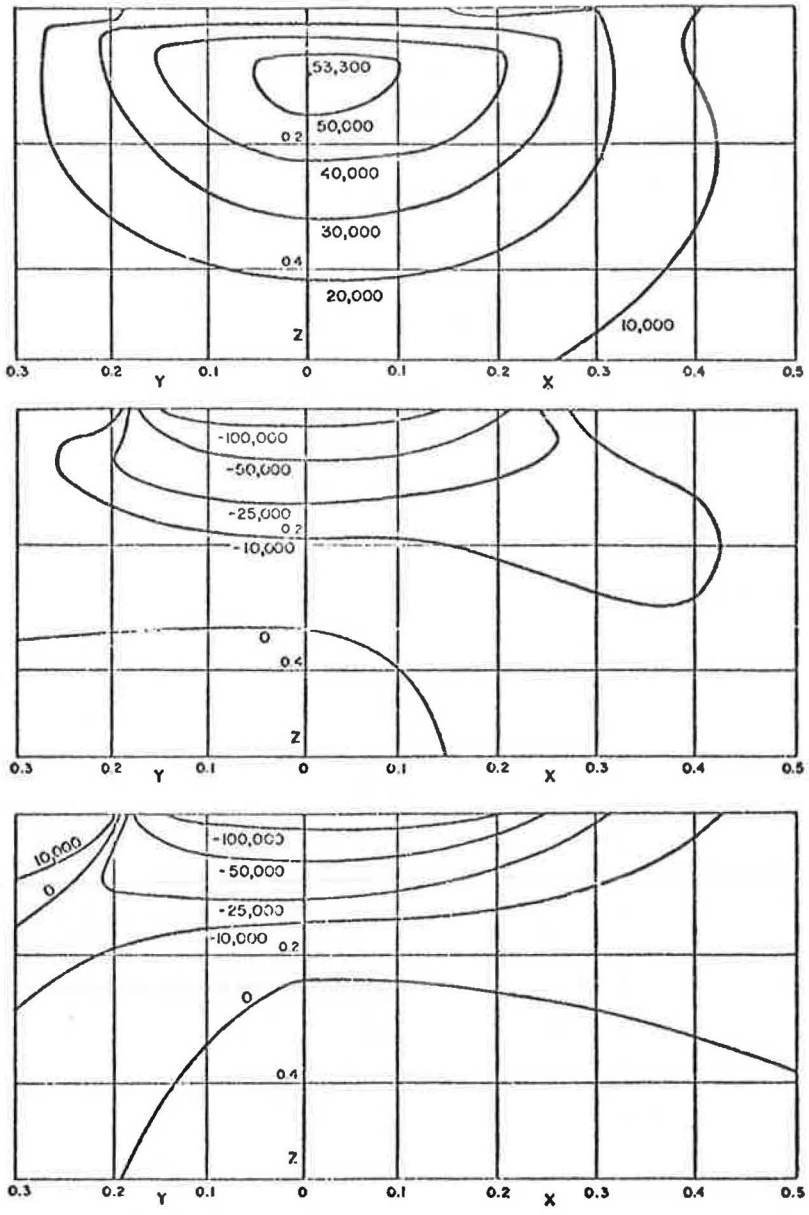

Figure 11. Maximum compression, octahedral stress: 0.83-m (33-in) diameter wheel and new and worn 65.6-kg/m 132-lb/yd) RE rail.

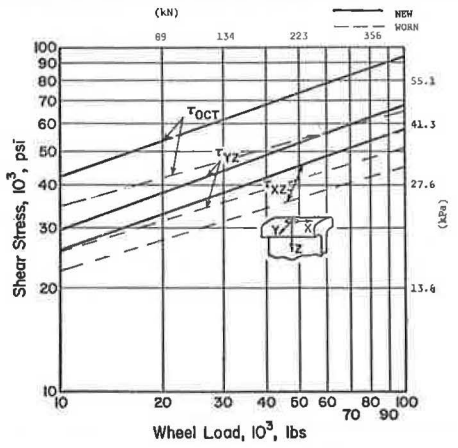

are transverse fissures and vertical and horizontal split heads.

Transverse Fissures

Transverse fissures occur at various depths in the railhead and may be initiated either on the surface from a shelling type of defect or internally from an imperfection (such as an inclusion, shatter crack, or blow hole). A transverse fissure is a progressive transverse fracture, Figure 1a, that starts from a nucleus within the head and then grows outward and downward throughout the head. Early downward growth of a transverse fissure is believed to be primarily influenced by flexural stresses induced by vertical wheel loading. These flexural stresses, however, tend to flex the crack toward the closed direction and, if it were not for the strong residual tensile stresses in the railhead caused by plastic flow, these flaws might have less tendency to propagate. Propagation in the upward direction is inhibited by the strong residual compressive stresses closer to

Figure 12. Transverse stresses developed due to full slip and 84.6-kN (19 000-lbf) wheel load.

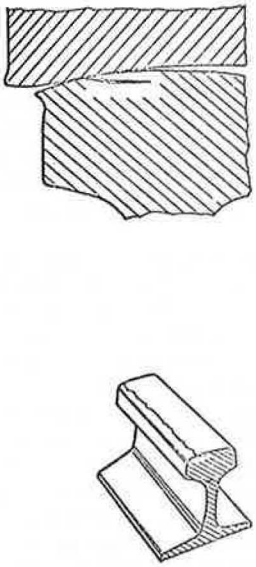

(a) Observed Edge Cracks in Rail Heads

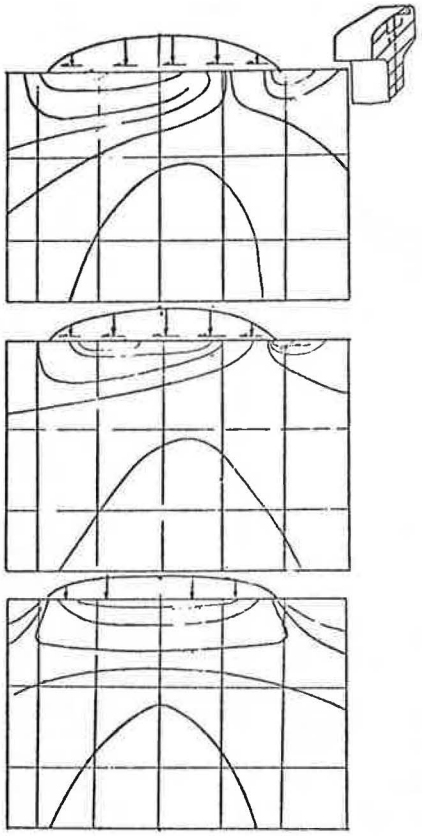

(b) Transverse Stresses in the Transverse Plane of the Rail Head

Figure 13. Analytical and experimental longitudinal, vertical, and transverse residue stresses.

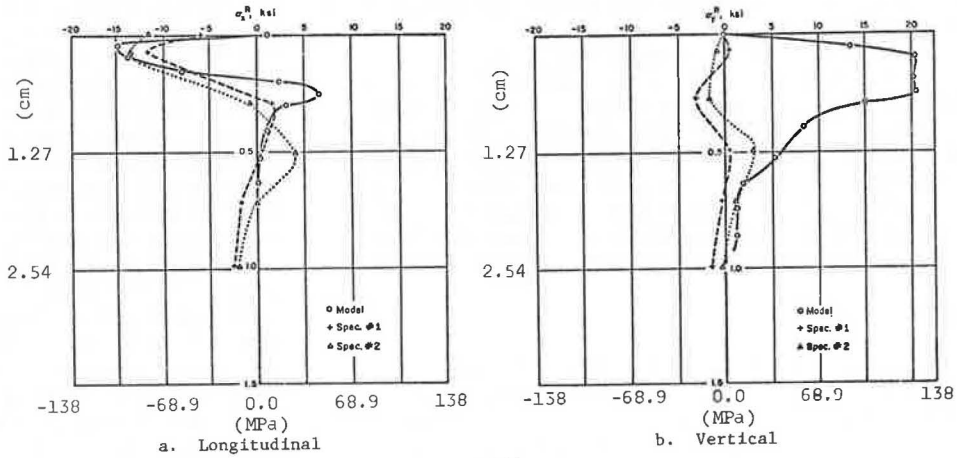

a. Longitudinal b. Vertical

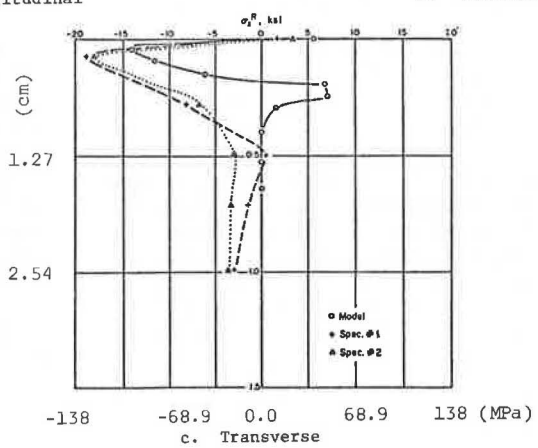

c. Transverse

Figure 14. Hardness profile of non-heat-treated standard rail specimen.

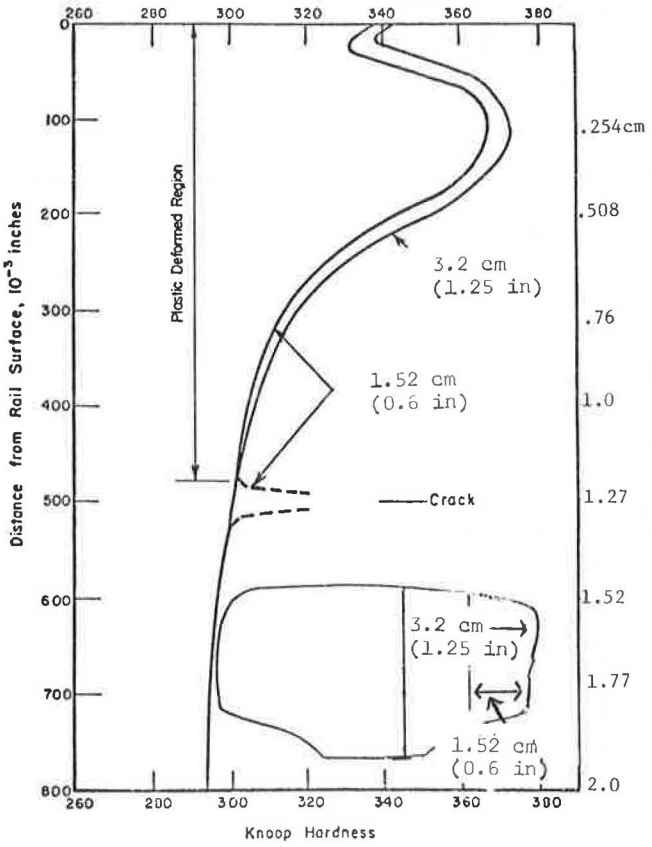

the running surface (Figure 13). Lateral growth of the flaw is greatly influenced by the flexure that results from the lateral load as in Figure 7.

As the flaw grows, a greater role is played in the growth by transverse shearing stresses in the railhead because of the local bending of the head on the elastic foundation of the web. The flaw growth remains slow until the crack covers 20 to 25 percent of the head area. The transverse fissure is regarded as particularly dangerous because final failure almost always results in a complete break in the rail and also because it seldom becomes visible before final failure occurs.

Vertical Split Heads

The vertical split is a progressive longitudinal fracture that grows through the head vertically and longitudinally near the center of the rail. It is initiated at a seam, segregation, or inclusion. The early growth of this defect is believed to be most influenced by flexural stresses. As the flaw grows to approximately 2.54 cm (1 in) in diameter, transverse shearing stresses begin to play a greater role in determining the action of vertical split defects under load.

In the case of the vertical split head, the tensile residual stresses that exist in the railhead make possible (particularly in the early stages of flaw growth) the propagation of these defects. Although it remains to be shown, we believe that the transverse shear stresses induced by lateral loading will also play an important role in the propagation of these flaws. This conclusion is drawn from the results found for horizontal splits.

The vertical split head may attain lengths of up to 3 m (10 ft), but does not become visible on the surface until it is at least a meter or so long. The flaw usually terminates by turning and growing out to the side of the railhead. This results in the breaking out of approximately half of the head.

Horizontal Split Heads

The horizontal split head is a progressive longitudinal fracture that grows parallel to the running surface at a depth of at least one-third of the railhead, Figure 1c. Early flaw growth is most affected by flexural stresses. The deeper the flaw is within the head, the less the effect. As the crack size approaches 2.54 cm in diameter, the effect of the longitudinal flexural stresses is overshadowed by that of the shearing stress due to the vertical wheel load.

These transverse shearing stresses are most influential on shallower horizontal split heads (at approximate depths of 0.76 cm). More deeply embedded flaws are also greatly influenced by transverse shearing stress, but this stress is caused primarily by the local bending of the head on the elastic foundation of the web.

Although these flaws usually initiate at an internal longitudinal seam, segregation, or inclusion, they usually develop into compound fissures that result in complete transverse breaks. After breaking out, the horizontal split head appears as a hairline crack on the side of the railhead. Before it reaches the free surfaces of the sides of the railhead, it often results in the appearance of a flat spot on the rail surface and a slight dropping of the entire railhead. Breakout first occurs in uncanted rail on the gauge side and in canted rail on the field side.

CONCLUSIONS

The failure of rails in service is strongly influenced by the interactions of rail stresses with the material characteristics of rail steels. These stresses in rails arise from four primary stressing mechanisms. Flexure of the rail includes the long-wave bending of the rail under wheel loads on the foundation of ties, ballast, and subgrade, as well as the local bending of the railhead on the web. These stresses typically are moderate and in the range of 13.8 to 68.9 MPa (2000 to 10 000 lbf/in^2) in the railhead. However, the magnitude and distribution of these stresses is strongly altered by variations in rail support and load-vector position and orientation. A moderate lateral load may increase these stresses by as much as 165 MPa.

Stresses induced locally by the contact of the wheel and rail are far more severe, often reaching values of octahedral stress of more than 400 MPa (58 000 lbf/in^2) in the railhead. Although the primary influence of these stresses is localized to a region of less than 0.5 cm from the tread surface, their action is felt to a depth of approximately half the depth of the head because of the development of residual stresses. Although local yielding of the rail is strongly influenced by surface tractions, indications are that, for typical wheel loads, plastic flow may stop and thus stabilize the residual stress state. Coupled with the quasi-steady state, thermal stresses of nearly 47.5 MPa that result from constrained expansion and contraction of the rail and residual stresses act to shift the mean stress during the passage of wheel loads, which strongly alters the stress environment to which inclusions and flaws in the rail are subjected.

The primary driving factor for midrail-region flaws is the stress induced by the flexural action of the rail under wheel loads. The residual stresses, in conjunction with the thermal stresses, in rails act to modify

the flexural stress cycles seen by flaws. Transverse fissures may be driven initially by longitudinal stresses due to flexure and later by the action of the fully reversed shear stresses due to bending of the head on the web. Similarly, vertical split-head flaws may be driven by the flexural action of lateral loads, again influenced by the action of the fully reversed shear stresses. The growth of horizontal splits in the railhead appears to be dominated by shear stresses, except in the very earliest stages of growth. For horizontal flaws at depths of less than 0.76 cm the effects of transverse shear stresses due to whole-rail flexure dominate but, below this depth, the shear stresses resulting from the bending of the head on the web become increasingly significant. However, in light of the complexities of the factors that control stresses in rails, these conclusions must be considered as preliminary.

ACKNOWLEDGMENT

The results summarized in this paper were developed at Battelle Columbus Laboratories and the U.S. Department of Transportation, Transportation Systems Center, under the sponsorship of the Federal Railroad Administration. We gratefully acknowledge the contributions of P. M. McGuire, S. G. Sampath, and E. F. Rybicki of Battelle Columbus Laboratories, A. B. Perlman of Tufts University, and J. J. Lanza of the Transportation Systems Center in the conduct of the rail-stress program summarized here.

REFERENCES

1. J. J. Hitz. Track-Related Accident Causes: Phase 1. Transportation Systems Center, Cambridge, MA; Federal Railroad Administration, May 1977.
2. M. M. Frocht and B. C. Wang. A Three-Dimensional Photoelastic Study of Interior Stresses in the Head of a Railroad Rail in the Region Under a Wheel. Proc., ASME, 4th U.S. National Congress on Applied Mechanics, Berkeley, CA, Vol. 1, 1962, pp. 603-609.
3. C. J. Code. Wheel Load, Wheel Diameter, and Rail Damage. Bulletin, AREA, Vol. 59, 1960.
4. G. H. Way, Jr. Heavy Cars: What Are the Issues? Bulletin, AREA, Vol. 76, No. 653, June 1975.
5. A. D. Kerr. On the Stress and Stability Analyses of Railroad Track. ASME, Journal of Applied Mechanics, Vol. 76, No. 1, 1973, pp. 1-5.
6. D. P. McConnell. Stresses in Rails. Transportation Systems Center, Cambridge, MA, Technical Memorandum, Nov. 1976.
7. T. G. Johns and K. B. Davies. Preliminary Description of Stresses in Railroad Rail. Federal Railroad Administration, Rept. No. FRA-ORD-77-35, Nov. 1976.
8. B. Paul. A Review of Rail-Wheel Contact Stress Problems. Proc., Princeton University Symposium on Railroad Track Mechanics, Elsevier, New York, 1975.
9. R. K. Steele. Requirements for the Reliability Assessment of Railroad Rail in Service. Proc., Princeton University Symposium on Railroad Track Mechanics, Elsevier, New York, 1975.
10. T. G. Johns and others. Engineering Analysis of Stresses in Railroad Rail: Phase 1. Federal Railroad Administration, June 1977.

Analytical and Experimental Study of Residual Stresses in Rails

Kent B. Davies and Thomas G. Johns, Battelle Columbus Laboratories, Columbus, Ohio

A mathematical model for the calculation of railhead residual stresses is presented together with the results for a specific case of wheel loading. These data are then compared with the results obtained by destructive evaluation of residual stresses in simulated railhead specimens. Finally, the results obtained are compared with published values for residual stress.

New rails have an initial residual stress field that is an artifact of the mechanical working of the manufacturing process. After their installation in track, this initial stress field begins to change under the recurring plastic deformation caused by passing wheel loads. The new residual stress state that is established, which may or may not continue to change during the life of the rail, is believed to have a profound effect on the formation of railhead cracks. But because of the difficulties implicit in the analysis, few investigations of rail residual stress have been reported in the literature. Those that have appeared, however, are of great interest. The most important of these are those due to Johnson (1), Merwin and Johnson (2), Johnson and Jefferis (3), Martin and Hay (4), and the Office for Research and Experiments of the International Union of Railways (ORE) (5).

Previous approaches to the study of rail residual stresses have involved both analytical and experimental methods. Analytical techniques have been based on the application of approximate numerical methods. Experimental approaches have relied on various destructive techniques, such as sectioning out and hole drilling. Figure 1 shows the results obtained by Martin and Hay (4) for the three normal, residual stress components calculated by a method based, in part, on that presented by Johnson and coworkers (1, 2, 3). Figure 2 shows both the experimental and the analytical results obtained by ORE (5) for rail removed from service. The data presented in Figures 1 and 2 represent the only residual stress calculations that have appeared in the literature so far.

NUMERICAL ANALYSIS OF RAILHEAD RESIDUAL STRESSES

A numerical method was developed for the calculation

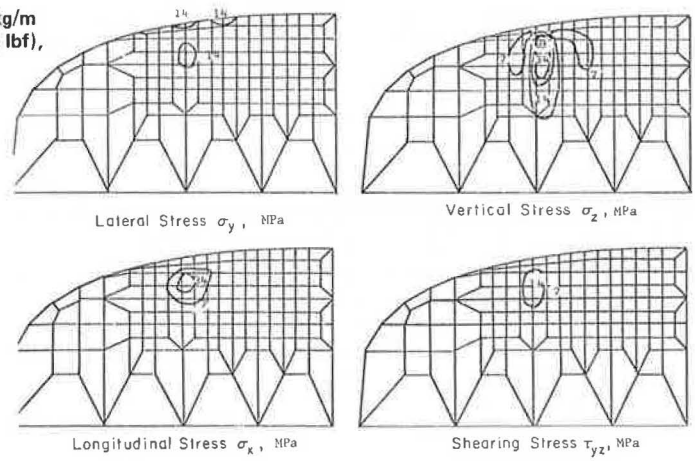

Figure 1. Residual stress components: 65.6-kg/m (132-lb/yd) RE railhead, P = 84.6 kN (19 000 lbf), and K = 379 MPa (55 000 lbf/in^2).

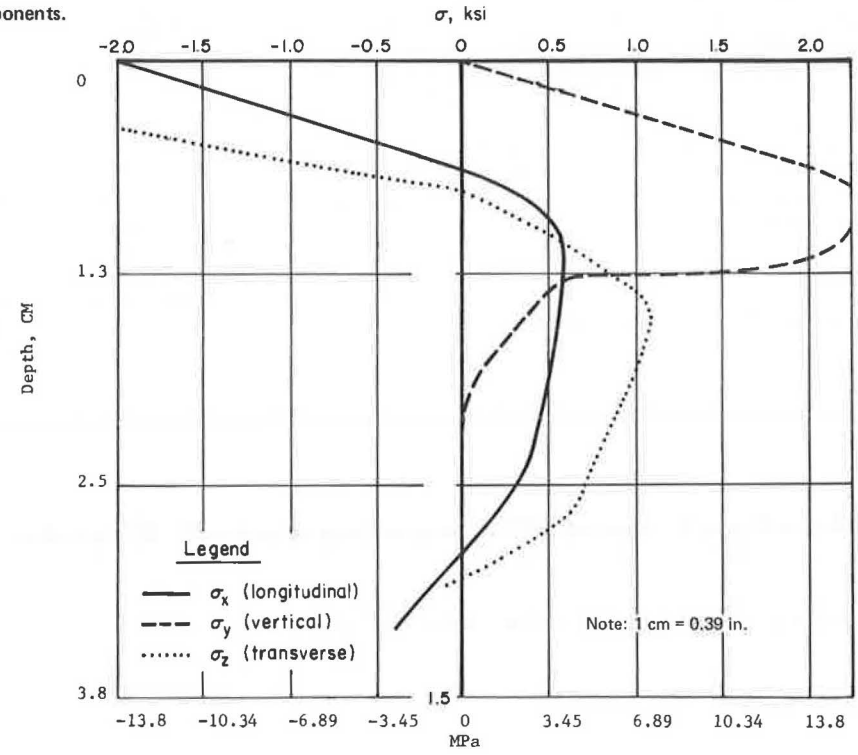

Figure 2. Experimental residual stress components.

of the residual stresses caused by wheel-rail contact. This analytical procedure extends the work of Merwin and Johnson (2) and of Martin and Hay (4) in that it is fully three dimensional (by using a direct finite-element approach) and includes the effect of work hardening.

The flow diagram shown in Figure 3 summarizes the calculation procedure. The first step in the computation is the determination of the subsurface strains by using the specified load and contact distributions and the three-dimensional finite-element model. This consisted of a quarter-section model of the railhead in which two vertical planes of symmetry were assumed. The model was a rectangular solid that had a 3x3.25-cm (1.2x 1.3-in) cross section. A constant-cross-section mesh was repeated at varying intervals along the length of the model. A cross-sectional view of the model is shown in Figure 4. It included 630 isoparametric-brick elements consisting of 1340 nodes. The loading was applied in the form of a 84.6-kN (19 000-lbf) Hertzian contact distribution having a 0.64-cm (0.27-in) semimajor axis and a 0.47-cm (0.19-in) minor axis. To avoid the additional complication of flexural stresses, the model was supported by a rigid foundation.

For the residual-stress analysis, it was necessary to construct a strain cycle that simulated the passage of a rolling load for a single cross-sectional plane. This was done from the simple static-contact cases analyzed by the finite-element method by using the GENTAPE program. It was assumed that the strain seen at any point in the railhead would be the same as that seen by any other point lying on the same longitudinal line at some time. Thus, the variation in strain along a given longitudinal line due to a static load was taken to be the same as the strain at a point as a loaded wheel passed by. The GENTAPE program assembled a magnetic tape of strain cycles for the nodal points of the cross section shown in Figure 4. The results of this compilation are shown for the elastic case in Figure 5. The elastic strain in the y-direction was compared with that determined by Martin and Hay (4) by an indirect finite-element solution, and good agreement was found

Figure 3. Flowchart of residual stress calculation procedure.

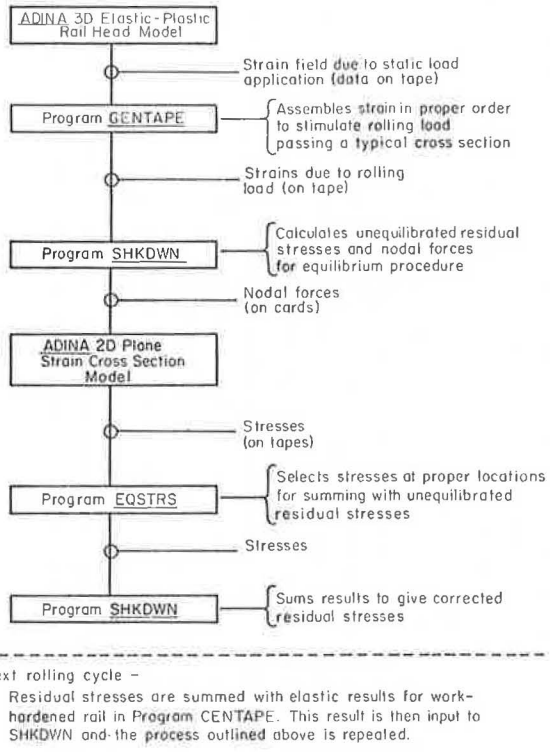

Figure 4. End-sectional view of three-dimensional finite-element grid for railhead analysis.

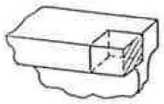

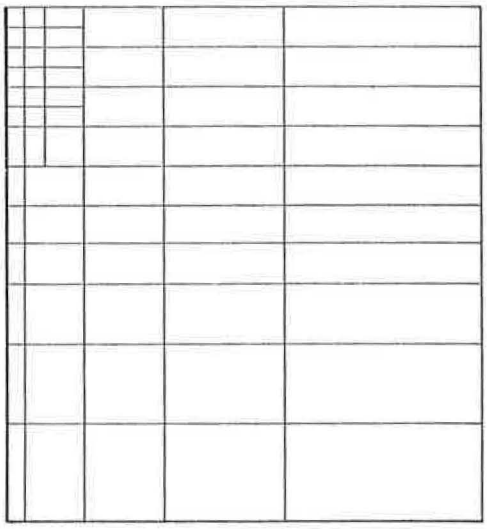

for the components. These particular strain cycles were computed for a point lying at a depth of 1.91 cm (0.75 in) below the rail surface. Similar cycles, differing only in the magnitudes of the components, exist for the other points in the plane.

The SHKDWN program calculates unequilibrated stresses on the basis of the following assumptions:

1. The elastic strain cycle that can be derived from a static-contact situation is a sufficiently close approximation to the true elastoplastic strain cycle of the rolling contact situation [as assumed by Merwin and Johnson (2)].
2. The material is isotropic and elastic-plastic and obeys an isotropic strain-hardening law. Its yielding is described by the Von Mises criterion and the Prandtl-Reuss equations.
3. Every plane of the rail remains identical to every other plane in the rail in terms of both residual stress and material properties. Thus, σ_{xz} and σ_{yx} are everywhere zero when no load is present.
4. A vertical plane of symmetry is assumed to exist on the longitudinal centerline of the rail. Thus, only half the railhead is included in the analysis.

Analysis proceeds in the program in the following manner:

1. Various problem parameters are read in, such as the coefficients of the linear equation that describes the stress-strain curve, the yield stress, Poisson's ratio, and the problem size.
2. Strain-cycle information is read from a tape on a mesh-point-by-mesh-point basis. For each increment of strain, the stresses at all of the points in the cross section are evaluated before moving on to the next increment. After the strain tensor at a point is read in, the strain components are transformed into deviatoric stress components by the relationships

$$S_{ij} = \sigma_{ij} - S_m \quad (i = j = 1, 2, 3) \tag{1}$$

where

$$S_m = \sigma_{ii}/3 \quad (i = 1, 2, 3) \tag{2}$$

At the same time, the strain-deviation gradient is calculated as a three-point divided difference approximation to the derivative. Thus,

$$(d\epsilon_{ij}/dx)\big|_n \cong [(\epsilon_{ij}\big|_n - \epsilon_{ij}\big|_{n-1})/(x_n - x_{n-1})] + (x_n - x_{n-1}) \times [(\epsilon_{n+1} - \epsilon_n)/(x_{n+1} - x_n)] - [(\epsilon_n - \epsilon_{n-1})/(x_n - x_{n-1})] \div (x_{n+1} - x_{n-1}) \tag{3}$$

is the gradient at the nth point in the mesh. Finally, the equivalent strain for the current strain level is calculated by using the familiar expression

$$\epsilon_{ef} = (2/3)[\epsilon_{11} - \epsilon_{22})^2 + (\epsilon_{22} - \epsilon_{33})^2 + (\epsilon_{33} - \epsilon_{11})^2 + (3/2)(\epsilon_{12}^2 + \epsilon_{23}^2 + \epsilon_{13}^2)]^{1/2} \tag{4}$$

3. By using the results of the uniaxial stress-strain curve, the Von Mises yield criterion

$$\sigma_{ef} < \sigma_y \tag{5}$$

where σ_y = equivalent stress at yield (for the first approach to yielding) is applied. If yield has not occurred at that mesh point, the stress is merely assumed to be that given by Equation 1. The program then proceeds to the next mesh point and repeats the sequence of computations. If, however, it is found that yielding has occurred, then the increment of stress due to the current value of strain is calculated by using the Prandtl-Reuss equations. These may be written in terms of deviatoric stress and strain. Specifically, the time rate of change visually indicated is replaced by the gradient in the rolling direction so that

Figure 5. Elastic strains along rail axis due to 84.6-kN (19 000-lbf) load: longitudinal plane of symmetry and depth of 1.91 mm (0.075 in).

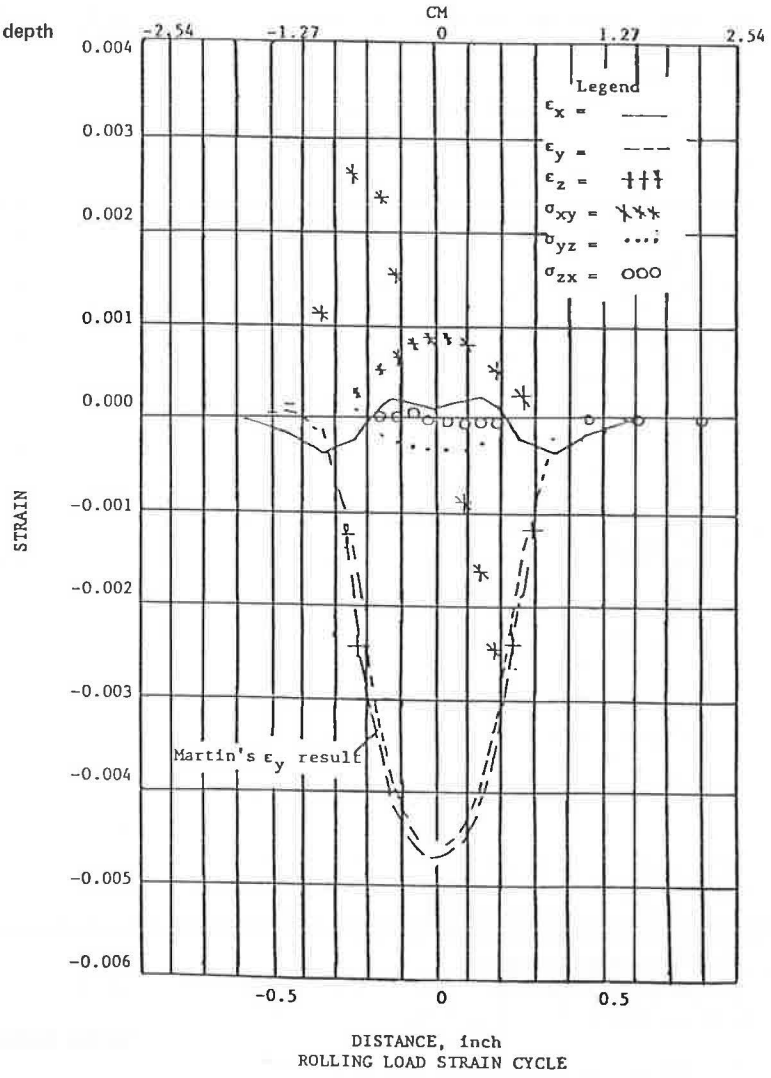

$$(\Delta S_x/\Delta x) = 2G[(\Delta\epsilon_x/\Delta x) - (\Delta W\Delta x^{-1}/K^2)S_x]$$
$$(\Delta S_y/\Delta x) = 2G[(\Delta\epsilon_y/\Delta x) - (\Delta W\Delta x^{-1}/K^2)S_y]$$
$$(\Delta S_z/\Delta x) = 2G[(\Delta\epsilon_z/\Delta x) - (\Delta W\Delta x^{-1}/K^2)S_z]$$
$$(\Delta\tau_{xz}/\Delta x) = G[(\Delta\gamma_{xz}/\Delta x) - (\Delta W\Delta x^{-1}/K^2)\tau_{xz}]$$
$$(\Delta\tau_{xy}/\Delta x) = G[(\Delta\gamma_{xy}/\Delta x) - (\Delta W\Delta x^{-1}/K^2)\tau_{xy}]$$
$$(\Delta\tau_{yz}/\Delta x) = G[(\Delta\gamma_{yz}/\Delta x) - (\Delta W\Delta x^{-1}/K^2)\tau_{yz}] \quad (6)$$

where $\Delta W/\Delta x$ = rate of plastic work and is given by

$$(\Delta W/\Delta x) = S_x(\Delta\epsilon_x/\Delta x) + S_y(\Delta\epsilon_y/\Delta x) + S_z(\Delta\epsilon_z/\Delta x) + \tau_{xy}(\Delta\delta_{xy}/\Delta x) + \tau_{yz}(\Delta\delta_{yz}/\Delta x) \quad (7)$$

and K, γ, τ, and δ have their customary meanings.

Equation 6 is the form of the Prandtl-Reuss relationship actually used in the program. The strain rates used for a particular point in the strain cycle were those given by Equation 3. The increments of stress computed by using Equation 6 are then added to the stresses computed at the previous increment of strain. This process continues during the strain cycle until unloading of a point occurs. After this, stress is again calculated elastically and further unloading proceeds elastically.

4. When the strain cycle has been completed, a system of compatible residual stresses remains. However, because the stresses at the various levels have been computed independently of each other, equilibrium is not satisfied. To remedy this, the resultant planar nodal forces are calculated that would give rise to the system of stresses just calculated if considered with respect to an assumed finite-element mesh. This is accomplished by integrating the equation of equilibrium over the indicated elements. Thus, the forces at the center of the element are given by

$$F_y = \int\int[(\partial\sigma_{yy}/\partial y) + (\partial\sigma_{yz}/\partial z)]\,dydz \quad (8)$$

and

$$F_z = \int\int[(\partial\sigma_{zz}/\partial z) + (\partial\sigma_{yz}/\partial y)]\,dydz$$

These resultant forces are apportioned equally to the four corner nodes of the assumed finite-element mesh. (The actual program is somewhat more involved than this, but the mechanical details, involved as they are with the finite-element method, will not be further elaborated upon. Nodal forces representing the residual stress system are finally output on punched cards.)

The two-dimensional, finite-element railhead cross-section model, which is exactly the same as the cross section of the three-dimensional railhead model, has 53 linear elements. The boundary conditions are appropriately arranged to simulate railhead support as described above. The analyses are performed by using the nodal forces produced from the unequilibrated residual stresses by the SHKDWN program. The resulting

stresses are output on tape.

The EQSTR program, which is structurally almost identical to the GENTAPE program, arranges the stress output from the two-dimensional finite-element model in a sequence that corresponds to that of the mesh points in the SHKDWN program. (Once again, this program is of little interest from a mechanical standpoint, so it will not be discussed further.)

The stress computation procedure is then completed by subtracting the stresses computed by the finite-element model (representing the unequilibrated portion of the computed stresses) from the original residual stress. Thus, at each mesh point

$$S_{ij}|_k = S_{ij}^{ur}|_k - S_{ij}^{fe}|_k \quad (9)$$

when $S_{ij}^{fe}|_k$ = finite-element component at the kth mesh point. The resulting stress deviations are then output as the final residual stress state for that load pass. This operation is also accomplished by using the SHKDWN program. A similar procedure is followed for the next pass of the load.

APPLICATION OF NUMERICAL METHOD TO CASE OF WHEEL-RAIL CONTACT

By using the computation procedure described above, residual stresses were calculated for the case of a 84.6-kN load on a rail modeled by a bilinear stress-strain curve that had a yield stress of 440 MPa (64 000 lbf/in^2). The stress cycle used was that described above and shown in Figure 5.

The results for one pass of the load are shown in Figure 13 of the preceding paper in this Record for the three normal stress components. It is observed that the respective maxima occurred below the surface of the rail. The vertical stress component is zero at the surface and tensile below the surface and reaches its maximum at a depth of about 2.5 mm (0.1 in). The other two normal stress components have compressive maxima and occur at somewhat shallower depths in the railhead. All of the components decay to insignificant levels at depths below 1.25 cm (0.5 in).

COMPARISON OF NUMERICAL AND EXPERIMENTAL RESIDUAL STRESS RESULTS

A destructive experimental determination of rail residual stresses was performed on simulated rail specimens that had been subjected to known rolling loads. Specimens were subjected to one or three passes of the wheel load.

The simulated specimens consisted of 25.4-cm (10.0-in) crown-radius head sections machined from a 79.5-kg (175-lb) crane-rail section. The resulting specimens were thoroughly stress relieved to eliminate any initial residual stress field. After rolling in a rolling-load machine, each specimen was dissected by using the Battelle Columbus Laboratories' sectioning technique for the determination of the three-dimensional residual stress field (6). The results from the experimental residual stress investigation are also shown in Figure 13 of the preceding paper in this Record. The rolling-load test specimens had a yield stress of 326 MPa (47 300 lbf/in^2). The specimens were loaded to a level of 64.5 kN (14 500 lbf). If the two sets of properties and loads are considered in relation to each other, it is seen that the laboratory specimen was the more severely loaded. By using the ratio of the maximum contact pressure to the shear yield stress as a means of comparison (1), it is found that the mathematically modeled case had a ratio (R) of 4.1116 and the laboratory case had R = 6.1616. Thus, it would be expected that the residual stress formation would be more developed in the experimentally measured case. Examination of the plot of longitudinal stresses shows that the results predicted by the model are slightly larger than the experimental results. In addition, the effects occur somewhat more shallowly in the model. The transverse stress results show the expected trend; the laboratory stresses are the larger and occur at the greater depth. Examination of the vertical stress results shows very poor agreement. At this time, no rationale can be offered for this disparity. It is interesting to note that, in the case of the horizontal plane stress components, the greatest difference between the one-pass and the three-pass specimens occurred on the surface. Thus, it was concluded that, with the exception of the vertical stress, there was reasonably good agreement between the mathematical model and the laboratory validation experiments when the strain cycle was assumed to be an elastic one.

COMPARISON WITH PUBLISHED RESULTS AND CONCLUSIONS

A mathematical model of residual stress formation in railroad rails was developed. The results obtained by using this numerical method were in reasonable agreement with the experimentally determined values obtained in this study. It is useful to compare these results with data published in the literature.

The experimental and analytical results can be most conveniently compared with those obtained by ORE (5). Such a comparison is made difficult by the fact that the ORE work was conducted on rail removed from service that had a tensile yield strength of approximately 689 MPa (100 000 lbf/in^2). Thus, the situation analyzed here was significantly different than that reported by ORE.

Comparison of the vertical stress results shows that the tensile maximum in the specimens examined by ORE was located at a depth approximately 0.62 cm (0.25 in) lower than the tensile maximum in the analytical results. Although this component is also about 34.5 MPa (5000 lbf/in^2) greater in magnitude, the agreement is considered measurable. The ORE curve disagrees with the experimental curves. Martin and Hay (4) showed a tensile maximum of about 68.9 MPa.

Comparison of the transverse component results shows several differences between the analytical results and those reported by ORE. The tensile maximum occurs at a considerably greater depth, and a very high compressive value is indicated at the surface of the rail.

The longitudinal residual stress results showed better agreement, although the ORE maximum once again occurred somewhat deeper in the railhead. Once again, the high compressive stress reported on the running surface by ORE was not found in our work.

Despite the degree of success with which it predicted residual stress magnitude, the model is sufficiently complex to make the calculation of the effect of many cycles of the load application both difficult and costly. Thus, it is recommended that future residual stress determinations be carried out experimentally by using rail removed from service for which the service history is accurately known.

ACKNOWLEDGMENTS

This work was supported by the Federal Railway Administration. We are pleased to acknowledge the assistance in all phases of the program of Donald McConnell of the U.S. Department of Transportation, Transportation Systems Center. Jack Groom was responsible for con-

ducting the experimental work reported in this paper.

REFERENCES

1. K. L. Johnson. A Shakedown Limit in Rolling Contact. Proc., ASME, 4th U.S. National Congress on Applied Mechanics, Berkeley, CA, Vol. 1, 1962, pp. 971-975.
2. J. E. Merwin and K. L. Johnson. An Analysis of Plastic Deformation in Rolling Contact. Proc., Symposium on Fatigue in Rolling Contact, Institute of Mechanical Engineers (London), Vol. 177, No. 24, 1963, pp. 676-688.
3. K. L. Johnson and J. A. Jefferis. Plastic Flow and Residual Stresses in Rolling and Sliding Contact. Proc., Symposium on Fatigue in Rolling Contact, Institute of Mechanical Engineers (London), Vol. 177, 1963, p. 95.
4. G. C. Martin and W. W. Hay. The Influence of Wheel-Rail Contact Forces on the Formation of Rail Shells. Trans., ASME, 72-WA/RT-8, 1972.
5. Study of Fatigue Phenomena of the Rail in the Contact Zone With the Wheel. Office for Research and Experiments of the International Union of Railways, Rail International, Vol. 3, No. 13, Sept. 1973, pp. 741-794.
6. T. G. Johns and others. Engineering Analysis of Stresses in Railroad Rail: Phase 1. Federal Railroad Administration, June 1977.

Mathematical Model for Lateral Thermal Buckling and Displacement of Curved Track

W. So, Research and Test Department, Association of American Railroads, Chicago
W. W. Yang, Consolidated Rail Corporation, Chicago

One disadvantage of continuously welded rails is that the possibility of track buckling because of temperature increases is increased significantly by the elimination of rail joints. Many mathematical models have been developed for the buckling of tangent tracks, but there are very few that deal with curved tracks. The objective of this paper is the development of methods for the prediction of both the lateral thermal-buckling load and the corresponding displacement of curved tracks so that criteria for track design, maintenance, and evaluation can be formulated. This objective has been achieved by using a two-dimensional finite-element model that simulates the lateral stability of a track subjected to temperature increases and train wheel loads. This paper illustrates only the basic applications and the potential of the model. A parameter investigation was made that included tracks that had curvatures varying from 0 to 10° and studied the effects of various track parameters on the buckling temperature and the lateral track displacement. The results indicate that the buckling temperature and lateral displacement of a curved track are significantly affected by changes in lateral ballast resistance, misalignment and curvature, and by the presence of ineffective ties. The model provides a promising new approach to the track-buckling problem; however, test data are needed to validate it.

Continuously welded rail is being increasingly used in railway track construction in the United States. A well-known disadvantage of such rails is that the possibility of track buckling because of temperature increases is increased significantly by the elimination of rail joints. Derailments attributed to track buckling have been reported (1). This track-buckling problem—also called the track-stability problem—is consequently of great importance on continuously welded tracks.

Track stability can be subdivided into two main categories according to the plane in which buckling occurs: lateral and vertical. Lateral stability refers to buckling that occurs in the plane of the track, and vertical stability refers to the uplift of the track. Vertical buckling is unlikely to occur, because the initial uplift of the track reduces the lateral ballast resistance and usually causes lateral buckling.

Many mathematical models have been developed for the lateral stability of tangent track, but there are very few that deal with curved track. The objective of this paper is the development of methods for the prediction of both the lateral thermal-buckling load and the corresponding displacement of curved track so that criteria for track design, maintenance, and evaluation can be formulated. This objective is achieved by using a two-dimensional finite-element model that simulates the lateral stability of a track subjected to temperature increases and train wheel loads.

The model was first developed by So and Martin (2) to solve the problem of the lateral stability of tangent tracks. Reasonably good agreement was obtained between the model results and test data. There are no other known applications of finite-element models in this respect. Previous applications of the finite-element method in the analysis of tracks were primarily for the calculation of stresses in the rails under wheel loads.

The finite-element model is quite powerful and efficient in simulating track stability because it uses standard structural-analysis computer programs for elastic frames. A remarkable advantage of the model is its versatility in incorporating all the main parameters that govern the lateral stability of track (3): (a) condition of lateral rail support, (b) rotational resistance of rail fasteners, (c) flexural rigidity of rails, (d) track curvature, (e) track irregularities (such as misalignments and ineffective ties or rail fasteners), and (f) loading on the track (such as thermal loads due to heating of the rails; vertical, lateral, and longitudinal loads due to normal traffic; dynamic vibrations; and train braking and acceleration). Longitudinal loading here refers to loading along the rails. The model uses geometrically nonlinear-beam-deflection theory (large-deflection theory). Geometrically linear-beam-deflection theory (small-deflection theory) has been used for track-

stability problems in most previous research. As demonstrated by Kerr (4), this approach yields inaccurate results because buckling deflections are not small.

The finite-element model presented here has not been thoroughly validated because of the lack of test data. Once its validity is fully established, the model should provide a useful approach to track-stability problems. In this paper, only the basic applications and the potential of the model will be illustrated.

REVIEW OF LITERATURE

Experiments on track stability have been conducted in other countries (5, 6, 7, 8); however, no available test data on curved tracks are complete enough to be used for the validation of the finite-element model presented here. Because of the importance of the track-buckling problem, it is recommended that tests be conducted in the United States.

Many theories have been developed for analysis of the buckling problem of the continuously welded track (9). Some of the published theories and test results have been critically reviewed by Kerr (10). Most of the published theories were developed for the lateral track-stability problem. Several important ones are reviewed here. Prud'homme and Janin (11, 12) assumed a beam that had continuous lateral elastic support from the ballast and continuous rotational resistance from the rail fasteners and formulated a set of differential equations. By using a semiempirical method, Bartlett (7) obtained a similar solution. Bijl (13) and Amans and Sauvage (14) formulated the differential equations for nonlinear rail-fastener and ballast characteristics. Using the finite-difference method, Bijl (15) assumed the rail to be a beam with axial loading and discrete elastic supports and the ballast and rail-fastener behavior to be nonlinear, and formulated the equations of equilibrium. Kerr (16) derived the equilibrium equations for a buckling model by using the principle of stationary total potential energy. Three different assumptions were used for the lateral resistance: constant, linear, and a combination of constant and linearly varying resistance. The results indicated that the simplifying assumption of constant lateral ballast resistance was more suitable for use in the analysis of lateral track buckling. Furthermore, by assuming constant lateral ballast resistance, negligibly small longitudinal ballast resistance in the buckled zone, constant longitudinal ballast resistance in the adjoining regions, and negligible fastener rotational resistance, Kerr (17) derived the equilibrium equations for a track beam representing the rail-tie structure by the principle of virtual displacement. The solutions for four buckled configurations were presented. By using the energy method, Numata (18) formulated the strain energy in the ballast and in the bending of the rails and the potential energy of the external loads, assuming constant lateral ballast resistance and certain buckling wave patterns for both curved and straight tracks.

The lateral track-stability problem is more complicated on curved tracks than on straight tracks. The radial displacement of the curved track will decrease the compressive force in the rails and influence the buckling load or temperature. Calculations with regard to this effect have been published by Numata (18), Engel (19), and Nemesdy (20); all indicated that, for track curvature up to about 3.5°, this phenomenon might be neglected.

None of the models reviewed above possess all the following capabilities: simulations of discrete tie supports, track curvatures, track irregularities such as misalignments and ineffective ties or rail fasteners, nonlinear ballast resistance, nonlinear fastener rotational resistance, lateral wheel loads, and geometrically nonlinear track deflections. The finite-element model presented here has the advantage of possessing all of them.

FORMULATION OF MODEL

The finite-element model uses a general-purpose computer program for the linear analysis of elastic frames (21). The program is modified by using the incremental approach for geometrically nonlinear deflection theory (22). Thus, the modified program can be used to determine large buckling deflections of rails and the corresponding buckling loads.

Figure 1 shows the general formulation of the model. The track structure is represented by a finite number of beam elements. The track curvature is simulated by piecewise linear approximation. The ties are assumed to be rigid and fixed by the ballast against any rotation so that both rails will have exactly the same response in the lateral plane. Hence, the two rails are combined into one for simplification. The ends of the track are assumed to be fixed; however, a parameter investigation of the length of the track will determine how the track model approximates the real track in the field. The lateral ballast resistance and the fastener rotational resistance are simulated respectively by the axial and flexural stiffnesses of the radial elements. The longitudinal ballast resistance is simulated by the axial stiffnesses of the elements that are tangent to the rail elements but shown as on one side of the rail elements for clarity. The simulation of thermal and wheel loads can be achieved by the input of fixed-end compressive forces in the rail elements and concentrated quasi-static loads respectively. Piecewise linear approximation is used to simulate track misalignments, nonlinear rail-fastener behavior, and nonlinear ballast resistance.

The definition of buckling load or temperature used here is based on the curve of the relationship between the thermal load or temperature increase and the maximum track deflection (see Figure 2). When a slight increase in thermal load or temperature increases the maximum track deflection appreciably, buckling is said to occur in a sudden manner and the buckling load or temperature increase (P) is defined as a single value. The slope of the load-deflection curve is smallest in the buckling region (see Figure 2a). However, this region is not always distinct. The variation in the slope of the curve may be gradual over a range of load levels (see Figure 2b). The buckling load can then be specified only as a range of values, and buckling is said to occur in a gradual manner. The change in the slope of the curve may be so gradual that the buckling load becomes undefined. In such a case, the track deflection is more meaningful than the buckling load, and the curve is used to predict track deflection rather than buckling load or temperature.

It should be noted that other criteria have been used [such as the definition of a safe buckling temperature formulated by Kerr (4) and discussed by So and Martin (2)]. Moreover, it should be emphasized that the load-deflection curve shown in Figure 2 is based on the thermal load or temperature increase and not on the equilibrium thermal load or equilibrium axial compressive force in the rails. As shown by Kerr and also as obtained by the finite-element model here, the equilibrium thermal load (or equilibrium axial compressive force) decreases in the buckled parts of the rails when buckling occurs; therefore a plot of this against the track deflection would not be similar to Figure 2.

Figure 1. Finite-element model of buckling of curved track.

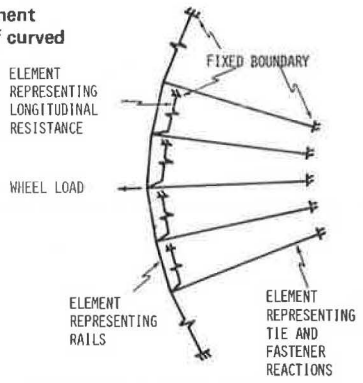

Figure 2. Definition of buckling load or temperature (P).

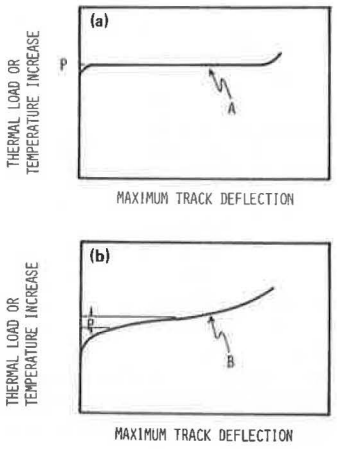

Figure 3. Longitudinal ballast resistance.

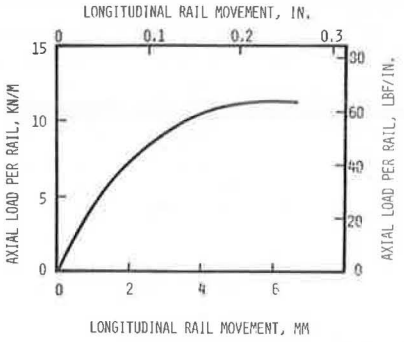

PARAMETER INVESTIGATION

The main parameters that affect the lateral thermal-buckling load of a curved track are investigated here by using the finite-element model. These parameters are track length (L), degree of track curvature (D), initial misalignment (M), ineffective ties, and lateral ballast resistance (R). In this limited investigation, the rail is assumed to be 67.5-kg/m (136-lb/yd) RE specification. The center-to-center spacing between the ties is taken as 0.508 m (20.0 in). An initial misalignment of sinusoidal shape, 12.2 m (40.0 ft) in length, is assumed to exist in the middle of each model track. The longitudinal ballast resistance, the fastener rotational resistance, and the lateral ballast resistance are shown in Figure 3 [test data taken from American Railway Engineering Association (23)], Figure 4 [test data taken from British Railways (7)], and Figure 5 [test data for curve A taken from French National Railways (12) and test data for curve B taken from British Railways (7)] respectively.

Figure 4. Fastener rotational resistance.

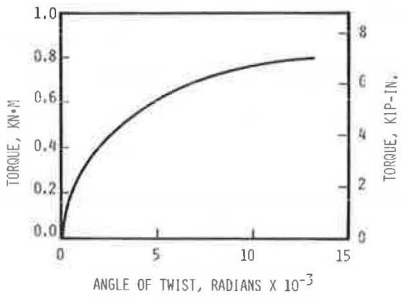

Figure 5. Lateral ballast resistance.

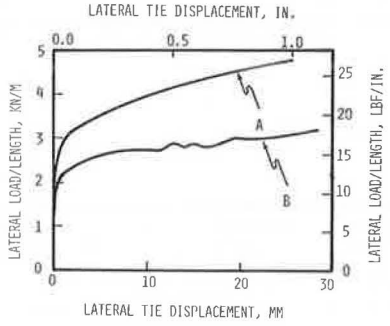

Because of symmetry, it is necessary to represent only half of the length of the track by the finite-element model. Figure 6 shows the model configuration of the reference track (no. 1 in Table 1)—a 61-m (200-ft) track that has 2° curvature and 12.7-mm (0.5-in) misalignment at its center. As described above, the track is assumed to be fixed at two ends and the two rails are combined into one and simulated by elements 32 to 47. Each of these elements has a sectional area and a moment of inertia equal to twice those of a single rail. The lateral ballast resistance and the fastener rotational resistance are simulated respectively by the axial and flexural stiffnesses of elements 1 to 16. The longitudinal ballast resistance is simulated by the axial stiffnesses of elements 17 to 31. By symmetry, the center point of the track can move only in the lateral direction. The thermal load, input as fixed-end compressive forces in the rail elements 32 to 47, is started at 89 kN (20 000 lbf) and increased by increments of 89 kN until buckling occurs.

To convert the fixed-end compressive force into a temperature increase in the rails, the following formula is used:

$$T = F/EA\alpha \qquad (1)$$

where

T = temperature increase,
F = fixed-end compressive force,
E = Young's modulus of the rail steel [20.7 GPa (30 000 000 lbf/in^2)],
A = total cross-sectional area of two rails [172.3 cm^2 (26.7 in^2)], and
α = coefficient of rail-steel expansion [1.1×10^{-5}/°C (0.61×10^{-5}/°F)].

To simulate track structures that have parameters different from those of the reference track, other model configurations were constructed in a similar way. The model simulations and the lateral thermal-buckling loads are summarized in Table 1. The following conclusions are based on this limited investigation.

Figure 6. Finite-element model of reference track.

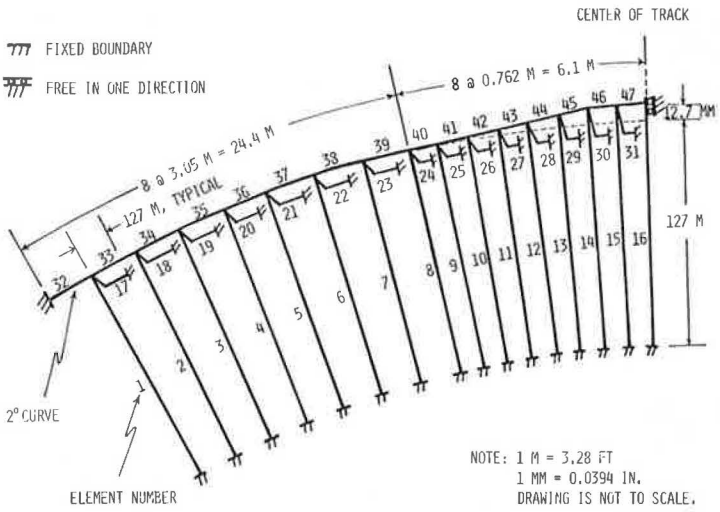

Table 1. Parameter investigation of lateral buckling of curved tracks.

Track No.	Parameter L (m)	M (mm)	D (°)	R	P Load (kN)	Temperature Increase (°C)
1[a]	61	12.7	2.0	Curve 5A	1920	49
2	122	12.7	2.0	Curve 5A	1930	49
3	244	12.7	2.0	Curve 5A	1970	50
4	61	12.7	0.0	Curve 5A	2820	72
5	61	12.7	0.5	Curve 5A	2440	62
6	61	12.7	1.0	Curve 5A	2230	57
7	61	12.7	1.5	Curve 5A	2080	53
8	61	12.7	2.5	Curve 5A	1760-1810	45-46
9	61	12.7	3.0	Curve 5A	1660-1780	42-45
10	61	12.7	3.5	Curve 5A	1570-1730	40-44
11	61	12.7	4.0	Curve 5A	1480-1680	38-43
12	61	12.7	5.0	Curve 5A	None	None
13	61	12.7	7.0	Curve 5A	None	None
14	61	12.7	10.0	Curve 5A	None	None
15	61	38.1	0.0	Curve 5A	1470-1680	38-43
16	61	38.1	1.0	Curve 5A	1390-1600	35-41
17	61	38.1	2.0	Curve 5A	1310-1550	33-40
18	61	38.1	3.0	Curve 5A	1240-1500	32-38
19	61	38.1	4.0	Curve 5A	1160-1450	30-37
20[b]	61	12.7	2.0	Curve 5A	1830	47
21[c]	61	12.7	2.0	Curve 5A	1640	42
22	61	12.7	0.0	Curve 5B	2420	62
23	61	12.7	1.0	Curve 5B	1880	48
24	61	12.7	2.0	Curve 5B	1570	40
25	61	12.7	3.0	Curve 5B	1340-1420	34-36
26	61	12.7	4.0	Curve 5B	1180-1340	30-34

Note: 1 m = 3.28 ft, 1 kN = 225 lbf, and temperature difference in °C = 1.8 x temperature difference in °F.

[a] Reference track.
[b] Simulation of track that has one ineffective tie at center.
[c] Simulation of track that has three consecutive ineffective ties at center.

Figure 7. Relationship between thermal-buckling load and track curvature.

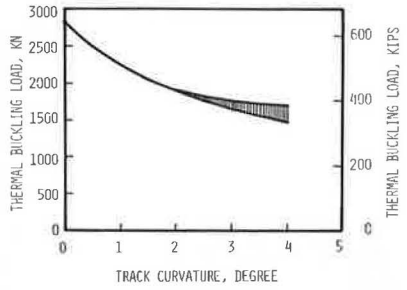

Figure 8. Relationship between thermal load and displacement: 0 to 2° model tracks.

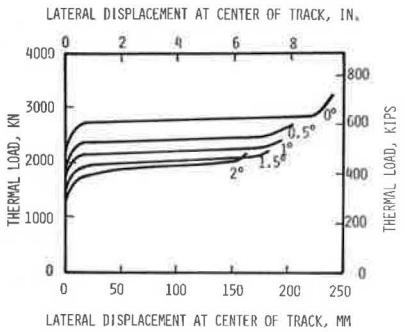

1. Track length: Track lengths of 61, 122, and 244 m (200, 400, and 800 ft) were investigated (nos. 1, 2, and 3 in Table 1). The buckling loads found for these tracks were 1.92, 1.93, and 1.97 MN (432 000, 434 000, and 443 000 lbf) respectively. There is only a negligible effect, an increase of about 0.5 percent, on the buckling load when the length of a 2° curved track is varied from 61 to 122 m. Again, only a 2 percent increase results when the length is increased from 122 to 244 m. This indicates that the 61-m track length can be considered a good approximation to the real track length in the field as far as the buckling load is concerned. Hence, as an approximation, a track length of 61 m was used for the remainder of the parameter investigation.

2. Track curvature: Simulations no. 1 and nos. 4 to 14 in Table 1 represent a set of model tracks that have curvatures that vary from 0 (a straight track) to 10°. Figure 7 shows the effect of track curvature on the buckling load for this set of model tracks. The reduction in the buckling load when the curvature is increased from 0 to 4° is about 44 percent.

For each of the tracks that have curvatures of 0 to 2°, there is a distinct decrease in the slope of the load-deflection curve at a particular load level (see Figure 8). According to the criterion for the buckling load discussed above, that load level is the buckling load of the track. As the track curvature increases from 2.5 to 4° (see Figure 9), the change in the slope of the load-deflection curve becomes more and more gradual and the buckling load of each track can be specified only as a range of load levels. For each of the curved tracks sharper than 4° (see Figure 10), there is hardly any significant change in the slope of the load-deflection curve. This no longer meets the criterion of the buckling load. Hence, the buckling loads of the tracks sharper than 4° are undefined and the track deflections are more meaningful than the buckling loads.

Attention should also be drawn to another important effect related to the track curvature, namely, the radial

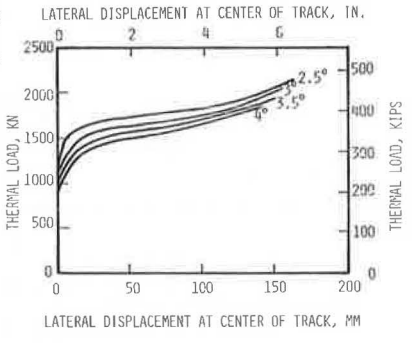

Figure 9. Relationship between thermal load and displacement: 2.5 to 4° model tracks.

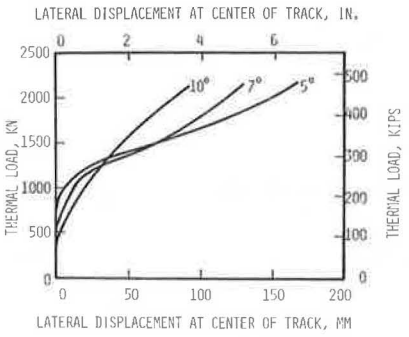

Figure 10. Relationship between thermal load and displacement: 5, 7, and 10° model tracks.

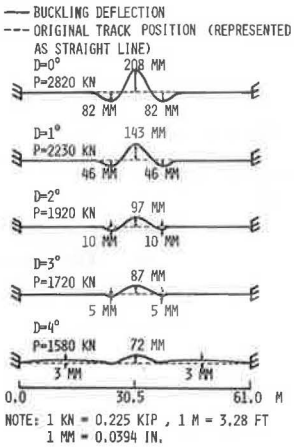

Figure 11. Buckling deflections: 0 to 4° model tracks.

displacement of the track as a whole. The wave patterns and the amplitudes of the postbuckling deflections of the tracks that have curvatures between 0 to 4° (nos. 4, 6, 1, 9, and 11 in Table 1) vary as shown in Figure 11. As the track curvature becomes sharper, the amplitudes of the buckling waves diminish and the track has a tendency to deflect radially. As shown in Figure 11, the postbuckling deflections of the 4° curved track have some radial displacements and, when the curvature is greater than 4° (nos. 12 to 14 in Table 1), the radial displacements increase rapidly (see Figure 12). Consequently, the track deflections are no longer confined to the local phenomenon of buckling. Instead, the whole track is displaced radially.

3. Track misalignment: The results of two sets of simulations of model tracks that had different misalignments and 0 to 4° curvatures (simulations no. 1 and nos. 4 to 11 and nos. 15 to 19 in Table 1) are shown in Figure 13. The buckling loads for the tracks that had the larger misalignment are about 17 to 44 percent lower. The effect is more significant for curvatures of less than 2°.

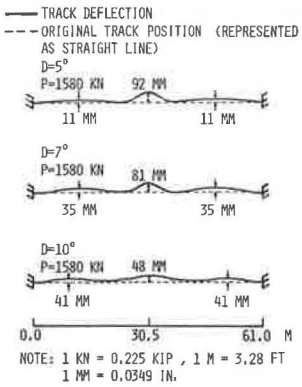

Figure 12. Deflections: 5, 7, and 10° model tracks.

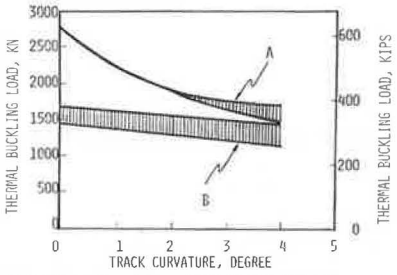

Note: Curve A—misalignment = 12.7 cm (0.5 in); curve B—misalignment = 38.1 cm (1.5 in).

Figure 13. Relationship between thermal-buckling load and track curvature at different track misalignments.

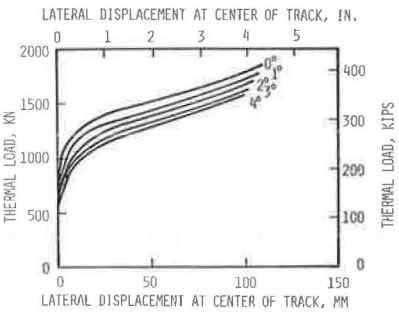

Figure 14. Relationship between thermal load and displacement: 0 to 4° model tracks that have 38.1-mm (1.5-in) misalignments.

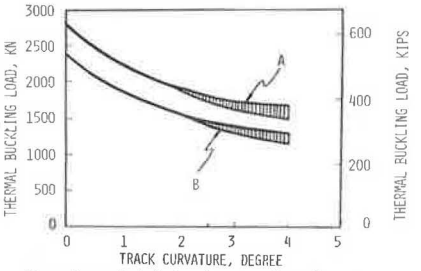

Note: Curve A—ballast resistance as shown in curve A of Figure 5; curve B—ballast resistance as shown in curve B of Figure 5.

Figure 15. Relationship between thermal-buckling load and track curvature for tracks that have different lateral ballast resistances.

Note that the buckling loads of the tracks that had 38.1-mm (1.5-in) misalignments are all specified as ranges of values. This indicates that buckling usually occurs in a gradual manner for those tracks that have relatively large misalignments (see Figure 14).

4. Ineffective ties: Two cases (nos. 20 and 21 in Table 1) that simulated respectively one and three totally ineffective ties located at the center of the track were investigated. When compared with the reference track (no. 1 in Table 1), the reductions of buckling loads were 5 and 15 percent for the tracks with one and three ineffective ties respectively.

5. Lateral ballast resistance: Two sets of model tracks that had different lateral ballast resistances (see Figure 5) and 0 to 4° curvatures were investigated (simulations no. 1 and nos. 4 to 11 and nos. 22 to 26). The results are shown in Figure 15, which indicates that, for the tracks that had the lower lateral ballast resistance, the buckling loads were about 14 to 20 percent lower. The effects are about the same for track curvatures from 0 to 4°.

CONCLUSION

This study has indicated that the finite-element model is an efficient and powerful method for the calculation of the thermal-buckling strength and the corresponding deflection of continuously welded curved tracks. The model uses general-purpose computer programs for structural analyses and incorporates all the main parameters that govern the lateral stability of track. The results of a parameter investigation indicated that the buckling temperature and lateral displacement of a curved track are significantly affected by changes in lateral ballast resistance, misalignment, and curvature and by the presence of ineffective ties. The model appears to be a promising new approach to the track-buckling problem; however, test data are required to validate the model.

ACKNOWLEDGMENT

This research was sponsored by the Research and Test Department of the Association of American Railroads. We wish to thank James R. Lundgren and Allan M. Zarembski at the association for reviewing the manuscript and making valuable suggestions.

REFERENCES

1. C. F. Rose. Railway Accidents. Her Majesty's Stationery Office, London, 1970.
2. W. So and G. C. Martin. Finite-Element Track Buckling Model. ASME, paper presented at IEEE-ASME 20th Joint Railroad Conference, Washington, DC, March 30-April 1, 1977, paper 77-RT-5.
3. J. W. Klaren and J. C. Loach. Lateral Stability of Rails, Especially of Long Welded Rails. Office for Research and Experiments of International Union of Railways, Utrecht, Netherlands, Question D14, Interim Rept. 1, April 1965.
4. A. D. Kerr. A Model Study for Vertical Track Buckling. Federal Railroad Administration, Rept. DOT-FRA-OHSGT, Oct. 1971.
5. F. Birmann and F. Raab. To the Development of Continuously Welded Track: Test Results of the Karlsruhe Test Facility, Their Analysis and Interpretation [in German]. Eisenbahntechnische Rundschau, Aug. 1960.
6. E. M. Bromberg. The Stability of the Jointless Track [in Russian]. Izdatelstvo Transport, 1966.
7. D. L. Bartlett. Experiments on the Stability of Long-Welded Rails. British Transport Commission, London, 1961.
8. Japanese National Railways. The Test on Buckling of Curved Tracks. Permanent Way, Permanent Way Society of Japan, Tokyo, Nov. 1958.
9. A. D. Kerr. A Bibliography on the Determination of Stresses in Rails and Ties and Thermal Track Buckling. U.S. Department of Transportation, Transportation Systems Center, Cambridge, MA, Technical Rept., Feb. 1976.
10. A. D. Kerr. The Lateral Buckling of Railroad Tracks Due to Constrained Thermal Expansions. Paper presented at Symposium on Railroad Track Mechanics, Princeton Univ., NJ, 1975.
11. M. A. Prud'homme. The Resistance of the Permanent Way to the Transversal Stresses Exerted by the Rolling Stock. Monthly Bulletin of International Railway Congress Association, Vol. 44, No. 11, Nov. 1967, pp. 731-766.
12. M. A. Prud'homme and M. G. Janin. The Stability of Tracks Laid With Long-Welded Rails. Monthly Bulletin of International Railway Congress Association, Vol. 46, No. 7-8, July-Aug. 1969, pp. 459-487.
13. F. Bijl. The Horizontal Buckling of Long Welded Tracks. Office for Research and Experiments of International Union of Railways, Utrecht, Netherlands, DT5, Document 2, 1958.
14. F. Amans and R. Sauvage. Railway Track Stability in Relation to Transverse Stresses Exerted by Rolling Stock. Monthly Bulletin of International Railway Congress Association, Vol. 46, No. 11, Nov. 1969, pp. 684-716.
15. F. Bijl. Determination of the Snaking Effort in Track Laid With Long-Welded Rails by Means of a Nonlinear Calculation. Monthly Bulletin of International Railway Congress Association, Vol. 42, No. 8, Aug. 1965, pp. 580-588.
16. A. D. Kerr. The Effect of Lateral Resistance on Track Buckling Analysis. Rail International, Jan. 1976.
17. A. D. Kerr. Analysis of Thermal Track Buckling in the Lateral Plane. Princeton Univ., NJ, Rept. 76-TR-6; Federal Railroad Administration, Rept. DOT-TSC-FRA-76-17, Feb. 1976.
18. M. Numata. Buckling Strength of Continuous Welded Rail. Monthly Bulletin of International Railway Congress Association, Vol. 37, No. 1, Jan. 1960, pp. 33-49.
19. E. Engel. The Stability of Jointless Tracks [in German]. Zeitschrift des Vereine Deutscher Ingenieure, Vol. 102, 1960.
20. E. Nemesdy. Analysis of Horizontal Track Buckling in Accordance With the New Hungarian Tests [in German]. Eisenbahntechnische Rundschau, Vol. 12, 1960.
21. F. Beaufait and others. Computer Methods of Structural Analysis. Prentice-Hall, New York, 1970.
22. O. C. Zienkiewicz. Nonlinear Problems: Plasticity, Creep, and Large Deformations. In The Finite-Element Method, McGraw-Hill, London, Revised 1st Ed., 1968, pp. 192-211.
23. J. P. Hiltz and others. Field Measurement of Forces Resulting From Rail Anchorage. Proc., 54th Annual Convention of American Railway Engineering Association, Palmer House, Chicago, Vol. 56, March 1955, pp. 283-322.

Statistical Description of Service Loads for Concrete Crosstie Track

Robert H. Prause, Applied Dynamics and Acoustics Section, Battelle Columbus Laboratories, Columbus, Ohio
Andrew Kish, Transportation Systems Center, Cambridge, Massachusetts

Measurements of loads and bending moments on concrete crossties for several days of revenue traffic were used to develop a statistical description of track loads for tangent and curved tracks that have variable tie spacing. The measured data show large tie-to-tie variations in loads and a load-dependent tie support condition. Many ties were center-bound for loads from light or empty cars, but the tie support became more uniform for heavy wheel loads. Maximum tie bending moments measured on curved track were considerably higher than those on tangent track because of the increase in vertical and lateral loads on the high rail when trains exceed the balance speed of the curve. Tie bending moments measured in this program were considerably lower than the current static flexural strength requirements for a probabilistic prediction of maximum load for a 50-year life. These and data from other concrete-tie test installations indicate a need to identify the failure mechanism for concrete ties so that statistical load descriptions can be used for future design and testing. Low-probability maximum loads will be very important if failures result from infrequent loads that exceed the static strength. However, the higher probability mean cyclic loads will be the more important factor if fatigue is identified as the governing failure mechanism.

There is currently considerable interest in the development of concrete crossties for main-line use in North America. Experience in several other countries has indicated that these ties have the potential advantages of longer tie life, reduced lining and surfacing maintenance, and increased rail life on curves. However, the premature cracking of concrete ties at several U.S. test installations during the past decade has prevented these ties from becoming a workable alternative to wooden ties.

Much of the difficulty in obtaining acceptable performance from concrete ties results from a lack of knowledge about tie loading and the effective support provided by the ballast. Tie center binding and end binding are familiar conditions for wooden-tie track, but the inherent resilience of wood minimizes the damage that results from these undesirable loading conditions. Concrete, however, is a very brittle material that is, therefore, less forgiving when stressed beyond its design limits.

The development of concrete ties in the United States has followed the development of the American Railway Engineering Association (AREA) specifications (1). Those specifications have evolved through several modifications in which tie-strength requirements have been gradually increased because of premature tie cracking. Specifications for the minimum bending strength at the rail seat and tie center and the corresponding static acceptance tests are the major considerations. The lack of sufficient field-test data to provide accurate descriptions of tie service loads that reflect realistic variations in support and loading conditions has been a major deterrent to the development of these specifications. This paper presents some statistical data on service loads for concrete ties and rail-fastener assemblies for typical main-line revenue railroad traffic.

TEST-SITE DESCRIPTION

The test sites selected for this extensive measurement program were on the Florida East Coast Railway (FEC) about 32 km (20 miles) north of West Palm Beach. This track was selected from among the several available sites (such as the Kansas test track; the Atchison, Topeka, and Santa Fe Railway test track at Streator, Illinois; the Chessie System test track at Lorraine, Virginia; or the Norfolk and Western Railway test track at Roanoke, Virginia), because it provided the best combination of track variables required for this program. These included tangent and curved tracks, tie spacings of 0.51 and 0.56 m (20 and 22 in) for comparison with the 0.61-m (24-in) standard spacing, and mixed freight loadings that included 90.7-Mg (100-ton) cars and speeds up to 96.5 km/h (60 mph). Two sections of tangent track that had 0.51- and 0.61-m tie spacings were instrumented to evaluate the effect of tie spacing, a major track design variable. A third test site that had 0.61-m tie spacing on a 3° 52′ curve and a 72.4-km/h (45-mph) balance speed was selected for a comparison of loads on tangent and curved tracks. Track construction consisted of 60-kg (132-lb) rail, Railroad Concrete Crosstie Corporation (RCCC) ties with Cliploc fasteners and polyethylene rail pads, and granite ballast. The RCCC tie, a modification of the original MR-2 design, is somewhat smaller than the ties designed according to the most recent AREA specifications, but this was not detrimental to the objective of measuring tie and fastener loads. Also, the fact that the temperate Florida climate is not a typical North American environment was not considered critical for obtaining load data over a short time period.

The tangent-track sites had been in service for about 1 year and the curve site had been in service about 6 years when the measurements were begun during July 1976. However, the curve had been surfaced and lined at the same time that the tangent track was constructed, and measurements from the U.S. Department of Transportation track-geometry car showed that track geometry was excellent throughout. This track was located on old roadbed that had been scraped to provide an even surface and to remove the old limestone ballast. Excavations at each of the tangent-track test sites showed a ballast depth of about 16.5 cm (6.5 in) under the tie and a clear demarcation between the new granite ballast and the old roadbed. It was apparent that the old roadbed (subgrade) was actually a well-compacted mixture of sandy soil and old limestone ballast, which provided a very stable and relatively stiff foundation.

TRACK INSTRUMENTATION

The selection of the measurement parameters, instrumentation, and data requirements for meeting the objectives of this program are discussed elsewhere (2). As shown in Figure 1, the instrumentation at the test sites was extensive. As many as 72 different measurements were recorded for a few trains at each site. About 30 measurements were recorded continuously for several days of traffic. The major types of instrumentation used are described below:

Figure 1. Typical track instrumentation.

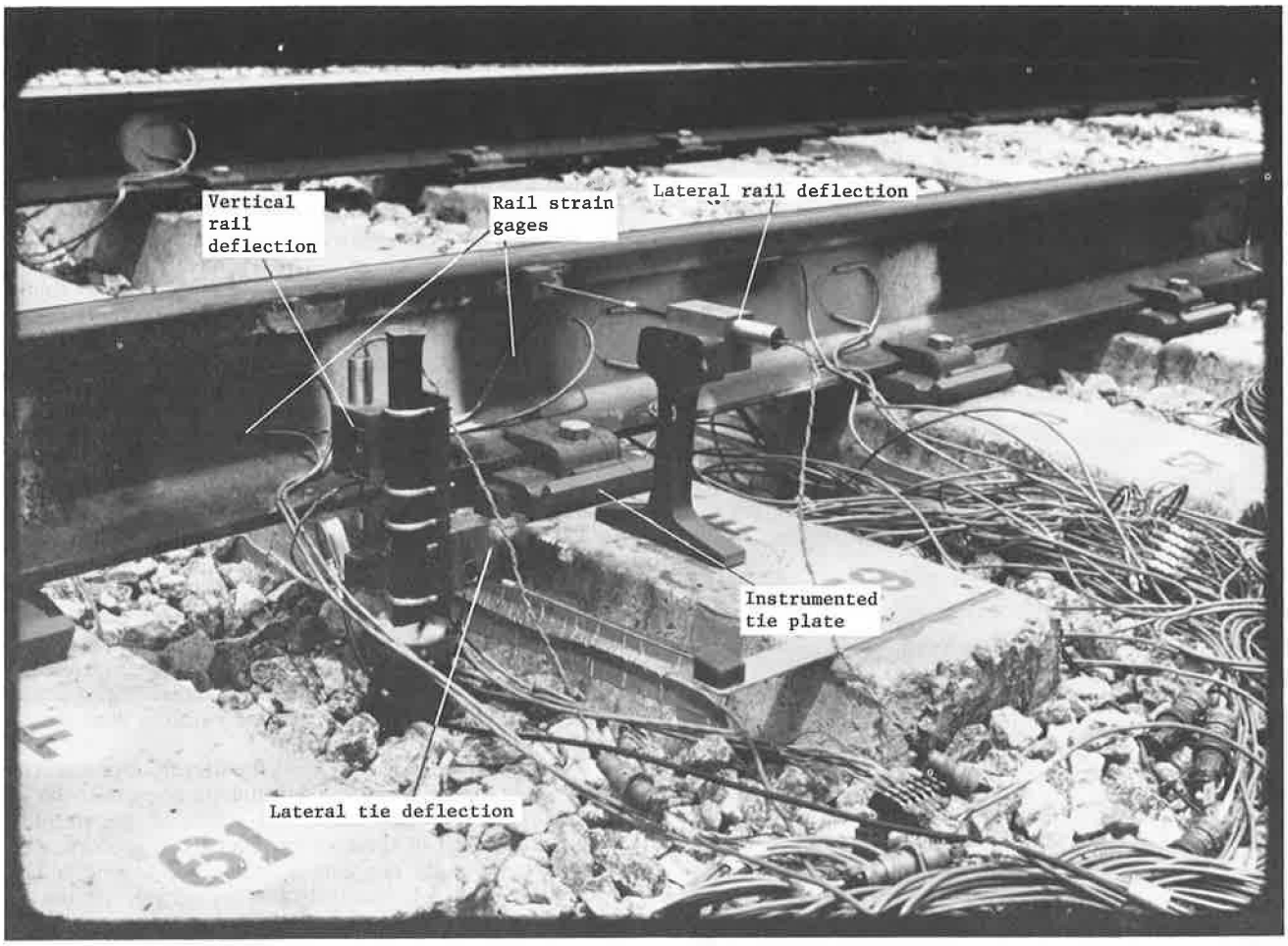

1. Strain gauge circuits applied to the rail web were used to measure the maximum (peak) vertical and lateral rail load for each passing axle. The signals from these circuits were also used to determine train speeds and approximate car loads. The vertical-load circuits were calibrated by using empty and loaded cars. A hydraulic ram placed between the two rails was used to calibrate the lateral load circuits.
2. Special-design instrumented tie plates were installed between the rail and the tie to measure the vertical rail-seat loads and the rail-seat rollover moments on five adjacent ties in each section. The load-cell washers in the tie plates were calibrated by using a laboratory loading fixture.
3. Strain gauge circuits were installed on several ties to measure the bending moments at the rail seat and the bending and torsional moments at the tie center. A full bridge with four active gauges was used for each measurement. Bridge output was calibrated directly in moment by using equivalent concrete ties in the laboratory.
4. Three FRA-Portland Cement Association (PCA) load-cell ties (see Figure 2) were installed to measure tie-support reactions at the interface of the tie and the ballast. The load-cell ties are steel and have a bending stiffness similar to that of concrete ties; they have 10 instrumented segments along the tie bottom to measure tie-to-ballast pressure.
5. Displacement transducers were used to measure the vertical track deflections and the lateral deflections of the rail head relative to the tie.
6. Instrumented load washers were used to record load variations on rail-fastener bolts.
7. Movable accelerometers were used to measure rail and tie vertical accelerations at several locations.

All three of the test sites included a main instrument array that extended over seven adjacent ties so that a complete set of load and response data could be obtained at one location. Additional instrumentation was located at random in a 15.2-m (50-ft) zone on either side of the main array and used to record load variations caused by dynamic motions of the cars as they passed the test site. The instrumented tie plates, which required lowering the ties in the main array about 2.54 cm (1 in), and the load-cell ties were all installed in the track 1 month before the measurement program was started to allow reconsolidation of the ballast under traffic.

STATISTICAL DATA ANALYSIS

Time-history records of track loads were recorded on frequency modulation tape for all trains passing during several days of revenue service. A special-purpose computer program was used to digitize these data and store a single peak value of load for each wheel (axle) that passed a particular measurement location. An identification for car load and car speed was used to separate the data into 16-km/h (10-mph) speed bands and into three car load categories before the data were stored on a disk file for subsequent analysis. Car load

was determined from the vertical wheel-rail load circuits in the main array, and car speed was determined from the transit time for a wheel to pass over a premeasured track section.

The final step in the data processing was to perform the statistical calculations needed to obtain mean values, SDs, probability densities, and probability distributions for the peak-value data from each measurement. The data in each of the speed and load categories were analyzed separately for each measurement (channel), and summations could be made for any category. Data from selected categories at different measurement locations could also be combined to form new data sets.

Figure 2. Load-cell tie.

For example, data from the five wheel-rail load circuits at site one could be combined for heavy cars in the 80- to 97-km/h speed range to include spatial variation effects.

Statistical calculations were made by dividing the total expected data range into 200 equal intervals and summing the number of peak values (wheels) falling in each interval. Graphs of probability density (histograms) and probability distribution functions were then plotted by using an interactive graphics terminal and the identification numbers for single categories and combinations.

The format for the results of the statistical analysis is shown in Figure 3 for measurement of the peak vertical wheel-rail loads. These data are for all cars and all speeds (all trains) at one measurement location. The probability density histogram shows the ratio of the number of peak loads within each of the fifty 5.3-kN [1200-lbf (1,2-kip)] load intervals that cover the total range of 267 kN (60 000 lbf). It is important to note that the quantitative results for the histogram depend on the load interval selected and are therefore not unique. Increasing the load interval (reducing the number of intervals) increases the number of occurrences at a particular load level. This improves the averaging used for the estimate but reduces the resolution—a trade-off decision. Load intervals that are too small for the data base cause irregularities in the density curve at extreme loads because there are insufficient data points to provide a reliable average for these low-probability events.

The amplitude of the probability-distribution function shown in Figure 3 gives the percentage of peak loads that exceed a specified load level. This is calculated from the integral of the density function; therefore, the quantitative results are unique and do not depend on the load interval used to generate the histogram. In the probability-distribution function format, the vertical axis has been expanded to provide greater resolution of the extreme values. Insufficient data points to provide reliable estimates for low-probability events appear in the distribution function as horizontal segments in some of the later figures. This shows that there were no data points at that load level. The accuracy of the estimates at these points is questionable.

Statistical data that have a normal (Gaussian) distribution will appear as the familiar bell-shaped curve

Figure 3. Formats for results of statistical analyses: (a) probability-density histogram and (b) probability distribution function.

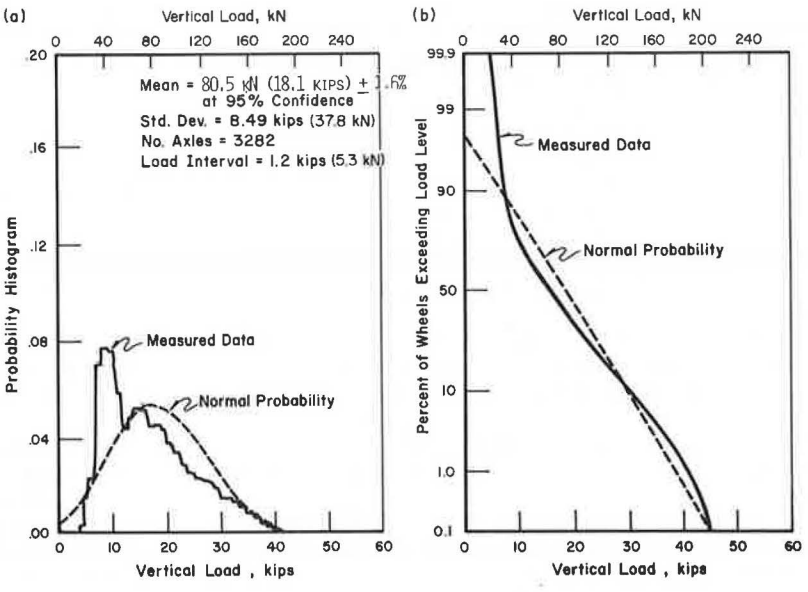

on the density plot and as a straight line on the scale used for the distribution curve. These curves are shown in Figure 3 for comparison. The 50 percent probability level gives the median load (50 percent higher and 50 percent lower) for any distribution. If the experimental data had had a perfectly normal distribution, then the median peak load would have been identical to the mean peak load [which is 80.5 kN (18 000 lbf) in this example]. The theoretical curves for the normal distribution shown in the figure have the same mean value and SD as the measured data. For this particular measurement, the normal curve gives a better estimate of the data at low probability levels than it does in the vicinity of the mean load because of the distortion caused by large numbers of empty cars. Other distributions such as a beta or a log-normal distribution may give a better estimate of extreme-value statistics, but these were not investigated.

The following sections of this paper summarize some of the more interesting results derived from statistical data on tie loads and show the effects of tie-to-tie spatial variations and of variations from the mix of vehicle types and operating conditions. For reference purposes, the vertical rail-seat loads and tie bending-moment requirements of the current AREA specifications are listed below (1 m = 3.3 ft, 1 kN = 225 lbf, and 1 kN·m = 8852 lbf·in).

	Vertical Rail-Seat Load		Bending-Moment Requirement (kN·m)			
Tie Spacing (m)	Percentage of Wheel Load	Value (kN)	Rail Seat (+)	Rail Seat (-)	Tie Center (-)	Tie Center (+)
0.533	46.5	214.5	25.4	13.0	22.5	10.1
0.61	51	234.1	28.4	13.0	22.5	10.1
0.69	55.5	254.1	31.0	13.0	22.5	11.3
0.76	60	273.7	33.8	13.0	22.5	12.4

The RCCC concrete tie used on the FEC is designed to have a minimum flexural strength of 17.0 kN·m (150 000 lbf·in) at the rail seat, and one of every 200 ties is checked to this limit after curing for 18 h. Although some additional increase in strength will occur with time, this smaller tie cannot meet the 28.3 kN·m (250 000 lbf·in) positive moment currently required for 0.61-m tie spacing. More detailed data from the measurement program are given elsewhere (3).

Vertical Wheel-Rail Loads

Figure 4 shows typical statistical distributions for all five measurements of vertical wheel-rail load at one site. There was no significant spatial variation in load measurements at this site, and the data for the other sites were similar. The 0.1 percent exceedance load levels for the most severely loaded location at each site are given below.

Test Site	Tie Spacing (m)	Vertical Wheel-Rail Load (kN)	Tie-Rail-Seat Load (kN)	Bending Moment (kN·m)	
				Tie Rail Seat (+)	Tie Center (-)
Tangent	0.61	200	107	7.4	3.4
Tangent	0.51	205	93	8.7	6.3
Curve	0.61	222	138	8.8	4.7

The 0.1 percent load level is exceeded by only 1 of each 1000 axles but, the annual traffic of 2.4 Tg (20 million gross tons) averages about 4000 axles/d. Therefore, the 0.1 percent load level would be exceeded about 4 times/d for this traffic.

Vertical Rail-Seat Loads

The data shown in Figure 5 for vertical rail-seat loads on several adjacent ties show that there is considerable tie-to-tie variation, which reflects local variations in support conditions. This causes a larger percentage variation in the average load than it does in the less frequently occurring high loads where the ties are firmly seated in the roadbed. The 0.1 percent exceedance rail-seat load of 138 kN (31 000 lbf) at the curve site given above occurred under the higher rail (where vertical loads are higher than those on tangent track when trains operate consistently above the balance speed for the curve).

Tie-Rail-Seat Bending Moments

Figure 6 shows the statistical distributions of the rail-seat bending moments measured on several different ties at site 1. A characteristic of tie bending-moment data is the large tie-to-tie variation in the mean and 0.1 percent moments. Also, all ties except one showed both positive and negative peak bending moments (which indicates a load-dependent ballast support condition). Negative rail-seat bending moments can be caused by a center-bound condition. Positive moments are expected for a uniform support condition, an end-bound support condition, or one in which a ballast pocket may have formed under the rail seat.

Figure 7 shows a typical load-dependent effect by comparing the bending-moment data for a single tie; locomotives, light cars [less than 45.5-Mg (50-tons) gross mass], and heavy cars [more than 45.5-Mg (50-tons) gross mass] are identified separately. For this particular tie, the peak rail-seat bending moment was positive for all of the locomotives and heavy cars, but some negative values were recorded for light cars. It is also evident that, as a class, locomotives cause the highest mean loads but heavy freight cars cause loads that are as high or higher at the 0.1 percent probability level. Also, the presentation of the data as percentage of wheels can obscure an important point. Because there are 10 to 15 heavy cars for every locomotive in a typical train, track damage from high vertical loads will occur much more frequently from heavy cars than from locomotives. It also appears that the probability-distribution curves for heavy cars and locomotives cross near the 0.1 percent load level so that the loads from heavy cars will dominate the high-load, low-probability tail of the probability-distribution curve.

The maximum 0.1 percent rail-seat bending moments listed above are quite similar for all three measurement sites, but the highest loaded tie at the curve site has a higher SD than any of those measured at the other sites. Table 1 gives the low-probability statistics that would be predicted by using the measured mean and SD for the highest loaded tie at site 3 and assuming a normal probability distribution and the corresponding number of axles between occurrences; e.g., a bending moment of 9 kN·m (79 300 lbf·in) would be exceeded by 0.1 percent of the axles or 1 of every 1000 axles. The comparison between the bending moments predicted by using a normal distribution and the actual measured distribution of moments shows very good agreement over the limited range of this particular measurement, but other theoretical distributions might be more appropriate for extreme-value estimates.

For reference purposes, Table 1 also lists the estimated number of days between exceedances for different annual traffic densities. These data indicate that bending moments greater than about 13 kN·m (115 000 lbf·in) would not be expected during a 50-year

Figure 4. Statistics of wheel-rail loads: typical railroad traffic.

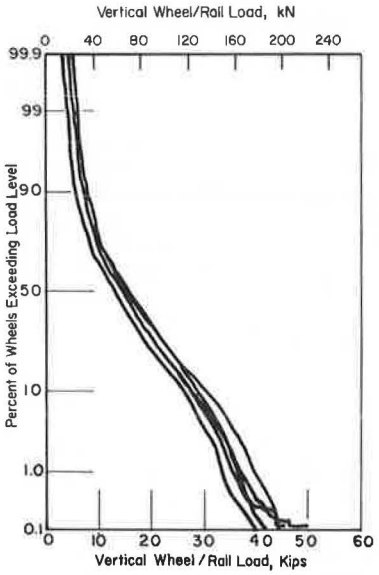

Figure 5. Statistics of rail-seat loads: typical railroad traffic.

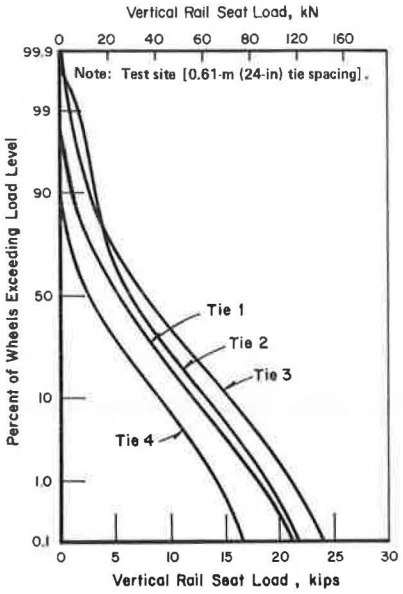

Figure 6. Peak tie-rail-seat bending-moments: all traffic at site 1.

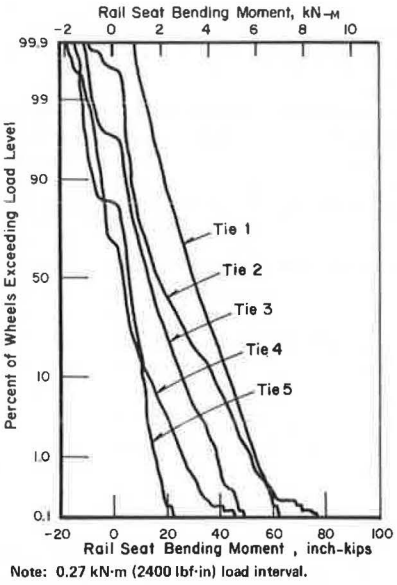

Note: 0.27 kN-m (2400 lbf-in) load interval.

Figure 7. Peak tie bending moments for different car sizes.

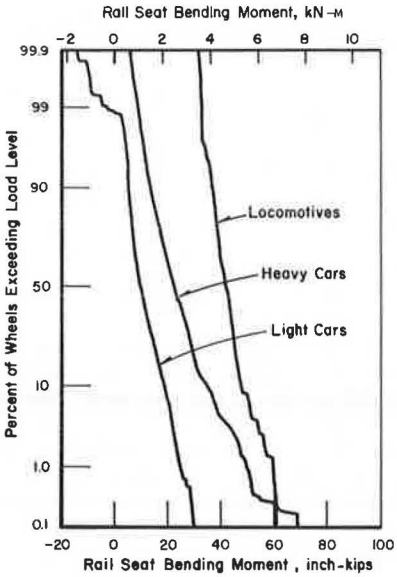

life at any normal traffic level, assuming that the predicted distribution is valid for this period of time. This is less than 50 percent of the 28-kN·m bending-moment requirement given in the current specifications. However, it should be cautioned that this extrapolation is based only on vehicle-load statistics for a specific, heavily loaded tie. The additional statistics for tie-to-tie variations have not been included. Also, the question of whether the normal distribution, or some other distribution, will give a conservative estimate of the very low probability high bending moments that might be caused by severe wheel-flat impacts cannot be answered completely without collecting data for a much longer time period. Experience at test installations where ties have failed, however, shows that a considerable number of ties crack within a few months after installation, which tends to dispute the hypothesis that cracking is due to very infrequent occurrences of high loads.

Tie-Center Bending Moment

The statistical data for the bending moments measured at the center of five different ties at each site showed considerable tie-to-tie variation. All ties except one had both positive and negative peak bending moments. Negative center bending moments represent a center-bound support condition and cause tension in the top surface of the tie. Bending cracks in the middle of concrete ties almost always start at the top surface; thus, negative bending moments have historically been of major importance. Positive bending moments at the tie center can be caused by an end-bound support condition. If the rail-seat loads were distributed symmetrically on a well-compacted support region under each rail seat, the bending moments in the tie center would be quite low.

The maximum bending moments at the tie center summarized above show a high value of 6.3 kN·m (56 000 lbf·in) at site two, and this was exceeded by a maximum positive moment (not listed) of 7.6 kN·m (67 000 lbf·in) on one tie at site three. These maximum moments at the tie center are only about 15 percent lower than the maximum positive moments in the rail-

Table 1. Extrapolated statistics for rail-seat bending moments based on most severe tie loading.

Percentage Level Exceeded	Rail-Seat Bending Moment (kN·m)		No. of Axles Between Exceedances	Estimated Time Between Exceedances (years)[a]		
	Predicted	Measured		2.4-Tg (20 million-ton) Load	4.8-Tg (40 million-ton) Load	7.2-Tg (60 million-ton) Load
50	4.3	4.2	2			
1.0	7.8	7.7	100			
0.1	8.9	8.8	1000	7.5×10^{-4}	3.7×10^{-4}	2.5×10^{-4}
0.01	9.4		10^4	7.5×10^{-3}	3.7×10^{-3}	2.5×10^{-3}
0.001	10.7		10^5	7.5×10^{-2}	3.7×10^{-2}	2.5×10^{-2}
10^{-4}	11.4		10^6	7.5×10^{-1}	3.7×10^{-1}	2.5×10^{-1}
10^{-5}	12.1		10^7	7.5	3.7	2.5
10^{-6}	12.7		10^8	75	37	25
10^{-7}	13.2		10^9	750	375	250

Notes: 1 kN·m = 8852 lbf·in.
Mean moment = 4.3 kN·m (38 400 lbf·in) and SD = 1.5 kN·m (13 200 lbf·in).
[a]Based on 3700 axles/d for 2.4-Tg annual traffic.

Figure 8. Load-dependent distribution of ballast pressure on bottom of load-cell tie.

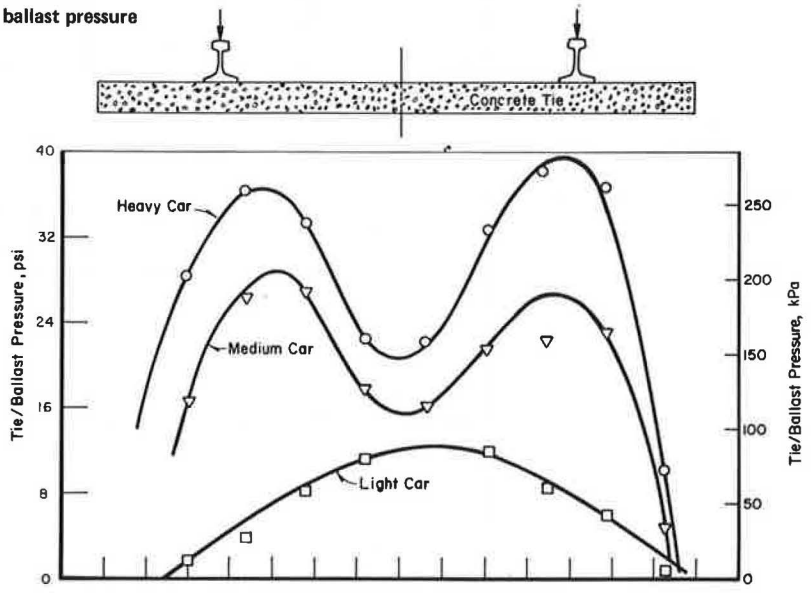

seat region. However, they are considerably lower than the 22.5 kN·m (200 000 lbf·in) negative and 10.2 to 12.4 kN·m (90 to 110 00 lbf·in) positive strength requirements in current specifications.

The data from the individual load categories show that the bending moment at the tie center is practically independent of car load for many ties. This indicates a nonlinear support condition in which the distribution of reaction loads along the tie length changes with load to maintain a relatively constant bending moment. For example, a center-bound tie that has voids under each end but is supported in the middle will develop negative bending at both the center and the rail seats with light loads. However, increased wheel loads will cause the tie to bear more fully on the ballast and shift the reaction load toward the tie end. This will produce positive bending at the rail seat and very little change in the bending moment at the tie center.

Tie-Ballast Pressure Distribution

The load-dependent support condition observed in the bending moments of several concrete ties was confirmed by load-cell-tie data. The graph of tie-ballast pressures along the tie length (Figure 8) shows a noticeably center-bound condition for light wheel loads [35.6 kN (8000 lbf)], whereby most of the tie load is supported by the middle of the tie. But for higher wheel loads [89 to 160 kN (20 000 to 36 000 lbf)] on the same tie, the peak pressures move toward the rail-seat region. This load-dependent behavior indicates that the high ballast pressures from heavy cars are causing voids in the rail seat region under the ties.

Recent results from repeated-load laboratory tests at the PCA and Queen's University in Canada have confirmed this load-dependent behavior for different size concrete ties. Reducing the variation in pressure distribution on the ballast and subgrade under ties may be a key factor in improving track performance. This is particularly important for track that has poor drainage or very moisture-sensitive subgrades. Under these conditions, depressions or ruts in the subgrade in the rail-seat region will retain moisture and the rate of track settlement will increase greatly. Changes in tie design, reduced tie spacing, and increased ballast depth are possible ways to reduce this mode of degradation.

Effect of Tie Spacing

The data given above for the maximum (0.1 percent exceedance) loads measured at each test site showed that, in most cases, the maximum tie loads and bending moments measured at site two, which has 0.51-m tie spacing, were not significantly lower than those measured at site one, which has 0.61-m spacing. Reducing the tie spacing from 0.61 to 0.51 m, a 16 percent reduction, is normally expected to reduce the ver-

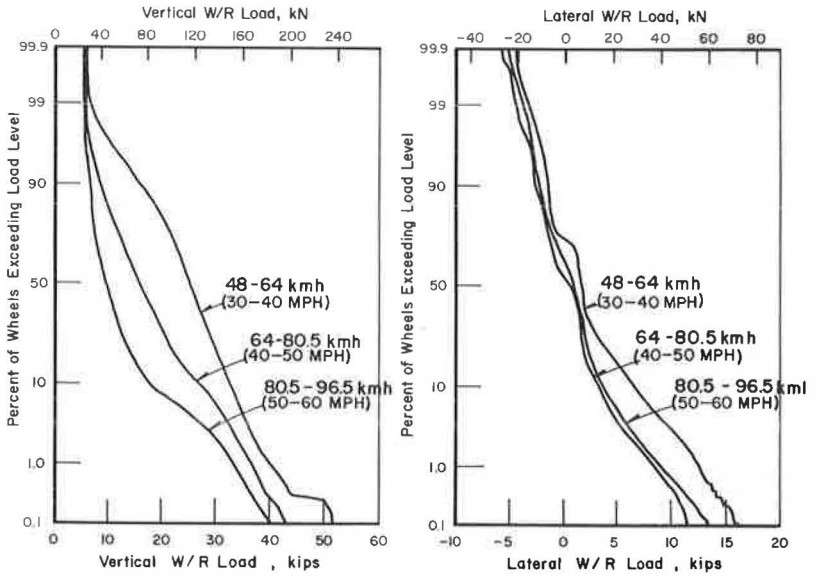

Figure 9. Effect of train speed on average vertical and lateral wheel-rail loads: all traffic at site 1.

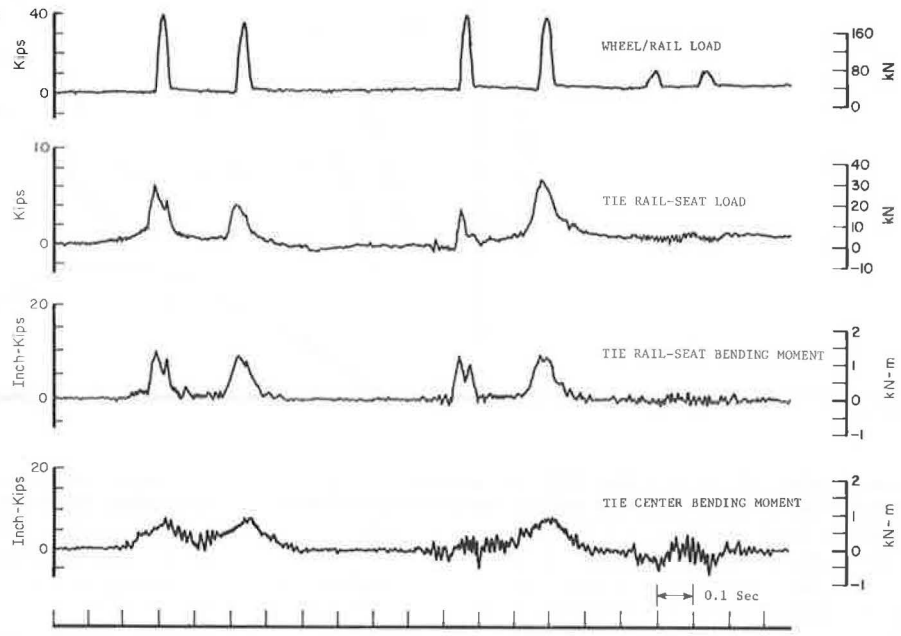

Figure 10. Time history of track loads for four-axle locomotive.

tical rail-seat loads and tie bending moments by about 16 percent. However, the large tie-to-tie variation in support conditions makes it difficult to compare results for different track designs by using single-tie measurements. It is more appropriate to average the data for identical measurements at several different locations to include these typical spatial variations.

The percentage changes in the average mean and 0.1 percent load levels caused by reducing the tie spacing from 0.61 to 0.51 m are given below.

Item	Change in Avg Mean			Change in Avg 0.1 Percent Load		
	All Cars	Locomotives	Heavy Cars	All Cars	Locomotives	Heavy Cars
Rail-seat vertical load	8.9	18.5	16.9	8.8	30.2	20.6
Tie-rail-seat bending moment	36.4	24.8	36.5	12.0	19.0	33.2

These data demonstrate the difficulties in reaching definitive conclusions by using track-response measurements. Reducing tie spacing by 16 percent reduces average and maximum vertical rail-seat loads by about 9 percent for all traffic. Average tie bending moments at the rail seat were reduced more than were rail-seat loads. This indicates a nonlinear support condition in which the reduced tie loading provides a substantially greater reduction in both average mean and average 0.1 percent bending moments; the maximum bending moments are reduced by 12 percent and the average mean is reduced by 36 percent for all traffic. It should be noted, however, that there is no difference in the maximum rail seat loads and tie bending moments for the most severely loaded tie at the different tie spacing locations although there should be fewer ties subjected to these maximum loads in the section that has 0.51-m spacing.

Many of the measured data indicate that nonlinear support conditions have a very significant effect on

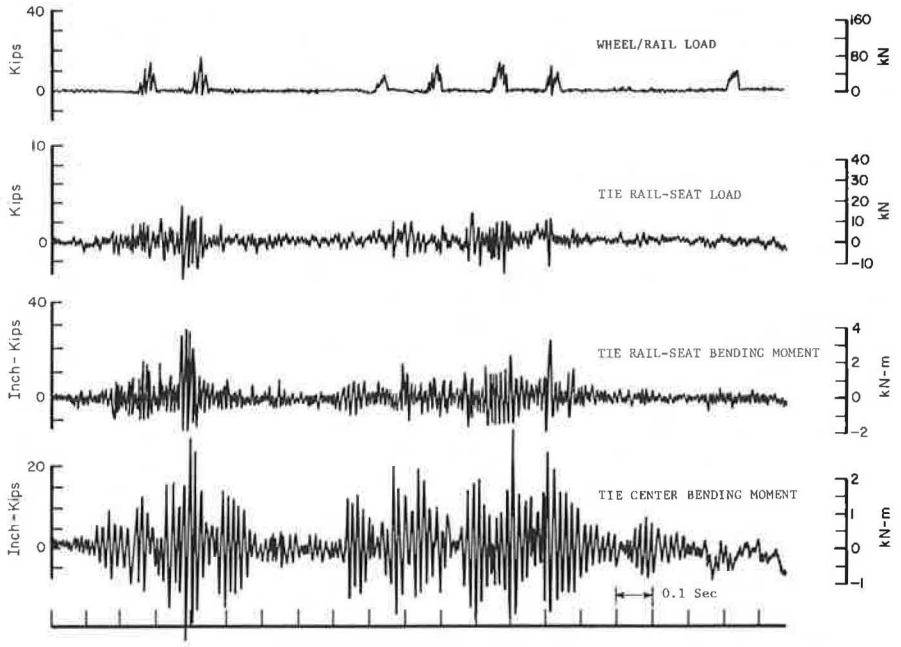

Figure 11. Time history of track loads for lightly loaded freight car that has wheel flats.

Table 2. Average track component loads: all traffic on track having 0.61-m (24-in) tie spacing.

Item	Tangent Track	Curved Track (high rail)
Vertical wheel-rail load (P), kN		
Avg mean	74.7	65.4
Avg SD	35.6	36.5
Avg 0.1 percent load	185	178.4
Rail-seat vertical load (Q)		
Avg mean, kN	29.4	40.4[a]
Avg SD, kN	18.2	26.2
Mean ratio, Q/P	0.39	0.62
Avg 0.1 percent load, kN	85.8	121.4
Rail-seat moment, kN·m		
Avg mean	0.06	0.29[a]
Avg SD	0.44	0.67
Avg 0.1 percent load	1.4, 1.3	2.4, 1.8
Tie-rail-seat bending moment (M_{rs})		
Avg mean, kN·m	1.7	1.9
Avg SD, kN·m	1.0	1.2
Mean ratio, M_{rs}/P	0.923	1.16
Avg 0.1 percent load, kN·m	4.5	5.9
Tie-center bending moment (M_c), kN·m		
Avg mean	1.0	1.1
Avg SD	0.72	1.3
Avg 0.1 percent load	3.3, 1.2	4.8, 2.7

Notes: 1 kN = 225 lbf and 1 kN·m = 8852 lbf·in.
Average 0.1 percent load levels predicted from average mean and SD by assuming normal probability distribution; i.e., 0.1 percent load = mean ± 3.1 (SD).

[a]Average based on data for only two instrumented tie plates.

track loads. The results suggest that if the population of heavy cars becomes a greater portion of revenue service, i.e., if there are more unit trains of 63.50 and 91.0-Mg (70- and 100-ton) hopper cars, changes in tie spacing might have a much greater effect on tie moments than would be normally expected by using conventional track design estimates. Therefore, although a reduction in tie spacing might provide a large benefit, an increase might cause an unexpectedly large increase in tie bending moments. This suggestion requires additional evaluation because the effect of these variations in tie support conditions cannot be predicted for an increase in average wheel load.

Effect of Train Speed

A review of the mean values of vertical wheel-rail loads in the different speed categories showed the somewhat unexpected result that the average loads in the 48- to 64-km/h (30- to 40-mph) low-speed range were as much as 50 percent higher than the all-traffic average. Further investigation showed that this was caused by the fact that trains that have very heavily loaded cars operate at lower speeds past the test site than do trains that have a higher percentage of lightly loaded or empty cars. This type of speed effect reflects railroad operations rather than vehicle dynamics. It is not known whether this is typical of operations at other track sites on the FEC or on other railroads.

Speed effects related to vehicle dynamics can be evaluated only by using data for a common type of vehicle. Measured variations in mean vertical loads for identical locomotives operating at different speeds were less than 5 percent from the mean for all speeds. It was concluded from this that the effect of operating speed on vertical track loads from vehicle-dynamic effects was negligible on the FEC tangent track test sites.

Figure 9 shows the effect of train operating speed on the vertical and lateral wheel-rail loads. It is evident that the vertical-load bias in the 48- to 64-km/h range was responsible for the fact that that speed also caused the highest lateral loads on an all-car basis. This is true also for the heavy-car category alone. However, data for light cars, where the load bias versus speed was small, showed that the highest lateral loads occurred above 80.5 km/h (50 mph) and the lowest lateral loads occurred at 48 km/h. This is indicative of hunting cars. Other investigators (4) have confirmed that lightly loaded and empty freight cars have a lower hunting critical speed than have heavy cars.

Effect of Wheel-Flat Impact Loads

Recordings of track-load time histories showed considerable vibration, especially from the impacts of wheel flats. Data from FEC indicate that about 10 percent of the car wheels have flats of sufficient size to excite noticeable vibration but that a much smaller portion of these cause loads that exceed the normal load for a heavily loaded car. Figure 10 shows load data for a locomotive and demonstrates track response to heavy cars that have no apparent wheel flats. Figure 11 shows

that the response to light cars that have wheel flats is clearly more severe, particularly at the tie center. The damping of the track structure is quite low for this case, and it is difficult to distinguish the load pulses for individual wheels from the general vibration.

Curved Versus Tangent Track

The two major effects of train speed on curved track are the differences in vertical loads on the low and the high rails and the increases in lateral loads due to the curving forces from the truck and the unbalanced centrifugal forces on the cars. Measurements of vertical wheel-rail loads on the low and high rails confirmed that trains running at 48- to 64-km/h were below the theoretical 72.4-km/h balance speed. Trains in the 80.5- to 96.5-km/h range were operating above the balance speed, and the mean vertical load was about 10 percent higher than at the balance speed.

The lateral wheel-rail loads from light cars were much lower than those for heavy cars and locomotives on the curve, and the lateral loads for the light cars also were lower on the curve than they were on tangent track. It appears that the flanging on curves reduced or eliminated car hunting, and forces from light cars due to truck curving were much lower than those from hunting.

Table 2 summarizes the overall statistics for all traffic (all cars, all speeds) at the curve site and compares these to the same data for the tangent site (site one) that has the same 0.61-m tie spacing. The major differences between the two sites are that the average tie bending moments at the 0.1 percent exceedance level are 25 percent higher at the rail seat and 50 percent higher at the tie center than they were on tangent track even though the mean bending moments were nearly identical. This is a result of the increase in load variation (SD) that occurs in the curve from trains operating both below and above the balance speed. The significance of the higher variability of loads in the curve is that the low-probability high loads will exceed those on tangent track even though the mean loads will be quite similar.

SUMMARY AND CONCLUSIONS

Data from measurements of rail and tie loads on concrete-tie track were used to develop a statistical description of track loading for typical railroad service. This description can be used to evaluate performance specifications for concrete ties and fasteners and to validate track analysis models for predicting the effects of tie spacing, ballast depth, and tie size on track loads.

Typical mean rail-seat loads were on the order of 40 to 60 percent of the mean vertical wheel loads, depending on tie spacing and whether the track was tangent or curved. Data from adjacent ties showed considerable tie-to-tie variations in support condition.

Data on tie bending moments and tie-ballast-interface pressure distributions indicated a strong load-dependent response. There was a noticeable center-bound support condition for light wheel loads, but the support shifted toward the rail-seat region for heavy wheel loads. The high ballast and subgrade pressures from heavy cars evidently cause voids or depressions in the roadbed under the rail-seat region of the ties.

Tie moments from revenue traffic on the FEC were considerably lower than the current flexural strength requirements, even for a probabilistic estimate of maximum loads for a 50-year life. Similar conclusions can be made based on tie-load data from other test installations such as at Streator and the Facility for Accelerated Service Testing (FAST) at Pueblo, Colorado (5) (1 kN·m = 8852 lbf·in).

Test Installation	Tie Bending Moment (kN·m) Rail Seat (+)	Center (-)	Center (+)
AREA	28.2	22.6	10.1
FEC	8.8	6.3	7.5
Streator	10.9	8.1	
FAST	9.0	14.6	

However, cracking of ties having static flexural strengths that exceed measured loads has persisted. It is conjectured that small cracks may be initiated at loads much lower than the static strength requirements and that, once initiated, the repeated fatigue loading of normal traffic will cause the cracks to grow until they reach a detectable size. Locating small cracks in prestressed ties is practically impossible, and this makes the investigation of the crack-initiation mechanism particularly difficult. However, if a fatigue mechanism is confirmed, it may be possible to improve tie life by design or material changes that are different from those used to increase ultimate strength.

The necessity for eliminating tie cracking has not been verified by service experience, and preliminary results of tests at FAST that used precracked ties indicate no major structural failure after 6 Tg (50 million tons) of traffic. The reason cited most frequently for the elimination of cracking is that a crack that reaches the prestress tendons will eventually cause bond failure from the cyclic loading of normal traffic. Other problems that could result from cracking are corrosion of the metal tendons and concrete damage from freeze-thaw cycles.

ACKNOWLEDGMENT

This paper is based on the results of a research project conducted by Battelle Columbus Laboratories and Bechtel. The research was sponsored by the U.S. Department of Transportation, Federal Railroad Administration, through the Transportation Systems Center. We gratefully acknowledge the assistance and enthusiastic cooperation of the staffs of Battelle Columbus Laboratories, Bechtel, and FEC. This paper presents our views and positions and does not necessarily reflect those of the U.S. Department of Transportation.

REFERENCES

1. Specifications for Concrete Tie and Fastening. Proc., AREA, 655, Nov.-Dec. 1975, pp. 193-236, and Bull. 660, Nov.-Dec. 1976, pp. 133-137.
2. R. H. Prause, H. C. Harrison, and R. C. Arnlund. Measurement Plan for the Characterization of the Load Environment for Crossties and Fasteners. Battelle Columbus Laboratories, Columbus, OH; Federal Railroad Administration, Rept. FRA/ORD-77/03, April 1977.
3. R. H. Prause, H. D. Harrison, J. C. Kennedy, and R. C. Arnlund. An Analytical and Experimental Evaluation of Concrete Crosstie and Fastener Loads. Battelle Columbus Laboratories, Columbus, OH; Bechtel, San Francisco; Federal Railroad Administration, Rept. FRA/ORD-77/71, Dec. 1977.
4. D. R. Ahlbeck, H. D. Harrison, and S. L. Noble. An Investigation of Factors Contributing to Wide Gauge on Tangent Railroad Track. Journal of Engineering for Industry, Trans., ASME, Vol. 99,

Series B, No. 1, Feb. 1977, pp. 1-9.
5. A. Kish, D. P. McConnell, R. M. McCafferty, H. Moody, and A. Sluz. Track Structures Performance: Comparative Analysis of Specific Systems and Component Performance. Federal Railroad Administration, Rept. FRA/ORD-77/29, June 1977.

Development of Multilayer Analysis Model for Tie-Ballast Track Structures

James C. Kennedy, Jr., and Robert H. Prause, Applied Dynamics and Acoustics Section, Battelle Columbus Laboratories, Columbus, Ohio

A multilayer analysis model for tie-ballast track structures has been developed. The model includes the effects of rail bending, rail-fastener stiffness, tie bending, variable ballast and subgrade material types, and variable tie spacing and ballast depth. The results predicted by using the model are compared with experimental results and excellent agreement is shown. The model offers the advantages of simplicity of use and reduced computer run time when compared with the finite-element codes currently used.

The evaluation of track performance and track design for vertical loads requires the ability to predict realistic pressure distributions at the interfaces between the tie and the ballast and between the ballast and the subgrade. This requires a model that includes the effects of tie bending; rail-fastener stiffness; and changes in ballast depth, roadbed material properties, and tie spacing in a unified manner. In such a model, changes in roadbed configuration that affect track moduli and the distribution of loads from the rails to individual ties are apparent.

A track model and computer code that incorporates the above features has been developed. This paper compares its ease of use, computer time required per run, and accuracy of results with those of other existing analysis codes. Analytical validation and a comparison of computer predictions and experimental results are also presented.

The Multi Layer Track Analysis (MULTA) computer routine discussed here is a two-stage numerical procedure for determining the three-dimensional load and stress distribution in a railroad track system subjected to static loads.

MULTA can be used to evaluate new or existing track-system configurations for various combinations of concentrated vertical loads or moments exerted on either or both rails.

TYPICAL METHODS OF ANALYSIS OF TRACK STRUCTURES

Currently, the analysis of track structures usually follows one of two paths: (a) the track structure is represented very simply (e.g., a beam on an elastic foundation wherein the substructure is represented as a series of discrete springs) or (b) the track structure is modeled in great detail by using a finite-element representation. In the first case, the system is represented so simply that individual contributions (such as ballast material type and depth, subgrade material type, and tie bending) are not sufficiently detailed or easily evaluated. On the other hand, the detail characteristic of most finite-element codes requires preparation of input data and running time for computer analysis of such magnitude that extensive analyses are quite often prohibitive.

A finite-element code was selected that could simulate variable ballast depth and material type and subgrade depth and material type so that the results obtained by using it could be compared with those obtained by using MULTA. MULTA is not a finite-element code as such; the differences between it and a typical finite-element code will be pointed out below. The finite-element code used for this comparison was the prismatic solid analysis (PSA) code originally developed at the University of California, Berkeley, and modified by the Association of American Railroads (AAR). The comparison between the results obtained by using the two codes showed negligible differences in predicted stresses and displacements. [A complete description of the PSA code and the comparison have been given by Prause and others (1)].

Typically, the preparation of input data for use in MULTA requires considerably less time than do seemingly equivalent finite-element codes. In the results that are discussed below, 11 ties are used in the simulation of the track structure. Preparation of input data for MULTA, including punched data cards, required about 3 person-h. Running time required about 400 computer s. On the other hand, the preparation of input data for the analysis that used the PSA finite-element code required about 8 person-h preparation time and about 750 s computer run time. Thus, the MULTA program has the advantage of being able to simulate and evaluate the effects of parameters such as ballast depth and material type, subgrade material type, tie bending, and rail-fastener stiffness where similar analysis codes (such as the beam-on-elastic-foundation formulation) do not. On the other hand, its relative ease of input-data preparation and considerably smaller amount of computer run time offer definite advantages over the more detailed finite-element codes without compromising the results for a vertical linear-elastic track-analysis tool.

The results predicted by using the MULTA code have also been compared with those predicted by using the ILLI-TRACK structures code. This is a two-dimensional finite-element code developed at the University of Illinois (2). The comparison shows that ballast pres-

sure, rail deflection, and rail bending-moment predicted values can be in serious error if the effective bearing area of the tie is not properly chosen when the ILLI-TRACK model is used. This is a key difference between the two models. It is necessary to assume an initial tie bearing area when ILLI-TRACK is used, whereas tie deformation and contact area are included directly in MULTA. [The comparison of MULTA and ILLI-TRACK predictions has been given by Prause and Kennedy (3)].

Figure 1. Track model for MULTA program.

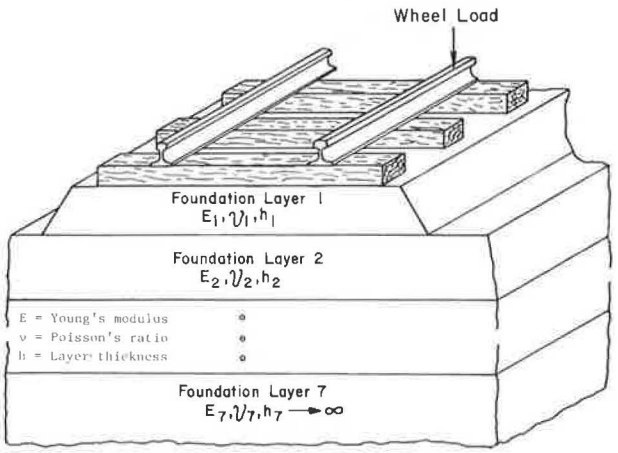

Development of Track Model

The two stages of solution in MULTA are modifications to two previously developed computer codes. The first stage is a modified version of the computer program developed by the AAR and models the ballast-subgrade system as a multilayered elastic system (4). The theoretical basis for the multilayered elastic system was first presented by Burmister (5). The second stage of solution in MULTA is a modified version of part of the program described by the AAR (6). The load-combination phase is that portion of the program that was revised for use in MULTA. This second stage of MULTA includes rail loads, rail bending, rail-fastener stiffness, and tie bending. The schematic for MULTA is shown in Figure 1.

Model Description

The first stage of MULTA analyzes the track substructure (ballast and subgrade) and provides information about displacement and stress influences as input to the second stage. The basic theory in the first stage assumes

Figure 2. Basic geometry for first stage of MULTA program.

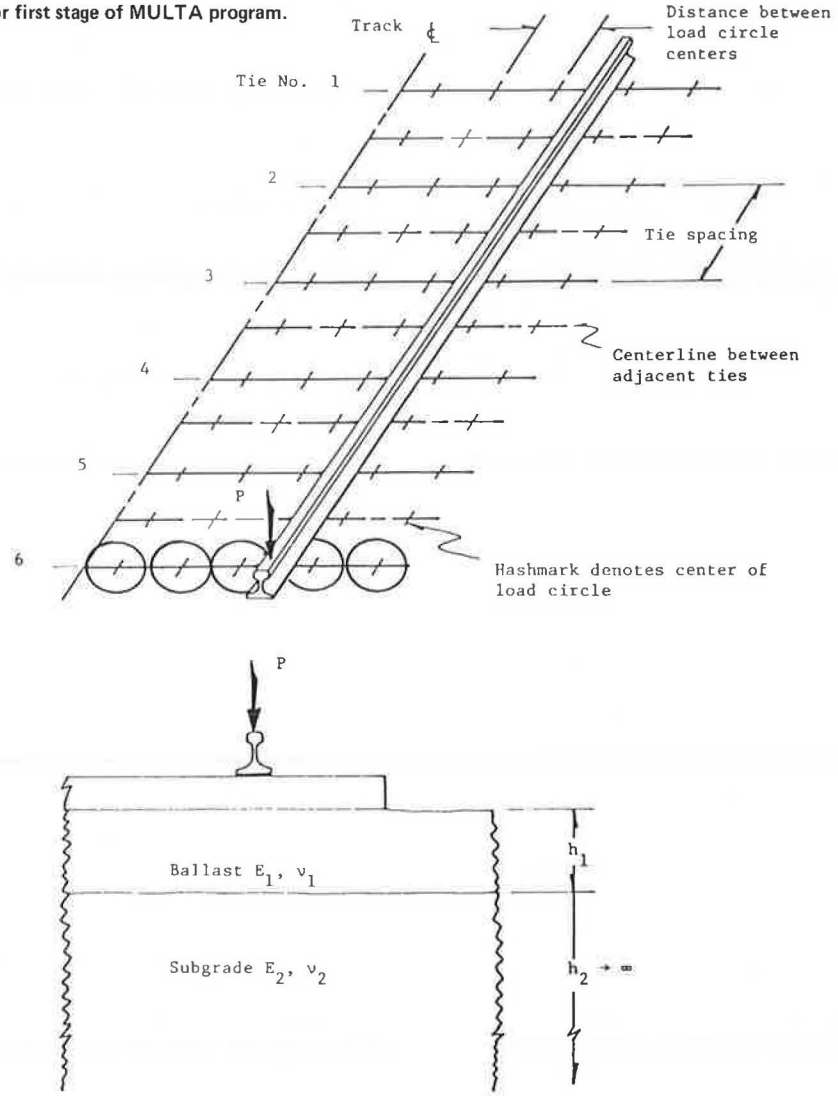

the ballast-subgrade structure to be that of an elastic half space and, as such, the horizontal and vertical (downward) dimensions of the track structure are infinite in extent. This precludes the simulation of actual ballast-profile geometries, such as sloping shoulders. However, the effects of infinite dimensions in the horizontal and vertical directions on the stress and displacement predictions for vertical loads have been evaluated, and it was concluded that the finite dimension of the ballast shoulder had a negligible effect on the ballast and subgrade pressure under the ties (1).

MULTA calculates stress and displacement influence functions in the form of the stress and displacement responses of the ballast-subgrade structure to unit vertical loads applied to specific locations on the horizontal surface of the ballast. These specific locations are at the tie-ballast interface for the particular tie-track system being simulated. Critical in the simulation of how the loads are transmitted from the tie onto the ballast is the choice of the effective load-distribution area on the ballast. This distribution is in the form of load circles that distribute the tie loads onto the ballast (see Figure 2). [Load-circle size (radius) and number of load circles necessary to achieve simulation efficacy and solution accuracy have been discussed by Prause and others (1)].

The second stage of MULTA is basically an equation solver. The equations that are solved in this stage include the magnitude and position of a wheel load on each rail, rail displacement, rail force and equilibrium, rail-fastener stiffness, and tie bending.

MODEL ASSUMPTIONS, FEATURES, AND LIMITATIONS

The track system model includes the following assumptions:

1. The entire system behaves in a linear fashion.
2. The loads and moments applied to the rails are static and concentrated.
3. The material of each component of the system is homogeneous, isotropic, and linear elastic.
4. The depth of the last soil layer is infinite.
5. The tie spacing is constant for all ties.
6. The track gauge is constant.
7. The rail-tie system (including the first and last ties) deforms compatibly on the elastic foundation.

MULTA has available to the user the following options and features:

1. The ballast-subgrade system can be modeled by as few as two or by as many as seven layers of homogeneous, isotropic, elastic materials, each of which has distinct material properties and depths. However, the last layer must have an infinite depth.
2. The vertical stiffness of the spring used to represent the combined stiffness of a rail fastener and tie pad can be selected arbitrarily but must be greater than zero.
3. Unequal loads are permitted for each rail and at any position along a rail.

Use of MULTA is subject to the following limitations:

1. All ties must have identical material and geometric properties.
2. The track roadbed representation as an elastic half space with infinite horizontal dimensions does not permit modeling the actual cross-section of a ballast section having sloping shoulders.
3. The model does not permit missing ties.
4. The model does not allow external loading in the lateral or longitudinal directions and thermal loads cannot be included.

Test Description

As discussed above, MULTA is analytically equivalent to other, more detailed codes, but it was also desirable to compare MULTA results with experimental results. The experimental results were extracted from tests conducted on the Florida East Coast Railway (FEC). The FEC test sites included two concrete-tie tangent track sections, one that had a nominal tie spacing of 0.61 m (24 in) (site 1) and one that had a nominal tie spacing of 0.51 m (20 in) (site 2) and a concrete tie curve site that had 0.61-m tie spacing (site 3). All three sites included a main instrument array that extended over 7 ties. The purpose of this continuous section was to obtain a complete set of track load and response data over a nominally uniform track section. [A detailed description of the test sites and the instrumentation used to record the various track quantities of interest have been given by Prause and others (1)]. Only the instrumentation that pertains to the validation of the analysis code (MULTA) is described here.

Measurement of Vertical Track Loads

Rail-Seat Loads

The main array of each test section contained six instrumented tie plates, of which five were along one rail. The instrumented tie plates were used to record rail-seat loading throughout the influence zone of the center tie. Each instrumented tie plate had a pair of load-cell washers. The signals from the two load-cell washers were summed to measure total vertical rail-seat load.

Tie-Ballast Pressures

The Federal Railroad Administration-Portland Cement Association (FRA-PCA) load-cell ties developed for the Kansas test track were used to measure the tie-support reactions at the tie-ballast interface. These steel ties have 10 separate segments along the bottom to convert bearing pressures to discrete loads. Each rail seat is instrumented to measure vertical rail-seat loads. [A detailed description of the construction of the FRA-PCA load-cell tie and a comparison of the bending stiffness between the load-cell tie and the Railroad Concrete Crosstie Corporation tie have been given by Kennedy and others (1)].

Two of the load-cell ties were installed at site 1, and one load-cell tie was installed on the curve at site 3. The purpose of using these load-cell ties was to simultaneously measure vertical rail-seat loads and the resulting distribution of tie-ballast pressure on the 10 instrumented segments along the tie length.

Generation of Input Data for MULTA

The input-data requirements of the MULTA track-analysis model include the elastic properties for a layered representation of the ballast and the subgrade. The following plate-bearing test procedure was used to obtain representative data for the elastic properties:

1. Two adjacent ties were removed, sufficiently far away to avoid any effect on the instrumentation, and load-deflection plate-bearing measurements were made on the ballast surface in the footprint of one tie. A 0.20-m (8-in)

diameter, circular loading plate was used on the ballast surface, and this area was covered with plaster of paris (dental cement) so that the loading plate would bear uniformly on the ballast. A fixed wooden reference beam supported outside the track was used as a displacement reference for two displacement transducers attached to the plate. Displacements were recorded for ballast loadings of up to about 862 kPa (125 lbf/in^2), which exceeds the ballast pressure encountered in actual service by a considerable margin [typical ballast pressures in service rarely exceeded about 345 to 414 kPa (50 to 60 lbf/in^2)].

2. The ballast crib was excavated at the location of the two removed ties to determine the actual ballast depth. The ballast depth under the bottom of the tie was 16.5 cm (6.5 in) at both site 1 and site 2. The plate-bearing tests were repeated on the subgrade without using the dental cement.

3. Data from steps 1 and 2 were used with the multilayer track-analysis model to determine representative values of Young's modulus for the ballast and subgrade layers.

The loading cycle was repeated three consecutive times at each of three positions along the length of the tie. As shown in Figure 3, the initial load cycle has a much lower slope (force versus displacement) than does the second load cycle. In fact, after the initial load cycle, the subsequent load cycles have almost the same slope. Data shown in Figure 3 are for the site 1 subgrade at 16.5 cm on the gauge side of the rail. Data for the other locations are characteristically similar.

Initial and final slope values from the subgrade tests were used to estimate Young's modulus (E_2) for the subgrade, by using theory-of-elasticity solutions for the deflection of an elastic half space loaded by a rigid circular plate. After E_2 was determined, the ballast-stiffness data were used to estimate Young's modulus (E_1) for the ballast. This estimate was made by using the multilayer program in an iterative scheme until the predicted load-deflection values for the circular plate load were sufficiently close to the experimental values. It was hoped that using initial and final stiffness values would place a bound on the value of E_2 so that the predicted value of track modulus (U) would compare favorably with the measured data for track modulus.

Figure 3. Relationship between force and displacement for subgrade plate-bearing test at site 1.

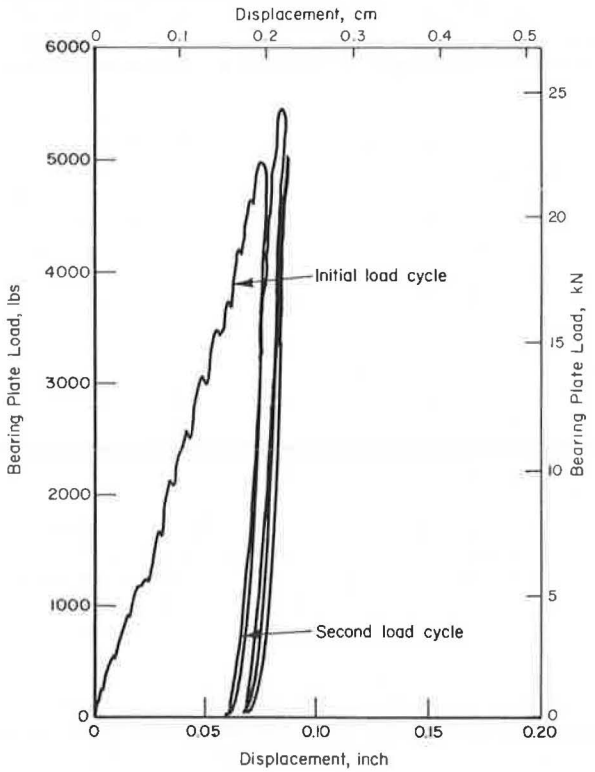

The values of Poisson's ratio for the subgrade and ballast layers are also needed as input to the MULTA program. Typical values of $\nu_1 = 0.4$ for the ballast and $\nu_2 = 0.4$ for the subgrade were chosen from the subgrade property data obtained from the results of soil tests conducted by Pittsburgh Testing Laboratories [as reported by Prause and others (1)].

The table below shows the values of E_1, E_2, and U, based on the initial and final plate-bearing-test stiffness data in conjunction with the MULTA program (1 MPa = 145 lbf/in^2).

	E_1(MPa)		E_2(MPa)		
Location	Initial	Final	Initial	Final	U(MPa)
Site 1	193	207	61.4	123	105-176
Site 2	103	193	33.1	123	72.5-210

Track modulus U is defined here as the force per 2.5 cm (1 in) of rail required to depress the track roadbed 2.5 cm. This parameter has been used historically to quantify the effective stiffness, or resilience, of a track structure and is a key parameter in the beam-on-elastic-foundation analysis procedure used for conventional track design. The predicted values of U are based on the beam-on-elastic-foundation equation for vertical rail-seat load in the form:

$$U = 4EI\,[(2/\ell_t)\,(Q/P)]^4 \qquad (1)$$

where

Q = maximum rail-seat load predicted by MULTA,
P = wheel load,
ℓ_t = tie spacing, and
EI = rail bending stiffness.

COMPARISON OF MEASURED AND PREDICTED LOADS

Effect of Track Modulus on Rail-Seat Loads

Vertical rail-seat load (i.e., the load that is absorbed by a tie in a track structure; for example, if a static wheel load is placed on a rail directly over a particular tie, that particular tie will absorb 40 to 60 percent of the applied wheel load) data from a slow roll-by of the work train were used to determine U. The work train consisted of one empty and one loaded 90.7-Mg (100-ton) hopper car and a four-axle locomotive. The effect of tie-to-tie variations in the main array was minimized by averaging the maximum rail-seat loads for a known wheel load during a slow traverse of the work train. The average ratio of the rail-seat load to the wheel load (Q/P) was used with the theoretical relationship from the beam-on-elastic-foundation formulation to determine an experimental track modulus. This is the same formula that was used to calculate the values of U given above.

The table below gives the maximum measured values of Q/P.

Item	Q/P (%) Tie 1	Tie 2	Tie 3	Tie 4	Tie 5	Avg
Site 1						
Light car	43	71	31	–	33	44.5
Heavy car	47	58	53	–	65	55.8
Site 2						
Light car	22	38	64	–	76	50
Heavy car	44	31	56	–	64	48.8

These data show a considerable load-dependent effect as well as large tie-to-tie variations. The average rail-seat load for heavy cars on track that has 0.51-m tie spacing was 12.5 percent lower than that of track that has 0.61-m tie spacing. A 16 percent reduction would normally be expected based on conventional guides for track design. However, individual ties in both sections carried as much as 65 percent of the heavy-car wheel load and as much as 76 percent of the light-car wheel load.

Figure 4 shows a comparison of measured and predicted rail-seat loads for a heavy-car wheel centered in the main array of site 2. The model parameters corresponding to a track modulus of 210 MPa/rail [(30 400 lbf/in^2)/rail] (final values given above) were used for the predictions. It is evident from the load distribution shape that the actual track was stiffer than the analysis model.

As discussed above, it was hoped that the data from the initial and final load cycles of the plate-bearing load-deflection tests would provide bounds to the estimation of the roadbed parameters. However, the comparison in Figure 4 shows that the plate-bearing test data did not provide a reliable prediction of roadbed stiffness even though the values for subgrade and ballast modulus appear reasonable when compared with the laboratory subgrade measurements and typical values for ballast.

Because the FEC roadbed is stiffer than that predicted by using the plate-bearing data, the following procedure was adopted in an attempt to synthesize the model parameters that determine roadbed stiffness and track modulus. The ratio of the moduli of the ballast and the subgrade determined from the plate-bearing tests was retained, and the actual values of E_1 and E_2 were increased so that the maximum predicted rail-seat load equals the average maximum experimental rail-seat load for the heavy car. The heavy car was chosen to reduce the effect of any nonlinearities. This procedure was used to adjust the E_1 and E_2 values so that the maximum predicted vertical rail-seat load was within 1.2 percent of the average experimental data for the 0.51-m tie spacing (site 2) and within 1.6 percent for the 0.61-m tie spacing (site 1). The adjusted values of foundation properties are given below (1 MPa = 145 lbf/in^2).

Property	Value
E_1, MPa	414
E_2, MPa	246
ν_1	0.4
ν_2	0.4

Figure 5 compares the measured and the predicted rail-seat loads when a heavy-car wheel is centered in the main array of the track that has 0.61-m tie spacing. In the case of a very stiff track (a high value of U), the loaded tie absorbs a large percentage of the applied load (>50 percent) and the loads absorbed by the adjacent ties drop off rapidly. The average maximum experimental rail-seat load was 84 kN (18 900 lbf) for an applied load of 151 kN (33 900 lbf) at site 1 (Q/P = 55.8 percent). This gives a track modulus of U = 329 MPa (47 700 lbf/in^2). The maximum predicted rail-seat load was 82.8 kN (18 600 lbf), and the predicted track modulus was 308 MPa (44 700 lbf/in^2). The lower predicted modulus is apparent from the comparison of the rail-seat load-distribution shapes shown in Figure 5.

This comparison shows that the actual track structure is at least as stiff as the value predicted using the adjusted modulus values of E_1 and E_2. The tie-ballast pressure distribution data in the following section also support this conclusion.

Tie-Ballast Pressure Distribution

Tie bending moments at the rail seat and bending and torsional moments at the tie center have been identified as the major causes of concrete-tie failures. The distribution of the support reaction between the tie and the ballast is the principal unknown factor in validating the bending moments predicted by analytical models. Therefore, measurements of tie-ballast pressure distribution along the length of the tie were needed to fully validate the analytical prediction of bending moments at the tie rail seat and at the center.

The vertical tie-ballast pressures along the length of one load-cell tie for heavy, medium, and light cars are shown in Figure 6. These pressure profiles indicate that this particular tie was noticeably center-bound for light-car loads. That is, the tie center bears almost the entire load, and the outer ends of the tie carry almost no load. As the magnitude of the load is increased, the peak pressures moved outward from the tie center toward the rail-seat regions. The experimental data show that the peak pressure shift from the tie center to the rail-seat region reaches a maximum on the gauge side of the rail seat. Pressures up to about 276 kPa (40 lbf/in^2) were measured in the rail-seat region for normal heavy cars.

Predicted results from the MULTA program for the medium-car load are shown for comparison in Figure 6. The MULTA program assumes a uniform elastic support for the roadbed. The resulting tie-ballast pressure distribution reaches its maximum under the applied load (rail seat) and its minimum at the tie center. The maximum predicted pressure [228 kPa (33 lbf/in^2)] is within 14 percent of the measured data for the medium load despite the center-binding effect for this tie.

The experimental data from the load-cell tie in the curved track section (site 3) are shown in Figures 7 and 8. Tie-ballast pressure distributions along the length of the tie for light-, medium-, and heavy-car wheel loads are shown in Figure 7. An integration of the pressure distributions showed that vertical equilibrium was satisfied to within 3 percent of the respective applied loads.

The results of the MULTA program shown in Figure 7 for medium-car wheel loads are in good agreement with the experimental data. Maximum pressures are predicted to within 5 percent, and the shapes of the distributions are very similar. It is also evident that the vertical load is considerably greater on the high rail and the case of unequal loads can be used as input to the model.

The normalized pressure distributions for the three cases of light-, medium-, and heavy-car wheel loads are shown in Figure 8. The small variations show that the support reactions for this tie behaved in a linear manner and that the uniform elastic foundation used in the MULTA program gave good predictions for the pressure distributions for all wheel loads.

Figure 4. Comparison of experimental and analytical rail-seat loads at site 2.

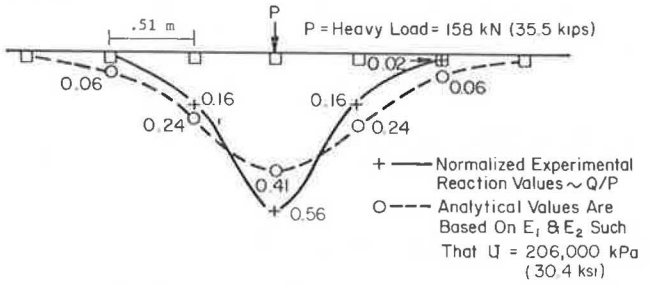

Track Displacement Predictions

The results from the MULTA program were used to determine how the track displacement compares to that for a Winkler foundation. The data in Figure 9 show that the predicted displacements are distributed over a greater length of track than the tie-load distribution. The difference between the displacement shape predicted by MULTA and that predicted by the tie-load distribution indicates that the rail is not behaving like a beam on a Winkler-type foundation; the two distributions would be identical for a Winkler foundation.

Vertical rail displacements were measured at two locations at each test site—the middle tie of the main

Figure 5. Comparison of measured and predicted vertical rail-seat loads at site 1.

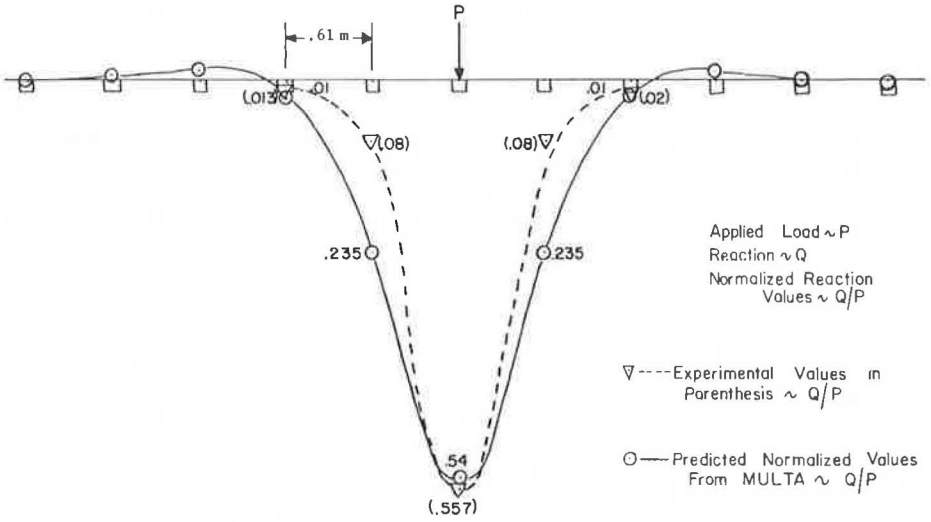

Figure 6. Tie-ballast pressure data at site 1.

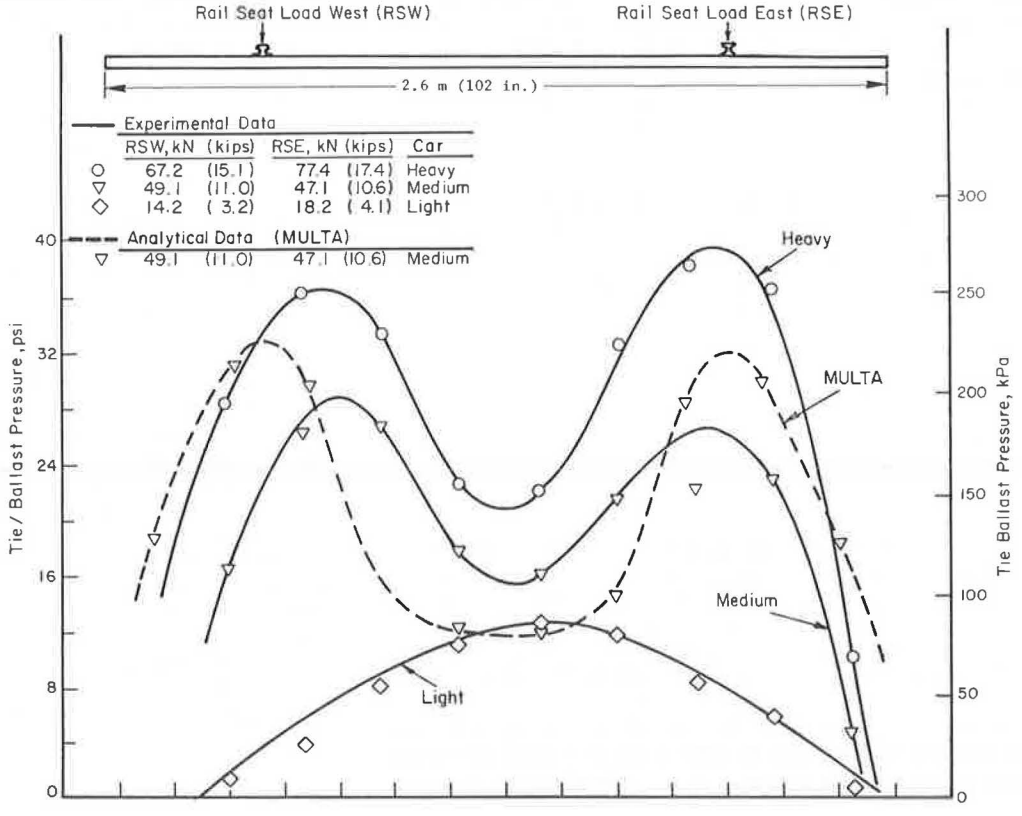

array and a tie about 10.7 m (35 ft) outside the main array. Because only two locations were instrumented at each test site for these data, it was difficult (in view of the local variations discussed above) to characterize the track structure by using experimental displacement values. It is believed that more values of displacement (per test site) are required so that average maximum displacement values could be used to better predict track modulus. However, the alternative approach of averaging data from five instrumented tie plates gave good results.

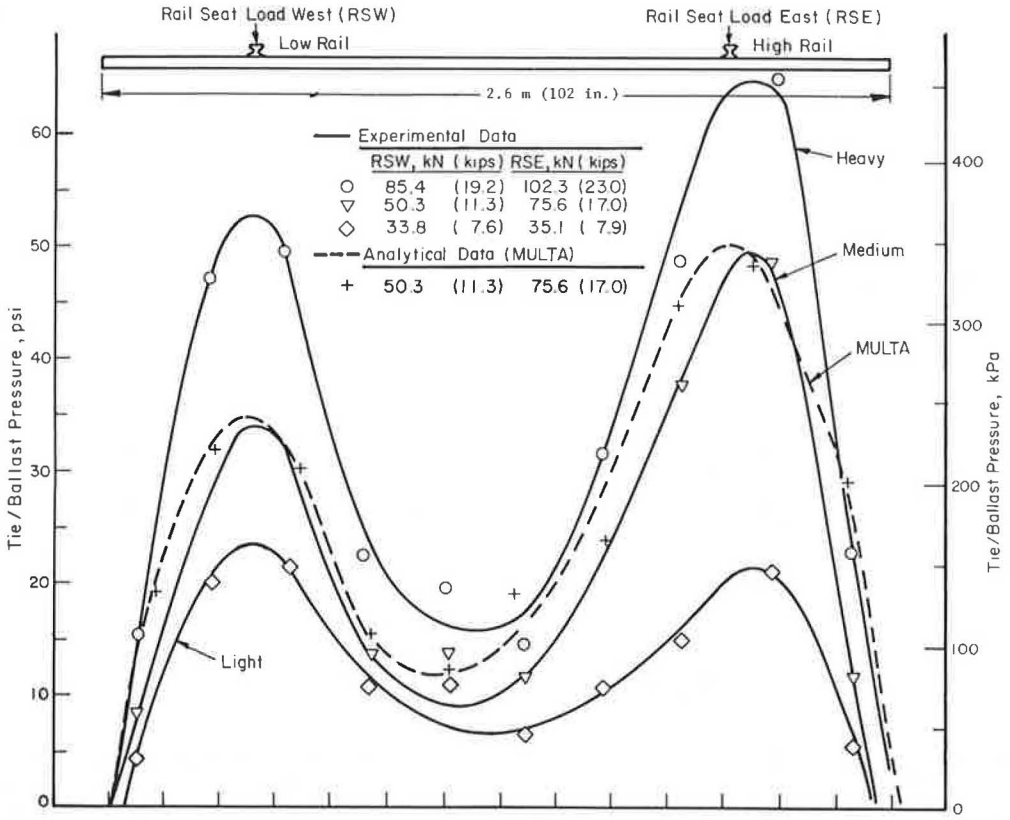

Figure 7. Tie-ballast vertical pressure data at site 3.

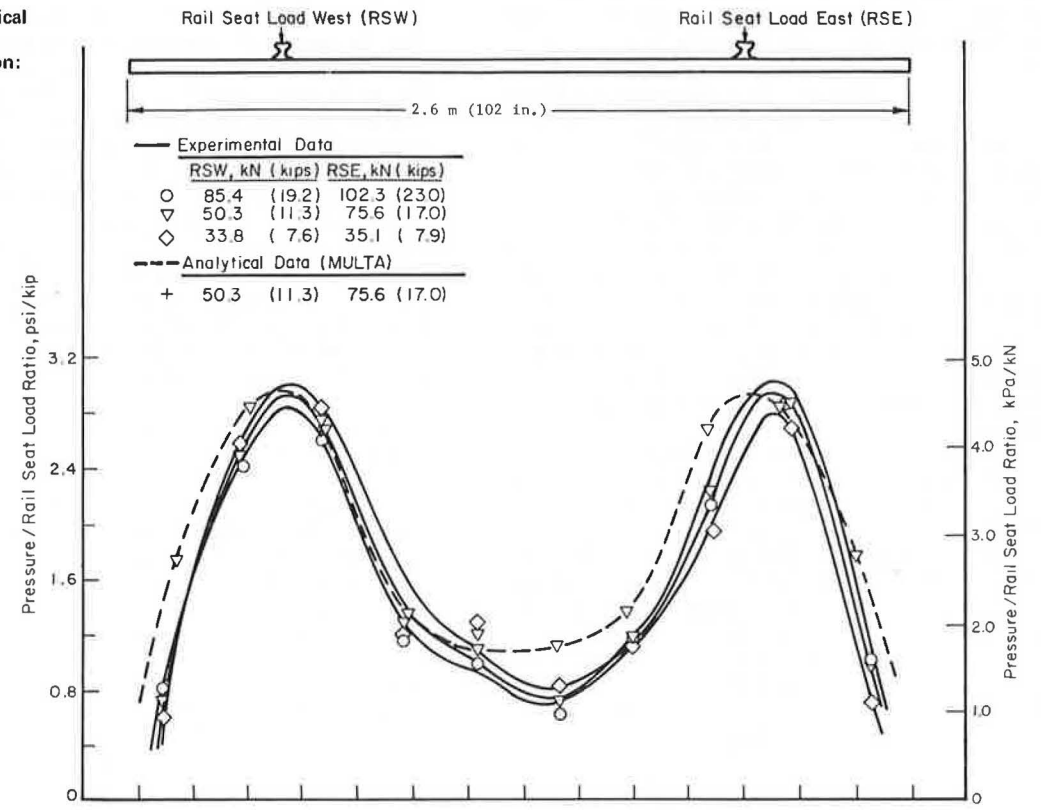

Figure 8. Tie-ballast vertical pressure normalized to respective rail-seat reaction: site 3.

Figure 9. Predicted tie load and displacement distributions: site 1.

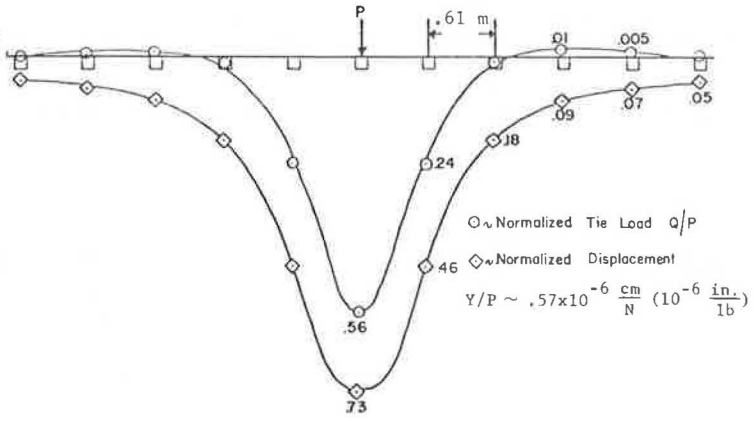

Table 1. Summary of track modulus values.

Location	Measured Track Modulus (MPa)				Predicted Track Modulus (MPa)	
	Displacement[a]	Strain[b]	Avg Tie-Plate Loads[c] Light	Heavy	Foundation Parameters From Plate-Bearing Tests[d]	Adjusted Values of E_1 and E_2[e]
Site 1						
Main array	270	316	130	328	105-176	308
Outside main array	283				105-176	
Site 2						
Main array	126	600	432-401		72.4-206	382
Outside main array	565				72.4-206	

Note: 1 MPa = 145 lbf/in^2.

[a]Calculated by using rail displacement for light- and heavy-car wheel loads.
[b]Calculated by using rail bending strains for light- and heavy-car wheel loads.
[c]Based on average maximum tie-plate loads on four ties [light load = 35.6 kPa (≈ 8000 lbf/in^2) and heavy load = 151.3 kPa (≈ 34 000 lbf/in^2)].
[d]Range for initial to final values for model parameters based on predicted maximum tie-plate load.
[e]E_1 = ballast modulus and E_2 = subgrade modulus, adjusted so that maximum predicted rail-seat load equals average maximum experimental rail-seat load at site 1.

Track Modulus Measurements

It was originally planned that rail bending strains measured under heavy and light loads similar to those used for measuring displacements would be used to provide a check on the track modulus determined from the displacement data. However, the lack of a sufficient number of strain gauges (i.e., at many positions along the length of the rail) prevents the sort of averaging process that subsequently was determined essential to minimize local variations. Difference (heavy-load-minus-light-load) stress and displacement values and corresponding track moduli are given in Table 1.

The values of track modulus given in Table 1 indicate that the track structure is quite stiff. However, the data resulting from displacement and strain measurements are for one or two discrete points along a rail at a particular test site; they do not represent any sort of averaged values. As such, they should not be considered truly representative of the overall track modulus.

Thus, the predicted calculations of track modulus shown above and in Table 1 are based on the beam-on-elastic-foundation equation for vertical rail-seat load (Q) as shown in Equation 1. Equation 1 is one of two forms used to calculate U. The other form is based on the maximum rail displacement (Y_0). Both forms are derived from beam-on-elastic-foundation theory. If, in reality, the track system behaves as a beam-on-elastic-foundation, then either form can be used to calculate U and the answers will be identical. However, if the shear coupling in the roadbed is significant, the track will not behave according to the assumptions used for the beam-on-elastic-foundation and the results from estimates of track modulus that use measured data for Q and Y_0 will not give equivalent values for U. This is also true for the MULTA model, where there is appreciable shear coupling in the simulation of the roadbed.

As we have seen, the measurements on FEC showed that the use of the average maximum rail-seat load to calculate U gives results that are more consistent with the loads and moments than does the use of rail displacements. As mentioned above, the rail-seat load distribution predicted by MULTA is qualitatively similar to the results of the beam-on-elastic-foundation solution and the FEC measurements, whereas the displacement distribution is different from beam-on-elastic-foundation solution because of coupling in the roadbed. However, if the predicted modulus values are calculated by using the rail displacements, the values will be approximately one-half to one-third those calculated by MULTA and the use of rail-seat loads and in the range of typical measured track-modulus data for concrete-tie track.

SUMMARY OF RESULTS AND CONCLUSIONS

The comparison of predicted and measured track-response parameters discussed above shows that the MULTA track-analysis program is capable of making good predictions of tie loads and tie-ballast pressures. The inclusion of tie bending has been shown to be quite important in predicting ballast pressures. The program can also be used to predict rail bending stresses and tie bending moments.

No experimental data on stresses in the ballast and subgrade below the tie were measured for comparison. However, the good agreement with the predicted ballast pressures immediately under the tie gave confidence

that pressures predicted elsewhere in the roadbed will be sufficiently accurate for track-design evaluations. Predictions of soil behavior are limited by the assumptions of linear elasticity in the MULTA model; thus, inelastic behavior of highly loaded soils could not be predicted accurately.

The major difficulty in using MULTA (or any other track-analysis program) is in the accurate modeling of the ballast and subgrade. The elastic continuum used in the MULTA model does show that the transfer of shear in the roadbed produces appreciable tie-to-tie coupling in displacements. This effect is also observed in track-response measurements, but it is not included in conventional beam-on-elastic-foundation models. However, the real difficulty is in establishing the material properties for a layered model of the ballast and subgrade that match the overall track-modulus measurements. The plate-bearing tests on the ballast and subgrade and independent vibroseismic measurements of subgrade properties did not give sufficiently accurate predictions of track modulus for the prediction of track loads under heavy-car wheel loads even though pressures greater than the maximum pressures under traffic were used for the plate-bearing tests. This difficulty cannot be explained at this time. In the meantime, it is recommended that the ballast and subgrade properties be adjusted to match the experimental measurements of track modulus under heavy-car wheel loads by using representative soil data for the relative ballast-soil stiffness. Predictions of tie loads, track deflections, and roadbed pressures will not be greatly influenced by changes in the relative ballast and soil stiffnesses as long as the track modulus is matched. Inaccurate estimates of these parameters will have their greatest effect on predictions of relative deflections in the ballast and subgrade layers.

ACKNOWLEDGMENT

This paper is based on the results of a research project conducted by Battelle Columbus Laboratories and Bechtel. The research was sponsored by the U.S. Department of Transportation, Federal Railroad Administration, through the Transportation Systems Center. We gratefully acknowledge the assistance and enthusiastic cooperation of the staffs of Battelle Columbus Laboratories, Bechtel, and FEC. This paper presents our views and positions and does not necessarily reflect those of the U.S. Department of Transportation.

REFERENCES

1. R. H. Prause, H. D. Harrison, J. C. Kennedy, and R. C. Arnlund. An Analytical and Experimental Evaluation of Concrete Crosstie and Fastener Loads. Federal Railroad Administration, Rept. FRA/ORD-77/71, Dec. 1977.
2. S. D. Tayabji and M. R. Thompson. Program ILLI-TRACK: A Finite-Element Analysis of Conventional Railway Support System—User's Manual and Program Listing. Federal Railroad Administration, Technical Rept. FRA-ORD-76-257, March 1976.
3. R. H. Prause and J. C. Kennedy. Parametric Study of Track Response and Performance. Federal Railroad Administration, Rept. FRA-ORD-77/75, Dec. 1977.
4. Ballast-Subgrade Model of Burmister Multilayer Elastic System. Report and Test Department, Association of American Railroads, Washington, DC, Rept. R262-13, Sept. 1975.
5. D. M. Burmister. The General Theory of Stresses and Displacements in Layered Systems. Journal of Applied Physics, Vol. 16, Feb. 1945, pp. 89-94.
6. Ballast-Subgrade Finite-Element Model: Prismatic Solid Analysis Program. Report and Test Department, Association of American Railroads, Washington, DC, Rept. 262-14, Vol. II, 14, Sept. 1975.

Permanent-Deformation Behavior of Railway Ballast

Reid M. Knutson, Department of Civil Engineering, University of Kansas
Marshall R. Thompson, Department of Civil Engineering, University of Illinois, Urbana-Champaign

Ballast materials were tested in the triaxial apparatus by using a repeated deviator stress and a constant confining pressure. Permanent deformation (plastic) characteristics at several stress levels were determined for a variety of types and gradations of material. Correlation analyses were made between the plastic response and the results of standard material-characterization tests. The results indicate that the most important factor influencing the repeated-load plastic-strain behavior of ballast is the degree of compaction. The stress level was also found to be an important factor; there was some indication that permanent deformation was less for the more nearly well graded specimens. Finally, unlike the resilient response, the permanent-deformation behavior of ballast is dependent on loading history.

One of the major problems of rail track support systems is the continual need for realignment of the rail-tie system by addition of ballast. Present maintenance practice dictates that only the portion of the ballast near the rail be tamped; the center is left undisturbed. This practice results in the addition of ballast primarily in the proximity of the rails; ballast pockets result (1).

Before the experience-oriented design of rail-tie support systems can be improved, the plastic-deformation behavior of ballast subjected to repeated loading must be investigated so that an understanding of its nature can be obtained. To accurately predict the deformation characteristics of ballast, the test method should simulate the in-service dynamic stress conditions.

BACKGROUND

There have been several investigations (2, 3, 4, 5) of the repeated-load behavior of granular materials. Both rigid-confinement and triaxial equipment have been used to study dense-graded aggregates and sand, but little work has been done that involved open-graded aggregates such as ballast. In addition, most of these investigations have been directed toward studies of the elastic (resilient) properties of the material; little attention has been paid to the plastic (permanent-deformation) behavior of aggregates subjected to repeated-load conditions.

Repeated-load triaxial testing of a variety of types of aggregate would appear to be the most appropriate method for the investigation of the plastic behavior of ballast materials. Previous investigations in which actual loading conditions were closely simulated have given excellent results.

Among the factors that affect the repeated-load permanent-deformation characteristics of granular materials are the confining pressure, the number of cycles, the load, and the stress history.

Lade and Duncan (6) have offered an explanation for the effects of stress history on permanent-deformation behavior. When a triaxial specimen (constant confining pressure) of a cohesionless material is subjected to an initial load, there is a large plastic deformation caused by the rearrangement of particles. This plastic deformation is accompanied by a smaller elastic deformation. When the specimen is unloaded and then reloaded to the previous stress level, theoretically only an elastic deformation will be observed. However, in the actual case, some additional plastic strain accumulates with each loading cycle. If, after several repeated loading cycles, the specimen is subjected to a deviator stress greater than that previously experienced, the stress-strain curve will continue in the direction of the original curve. Thus, the maximum load to which a material has previously been subjected becomes extremely important.

Field evidence of the effect of the maximum loading conditions (or primary loading) on the permanent deformation of ballast has been given in a report by the Office for Research and Experiments of the International Union of Railways (7). They concluded that smaller loads cause "negligible settlement" and that "small numbers of large dynamic loads . . . determine the deterioration of the track level, rather than the general level of the axle loads."

MATERIALS

Six materials commonly used for ballast were chosen so that their repeated-load behavior and natural properties could be compared. The materials selected were dolomitic limestone from Kankakee, Illinois; blast-furnace slag from Chicago; granitic gneiss from Columbus, Georgia; basalt from New Jersey; gravel (crushed and uncrushed) from McHenry, Illinois; and the type of slag used in the Kansas test track.

The materials were sieved, and the various size fractions of each were stored in separate containers for recombining into the desired gradations.

Characterization Tests

To relate the results of the repeated-load tests to the physical properties of the materials, the following standard tests were performed.

1. Particle index: ASTM D3398 (8),
2. Specific gravity: ASTM C127 (8) and AASHTO T85 (9),
3. Los Angeles abrasion: ASTM C131 (8) and AASHTO T96 (9),
4. Gradation parameter: that developed by Hudson and Waller (10),
5. Flakiness index: British standard 812-815 (11),
6. Soundness: ASTM C88 (8) and AASHTO T104 (9), and
7. Crushing value: British standard 812-34 (11).

The results of the characterization tests are summarized in Table 1.

Gradation

To examine the effects of different gradations on the resilient response, three different ones were included in the testing program. Two standard American Railway Engineering Association (AREA) gradations, nos. 4 and 5, were selected by using the center values of the recommended gradation bands. A third gradation was based on the use of the Talbot equation with an exponent of two-thirds. Because one of the main considerations of ballast is that it be free draining, the Talbot-equation gradation was maintained only through the 4.75-mm (no. 4) sieve. To ensure a high permeability, no material finer than that passing the 1.18-mm (no. 16) sieve was used. The gradation determined by using this analysis was labeled "well graded." A conservative estimate of the permeability of the well-graded material is 1500 m/d (5000 ft/d).

Equipment

A U.S. Army Engineer Waterways Experiment Station triaxial-cell design was modified, and the cell was fabricated at the University of Illinois. Because of the large maximum size of the aggregate to be tested, the cell was constructed to have an inside diameter of 279 mm (11 in) so that 203-mm (8-in) diameter cylindrical specimens 406-mm (16-in) high could be tested.

Air was used to supply the confining pressure and was not cycled during the tests. The repeated deviator stress was applied by a hydraulically actuated piston; control was by a closed-loop electronic system. Input for the load control was provided by a function generator connected through electronic controls to the hydraulic actuator.

To satisfy the constraints of the equipment and to approximate actual in-service conditions, a frequency of 50 cycles/min and a haversine load pulse of 0.15-s duration were selected.

The spacing of trucks on conventional railroad rolling stock varies, and the pulse caused by the second truck of one car overlaps that of the first truck on the following car. These two factors cause problems in analyzing the in-service frequency and duration of loading of ballast. The frequency (50 cycles/min) and duration of load (0.15 s) selected are equivalent to a train speed of approximately 129 km/h (80 mph).

The triaxial chamber pressure was monitored by a gauge on the air supply line. The axial load was monitored by a load cell mounted between the hydraulic actuator and the loading rod. A high-speed strip chart recorder was used to record the output of the load-cell amplifier.

Two methods were used to monitor the axial deformations. The primary method was provided by a linear variable differential transformer (LVDT) mounted at the top of the hydraulic actuator. The LVDT signal was observed on a strip chart recorder. In addition, two electronic-optical scanners were used to measure the vertical motion of targets placed at the upper and lower

quarter points of the specimen. The targets consisted of one black and one white rectangular strip, 32×64 mm (1.5×2.5 in) each, that were held to the specimen membrane by double-sided tape. The chamber pressure ensured that the membrane was molded firmly to the specimen, thereby eliminating slippage between the specimen and the targets. The optical scanners were rezeroed periodically, and the change in the distance between the two heads was observed on a dial indicator and thus provided a backup for the LVDT.

TEST PROCEDURE

Because one of the objectives of this study was the determination of the effects of gradation and maximum size on ballast behavior, two different sample sizes were used. Samples 152 mm (6 in) in diameter were used for the no. 5 ballast gradation specimens, which had a maximum particle size of 38 mm (1.5 in), and samples 203 mm in diameter were used for the no. 4 ballast-gradation specimens, which had a maximum particle size of 51 mm (2 in). Thus, the ratio of the diameter of the sample to the maximum particle size was always 4. All samples had a height-to-diameter ratio of 2:1 or more to minimize the end effects on deformation measurements.

To minimize segregation and to ensure gradation control, each specimen was weighed out by thirds for each of the size fractions, and each third was placed in a separate container. The material then was washed to remove the fines, drained, and compacted.

Because of the open-graded nature of ballast, vibratory compaction similar to that described by Rostron and others (12) was used. To determine the compaction characteristics of the aggregates and whether they were degraded during compaction, no. 5 ballast-gradation limestone was compacted in the standard split mold for various times by using the vibratory compactor. The results showed that there was little increase in density for compaction times greater than 45 s and that the gradation change (aggregate degradation) due to compaction was extremely small. For example, the amount of material passing the 4.75-mm sieve increased from 2.5 percent to 4.0 percent after compaction of 45 s/layer, and the increase was less (less than 1 percent) for shorter compaction times.

Because densities generally are not specified when ballast is placed, no attempt was made to attain a predetermined specimen density. Instead, three degrees of compaction were used. For the low-density specimens, each layer of aggregate was placed and hand rodded 10 times; for the medium-density specimens, each layer was compacted for 5 s by using the vibratory hammer; for the high-density specimens, each of the three layers was vibrated for 45 s.

The compaction was carried out in a split mold clamped to the sample base. A rubber membrane was used inside the mold, and a vacuum was applied through the attached tubing to hold the membrane against the mold. After compaction, the height of the specimen was recorded, the mold was removed, and a second membrane was placed over the specimen because, almost without exception, the original membrane was punctured during compaction.

The test specimen properties are given in Table 2.

All of the test specimens were conditioned for 5000 cycles at a deviator stress of 310 kPa (45 lbf/in^2) and a confining pressure of 103 kPa (15 lbf/in^2). The permanent deformations recorded by the LVDT method were divided by the specimen height to obtain the strains at 10, 100, 1000, and 5000 cycles. The plastic-strain data obtained during this conditioning phase have not been influenced by any stress-history effects and are probably the most representative results for making direct comparisons.

After the conditioning phase, the stress ratio was increased and 5000 additional load cycles were applied. Typical stress levels applied are given below (1 kPa = 0.145 lbf/in^2).

Deviator Stress (kPa)	Confining Pressure (kPa)
138	34
414	103
207	34
620	103
827	103

The stress state was increased until the sample failed or showed noticeable lateral bulging. The sample height at the beginning of each 5000 load cycles was taken as the gauge length for the strain determination.

RESULTS

The purpose of this part of the research was to determine the effects of material type and gradation on the plastic-strain behavior under repeated-load conditions of a variety of types of aggregates. The effects of stress history, degree of compaction, and stress level were also considered. [A more detailed description of these results has been given by Knutson and others (13).]

Linear regression analyses were used to develop relationships between the plastic strain and the corresponding number of loading cycles. Three types of regression analyses were used: arithmetic (strain versus number of cycles), semilog (strain versus logarithm of number of cycles), and log-log (logarithm of strain versus logarithm of number of cycles). In general, the best results

Table 1. Results of characterization tests.

Material	Gradation	Particle Index	Specific Gravity	Los Angeles Abrasion Loss (%)	Gradation Parameter	Flakiness Index	Soundness Loss (%)	Crushing Value
Limestone	No. 5	13.80	2.626	34.2	1.846	17.52	12.3	22.7
	No. 4	13.75	2.626	34.2	1.074	16.78	18.5	22.7
	Well graded	14.09	2.626	34.2	2.039	17.33	15.3	22.7
Granitic gneiss	No. 4	13.45	2.679	34.7	1.074	14.39	0.25	26.1
Blast-furnace slag	No. 4	15.68	2.133	37.8	1.074	3.59	0.75	37.3
Basalt	No. 5	15.10	2.775	12.3	1.846	19.69	6.14	12.4
	No. 4	15.40	2.775	12.3	1.074	17.33	4.93	12.4
	Well graded	14.83	2.775	12.3	2.039	16.11	4.86	12.4
Gravel	No. 5	7.54	2.658	23.2	1.846	4.03	5.06	13.8
	No. 4	10.17	2.658	23.2	1.074	5.79	5.78	13.8
	Well graded	8.86	2.658	23.2	2.039	6.58	5.84	13.8
Crushed gravel	No. 4	11.85	2.678	28.0	1.074	10.12	7.45	20.0
Kansas test-track blast-furnace slag	No. 5	14.10	2.521	26.7	1.846	5.39	0.87	25.2

Table 2. Properties of test specimens.

Material	Gradation	Compaction		Void Ratio
		Level	Density (kg/m³)	
Limestone	No. 5	Medium	1653	0.59
	No. 4	Low	1424	0.84
	No. 4	Medium	1536	0.71
	No. 4	High	1586	0.66
	Well graded	Medium	1792	0.46
Granitic gneiss	No. 4	Low	1490	0.76
	No. 4	Medium	1562	0.71
	No. 4	High	1639	0.63
Blast-furnace slag	No. 4	Low	1068	1.00
	No. 4	Medium	1137	0.87
	No. 4	High	1173	0.82
Basalt	No. 5	Medium	1722	0.63
	No. 4	Medium	1527	0.82
	Well graded	Medium	1853	0.50
Gravel	No. 5	Medium	2030	0.31
	No. 4	Low	1640	0.62
	No. 4	Medium	1722	0.54
	No. 4	High	1976	0.48
	Well graded	Medium	2110	0.26
Crushed gravel	No. 4	Medium	1615	0.66
Kansas test-track blast-furnace slag	No. 5	Medium	1585	0.59

Note: 1 kg/m³ = 0.062 lb/ft³.

were those obtained for plastic strain versus the logarithm of number of cycles. The slopes obtained from the linear regression equations were used in attempts to further analyze plastic-strain behavior. Because strain is zero at the beginning of testing and because only the trend of plastic strain is of practical importance, the equation intercepts were not included in the analyses.

The slopes and correlation coefficients of the data obtained at a repeated deviator stress of 310 kPa and a confining pressure of 103 kPa are summarized in Table 3. The slopes and correlation coefficients of the semilog analyses of the data obtained at the other stress levels are summarized in Table 4.

In all cases, an increase in the stress ratio (repeated deviator stress divided by confining pressure) resulted in an additional plastic-strain accumulation during the 5000 cycles. However, the stress ratio by itself cannot be used to predict adequately the plastic-strain behavior of ballast materials. Both the repeated deviator stress and the confining pressure must be considered together; for example, the application of a stress ratio of 4 and a confining pressure of 34 kPa (5 lbf/in²) is usually much less severe than is the same stress ratio and a confining pressure of 103 kPa.

The possibility of links between plastic-strain behavior and material properties was investigated by correlation analyses between the various plastic-strain parameters and the results of the material characterization tests.

There were significant ($\alpha = 0.05$) correlations between the four plastic strain values (10, 100, 1000, 5000 cycles) and both the initial density (inverse) and the void ratio. The strain value recorded after 5000 cycles also showed a significant correlation with the results of the crushing value tests. None of the other variables showed any significant level of correlation. The dependency of plastic strain on initial void ratio or on density (or porosity) reported by ORE (7) thus is reinforced.

To eliminate the effects of gradation, a correlation analysis was performed using only the results for the no. 4 ballast-gradation specimens. The significant correlations were much the same as in the previous analysis.

In the analysis of the no. 4 ballast-gradation specimens, not all of the material types were weighted equally; another analysis therefore was conducted that used only the six medium-density no. 4 gradation specimens. In this analysis, the particle index correlated significantly with two of the strain readings, but the results were not consistent. The results of the analysis, in general, were too erratic to draw any conclusions.

To include the effects of gradation, three gradation levels of each of three types of material (limestone, basalt, and gravel) were used in another correlation analysis. The results showed significant ($\alpha = 0.05$) correlations between the gradation and the recorded strain values. The relationship was inverse [which means that the strains were highest for the more uniformly graded (no. 4) specimens]. The slopes of the semilog relationships for all of the specimens (for a stress level of 310/103) showed significant ($\alpha = 0.05$) correlations between the strain and the Los Angeles abrasion number, density, void ratio, crushing value, and gradation parameter.

In general, none of the analyses considered resulted in consistently significant ($\alpha = 0.05$) correlations between the various strain parameters and the specimen properties. However, there was an inverse relationship between plastic strain and initial void ratio in several of the analyses. Because of the lack of consistent results and because of the difficulty in establishing causal relationships through correlation studies, an analysis of variance was used to assess possible differences among the plastic-strain responses of the samples due to gradation, compaction, and material effects.

Because changes in gradation affect both the compaction characteristics and the maximum theoretical density of aggregates, gradation effects on plastic-strain behavior are difficult to demonstrate quantitatively.

To show quantitatively the effects of gradation, a randomized complete block analysis was made of the plastic-strain data recorded at 10, 100, 1000, and 5000 cycles for several stress levels. Three types of material (limestone, basalt, and gravel) and three gradation levels of each were included. In only two cases were the strains significantly different.

Because of economic considerations, a ranking of ballast according to type of material (slag, granite, etc.) is desirable. The plastic-strain results of two no. 4 gradation gravel specimens compacted with the same effort—one containing rounded material and the other containing crushed particles—showed that the crushed gravel sample accumulated more plastic strain. However, for the same compactive effort, the uncrushed gravel attained a density 1.1 kN/m³ (7 lbf/ft³) greater than did the crushed material, which makes a direct comparison difficult.

A randomized complete block analysis was made to evaluate the effects of the material properties on the plastic strain after 10, 100, 1000, and 5000 cycles for various stress levels. Three materials (limestone, basalt, and gravel) and three gradations of each were considered in the analysis. No significant ($\alpha = 0.05$) differences were found among the strain readings with regard to material type.

A completely randomized design analysis was made to evaluate the effects of the various material properties on plastic-strain behavior. The stress-level values and the material properties (particle index, specific gravity, Los Angeles abrasion number, flakiness index, soundness loss, and crushing value) were included as the variables. The results show no significant differences for the effects of any of the material properties between the two stress level groups.

The effects on plastic-strain behavior of various levels of compaction were evaluated through the use of a randomized complete block analysis of the semilog regression equation slopes of five material types (limestone, basalt, granite, slag, and gravel) and three levels each of compactive effort. There were significant ($\alpha = 0.05$)

Table 3. Regression analyses of plastic strain during conditioning phase.

Material	Gradation	Compaction Level	Type of Regression Analysis: Arithmetic Slope	Arithmetic Correlation Coefficient	Semilog Slope	Semilog Correlation Coefficient	Semilog Standard Error of Estimate	Log-Log Slope	Log-Log Correlation Coefficient
Limestone	No. 5	Medium	0.0001	0.999[a]	0.219	0.943[a]	0.042	0.209	0.977[a]
	No. 4	Low	0.0008	0.612	1.470	0.981[a]	0.382	0.372	0.874[a]
	No. 4	Medium	0.0003	0.845[a]	0.678	0.995[a]	0.075	0.304	0.984[a]
	No. 4	High	0.0000	0.902[a]	0.088	0.967[a]	0.028	0.162	0.996[a]
	Well graded	Medium	0.0002	0.767	0.619	0.996[a]	0.057	0.284	0.932[a]
Granitic gneiss	No. 4	Low	0.0004	0.715	1.120	0.982[a]	0.210	0.296	0.942[a]
	No. 4	Medium	0.0002	0.800[a]	0.632	0.999[a]	0.029	0.276	0.969[a]
	No. 4	High	0.0001	0.942[a]	0.218	0.952[a]	0.077	0.177	0.991[a]
Blast-furnace slag	No. 4	Low	0.0005	0.727	1.260	0.964[a]	0.348	0.127	0.930[a]
	No. 4	Medium	0.0004	0.876[a]	0.797	0.985[a]	0.153	0.304	0.994[a]
	No. 4	High	0.0005	0.963[a]	0.936	0.879[a]	0.557	0.501	0.957[a]
Basalt	No. 4	Medium	0.0001	0.657	0.171	0.988[a]	0.107	0.168	0.938[a]
	No. 4	Medium	0.0003	0.791	0.668	0.999[a]	0.028	0.221	0.981[a]
	Well graded	Medium	0.0001	0.773[a]	0.327	0.997[a]	0.029	0.224	0.979[a]
Crushed gravel	No. 4	Medium	0.0002	0.846[a]	0.513	0.995[a]	0.058	0.202	0.995[a]
Gravel	No. 5	Medium	0.0001	0.795	0.297	0.995[a]	0.033	0.248	0.984[a]
	No. 4	Low	0.0003	0.796[a]	0.727	0.998[a]	0.045	0.160	0.988[a]
	No. 4	Medium	0.0002	0.923[a]	0.391	0.984[a]	0.089	0.265	0.997[a]
	No. 4	High	0.0000	0.854[a]	0.023	0.994[a]	0.003	0.111	0.999[a]
	Well graded	Medium	0.0000	0.840[a]	0.152	0.994[a]	0.018	0.128	0.999[a]
Kansas test-track blast-furnace slag	No. 5	Medium	0.0001	0.732[a]	0.151	0.999[a]	0.066	0.205	0.969[a]

[a]Significant at $\alpha = 0.05$.

Table 4. Regression analyses of plastic strain at stress levels other than conditioning.

Material	Gradation	Compaction Level	Stress Level (kPa/kPa)	Semilog Regression Results: Slope	Correlation Coefficient	Standard Error of Estimate
Limestone	No. 5	Medium	414/103	0.044	0.832	0.042
			207/34	0.021	0.901	0.014
			276/34	0.123	0.875[a]	0.090
			620/103	2.876	0.860[a]	1.716
	No. 4	Low	207/103	0.010	0.945[a]	0.004
			138/34	0.045	0.931[a]	0.019
			414/103	2.207	0.935[a]	0.969
			207/34	0.164	0.908[a]	0.083
		Medium	207/103	0.005	0.984[a]	0.001
			138/34	0.020	0.997[a]	0.002
			414/103	0.776	0.970[a]	0.232
			207/34	0.150	0.837[a]	0.117
		High	138/34	0.005	0.977[a]	0.001
			414/103	0.256	0.895[a]	0.126
			207/34	0.068	0.976[a]	0.017
			276/34	3.436	0.826[a]	1.985
	Well graded	Medium	138/34	0.014	0.932	0.006
			414/103	0.399	0.907[a]	0.202
			207/34	0.043	0.893[a]	0.024
			276/34	0.288	0.856[a]	0.190
			620/103	1.911	0.947[a]	0.698
			827/103	3.169	0.804	1.537
Granitic gneiss	No. 4	Low	138/34	0.052	0.998[a]	0.004
			414/103	0.107	0.967[a]	0.031
			207/34	0.016	0.993[a]	0.002
			276/34	0.452	0.883[a]	0.264
			620/103	7.500	0.777	3.924
		Medium	138/34	0.016	0.962[a]	0.005
			414/103	0.233	0.933[a]	0.079
		High	207/103	0.028	0.984[a]	0.004
			138/34	0.036	0.937	0.020
			414/103	0.243	0.902[a]	0.118
			207/34	0.051	0.897[a]	0.027
			276/34	0.125	0.892[a]	0.070
			620/103	2.478	0.930[a]	0.942
Chicago blast-furnace slag	No. 4	Low	138/34	0.061	0.843[a]	0.043
			414/103	1.444	0.872[a]	0.881
			207/34	0.163	0.811[a]	0.128
			276/34	0.461	0.778[a]	0.365
			620/103	2.706	0.849	1.458
		Medium	138/34	0.036	0.821[a]	0.027
			414/103	2.091	0.848	1.421
			207/34	0.231	0.819[a]	0.185
			276/34	0.514	0.792	0.430
			620/103	5.878	0.828[a]	2.742
		High	138/34	0.020	0.915[a]	0.010
			414/103	0.956	0.897[a]	0.512
			207/34	0.088	0.830[a]	0.064
			276/34	0.441	0.778	0.390
			620/103	3.298	0.876[a]	1.397

Note: 1 kPa = 0.145 lbf/in^2.

[a]Significant at $\alpha = 0.05$.

Table 4. Continued.

Material	Gradation	Compaction Level	Stress Level (kPa/kPa)	Semilog Regression Results: Slope	Correlation Coefficient	Standard Error of Estimate
Basalt	No. 5	Medium	414/103	0.076	0.921[a]	0.035
			207/34	0.015	0.996[a]	0.001
			276/34	0.104	0.958[a]	0.034
			620/103	0.547	0.962[a]	0.169
			827/103	0.936	0.959[a]	0.303
	No. 4	Medium	138/34	0.019	0.947[a]	0.008
			414/103	0.361	0.858[a]	0.235
			207/34	0.104	0.930[a]	0.049
			276/34	1.118	0.932[a]	0.478
			620/103	2.157	0.990[a]	0.313
	Well graded	Medium	138/34	0.010	0.939[a]	0.004
			414/103	0.135	0.948[a]	0.049
			207/34	0.018	0.945[a]	0.007
			276/34	0.048	0.910[a]	0.024
			620/103	0.691	0.965[a]	0.205
			827/103	0.745	0.940[a]	0.299
Crushed gravel	No. 4	Medium	138/34	0.023	0.934[a]	0.010
			414/103	0.451	0.890[a]	0.252
			207/34	0.116	0.903[a]	0.061
			276/34	2.064	0.850[a]	1.223
Gravel	No. 5	Medium	414/103	0.019	0.920[a]	0.009
			207/34	0.210	0.788	0.180
			276/34	3.075	0.793	1.501
	No. 4	Low	207/103	0.005	0.989[a]	0.001
			138/34	0.068	0.882[a]	0.039
			414/103	0.557	0.930[a]	0.203
		Medium	207/103	0.004	0.960[a]	0.001
			138/34	0.039	0.930[a]	0.017
			414/103	0.467	0.871[a]	0.286
			207/34	0.415	0.811[a]	0.326
			276/34	2.156	0.788	1.217
		High	138/34	0.011	0.974[a]	0.003
			414/103	0.058	0.941[a]	0.023
			207/34	0.992	0.866[a]	0.552
			276/34	5.063	0.946	1.098
	Well graded	Medium	138/34	0.008	0.915[a]	0.005
			414/103	0.102	0.907[a]	0.052
			207/34	0.034	0.912[a]	0.017
			276/34	1.244	0.700	1.368
			620/103	0.739	0.965[a]	0.216
			827/103	1.963	0.845[a]	1.141
Kansas test-track blast-furnace slag	No. 5	Medium	414/103	0.015	0.910[a]	0.007
			207/34	0.035	0.957[a]	0.010
			241/34	0.057	0.864[a]	0.036
			276/34	0.046	0.822[a]	0.035
			345/34	0.306	0.895[a]	0.169
			517/103	0.036	0.838[a]	0.031
			620/103	0.081	0.794[a]	0.068
			723/103	0.361	0.804[a]	0.260

Note: 1 kPa = 0.145 lbf/in^2.
[a]Significant at $\alpha = 0.05$.

differences among the slopes for the three levels of compaction. Further analysis by using Duncan's multiple range test showed that there was no significant ($\alpha = 0.05$) difference in slope between the high- and medium-compactive-effort samples, but both were significantly different from the low-compactive-effort samples. The lowest slope values were those obtained for the high-density samples.

SUMMARY

These analyses have shown that the most important factors influencing the permanent-deformation behavior of ballast are the number of repetitions, the degree of compaction, and the stress level. As previous studies have also shown, the increase in plastic strain is generally inversely proportional to the number of loading cycles. In every case, the permanent deformation was least for the specimens compacted by using the greatest effort. The stress-level effects are more difficult to discern because both the deviator stress and the confining pressure, not merely the ratio of the two, must be considered. However, the permanent-strain results agree well with the concepts of Lade and Duncan (6); large strains accumulated during primary loading, but almost no plastic strain occurred during reloading or during loading at reduced stress levels.

The effects on permanent deformation of gradation are less important than are those of the parameters discussed above. In general, the no. 4 ballast-gradation specimens tended to resist permanent deformation less than did the no. 5 specimens or the "well-graded" materials.

The effects of material properties (such as particle index and flakiness index) were not consistent, and therefore no conclusions are made with respect to such properties.

No other specimen parameter is as important in influencing the permanent strain behavior as is degree of compaction.

ACKNOWLEDGMENT

This paper is based on the results of a study of ballast and foundation materials conducted by the Transportation Research Laboratory of the Department of Civil Engineering, University of Illinois at Urbana-Champaign. The research was sponsored as a subcontract between the Association of American Railroads Research and Test Department and the University of Illinois that is

part of a larger cooperative effort between the Federal Railroad Administration and the Association of American Railroads. This paper represents our views and positions and does not necessarily reflect those of the Federal Railroad Administration or the Association of American Railroads.

REFERENCES

1. R. B. Peck. First Progress Report of the Joint Investigation of Methods of Roadbed Stabilization. Univ. of Illinois, Urbana-Champaign, Bulletin, Vol. 43, No. 66, Reprint Series No. 34, 1946.
2. J. H. Haynes and E. J. Yoder. Effects of Repeated Loading on Gravel and Crushed-Stone Base-Course Materials Used in the AASHO Road Test. HRB, Highway Research Record 39, 1963, pp. 82-96.
3. R. G. Hicks and C. L. Monismith. Factors Influencing the Resilient Response of Granular Materials. HRB, Highway Research Record 345, 1971, pp. 15-31.
4. R. D. Barksdale. Repeated-Load Test Evaluation of Base-Course Materials. Georgia Institute of Technology, Atlanta, 1972.
5. J. J. Allen. The Effects of Nonconstant Lateral Pressures on the Resilient Properties of Granular Materials. Univ. of Illinois, Urbana-Champaign, PhD thesis, 1973.
6. P. V. Lade and J. M. Duncan. Stress-Path Dependent Behavior of Cohesionless Soil. Journal of the Geotechnical Engineering Division, Proc., ASCE, Vol. 102, No. GT 1, 1976, pp. 51-68.
7. Stresses in the Rails, the Ballast, and in the Formation Resulting From Traffic Loads: Summary of Results Given in Reports 1-12. Office for Research and Experiments of the International Union of Railways, Utrecht, Netherlands, Rept. D 71/RP 13, 1970.
8. Annual Book of Standards. ASTM, 1976.
9. Standard Specifications for Transportation Materials and Methods of Sampling and Testing. AASHTO, 1974.
10. S. B. Hudson and H. F. Waller. Evaluation of Construction Control Procedures: Aggregate-Gradation Variations and Effects. NCHRP, Rept. 69, 1969.
11. British Standard 812. In Methods for Sampling and Testing of Mineral Aggregates, Sands, and Filters. British Standards Institution, 1967.
12. J. P. Rostron and others. Density Standards for Field Compaction of Granular Bases and Subbases. NCHRP, Research Results Digest 57, 1974.
13. R. M. Knutson and others. Materials Evaluation Study: Ballast and Foundation Materials Research Program. U.S. Department of Transportation, Rept. FRA-ORD-77-02, 1977.

Ballast and Subgrade Response to Train Loads

Ernest T. Selig, Department of Civil Engineering, State University of New York, Buffalo
Andrew Sluz, Transportation Systems Center, Cambridge, Massachusetts

Ballast and subgrade play major roles in the maintenance life of track structures because they are the source of the cumulative permanent deformation associated with the deterioration of surface and line. Ballast is also the principal means of correcting for this deterioration, which is caused by traffic and environmental factors. Better methods are still needed for the prediction of the effects of the controlling parameters on track performance for more rational track design and maintenance planning. The purpose of this paper is to provide a better understanding of these problems and describe progress being made toward their solution. The functions of ballast and subgrade are briefly discussed, and the mechanisms of permanent deformation are described. Newly developed or improved methods to measure the in situ physical state of ballast are presented, and examples of results from field tests are given. The capabilities of existing analytical track structure models for the prediction of track deterioration are assessed. New instrumentation techniques used for measuring the dynamic and permanent strains and deformations in ballast and subgrade are described. Finally, the characteristics of the stress, strain, and deformation in ballast and subgrade are illustrated with results of both analytical and experimental studies.

The type and condition of the ballast and the subgrade are key factors in the performance of a track structure. During the service life of a track, permanent strains accumulate in its substructure and cause permanent deformation that is visible as deterioration of surface and line. This deterioration of the track geometry leads to decreased safety (including increased potential for derailments) and increased damage to equipment and lading unless additional track maintenance is provided or train speed (and hence service level) is reduced. During the past few decades, traffic loads have increased and, at the same time, economic factors have restricted the amount of maintenance that can be done each year. In practice, the maintenance cycle frequency is often dictated by factors such as the availability of money and equipment to do the required work rather than by the amount of track deterioration. Thus, U.S. railroads have had increasing difficulty in maintaining the high service level desired. A recent estimate of the dollar value of the maintenance deficit for all of U.S. railroads was reported by Ward (1) to be $10 billion.

Raymond (2) has reported that approximately 40 percent of the $100 million that Canadian railroads spend on track-structure maintenance relates to ballast maintenance alone. Therefore, it is a safe assumption that, at least in dollar value, both the ballast and the subgrade parts of the track substructure are important in the upkeep of the service level of the track.

Ballast maintenance is the means by which the deterioration of track geometry is controlled, irrespective of the driving forces behind the geometry changes. Whether the structural deficiency is in the ballast, the subgrade, or the track superstructure (the crossties

and up), or even if the track degradation has been caused by an overloading of the normal traffic-carrying capacity of the track, the correction is usually affected by reworking the ballast. However, reworking of the ballast, in turn, changes its physical state and leaves it prone to increased deformation and, hence, track settlement. This problem is compounded not only by the limited amount of maintenance funds but also by an insufficiency of tools for assessing the cause of the problem and optimizing the use of the maintenance funds. Unfortunately, there are no uniform criteria for maintenance that can be applied to railroads in general. Although many railroads do keep some type of maintenance records, the definition of performance for any particular section of track is usually dependent on the subjective evaluation of the track foreman.

Some solutions to these problems are being developed and becoming available as a result of research sponsored by the Federal Railroad Administration (FRA), Office of Research and Development. Performance data are being generated and measurement tools are being tested under FRA sponsorship at the facility for accelerated service testing (FAST) track at the Transportation Test Center in Pueblo, Colorado.

In addition to discussing the responses of ballast and subgrade to train loading, this paper will present some of the ideas that are currently being developed under FRA sponsorship, including concepts in performance assessment and methods of measuring the physical state of the substructure.

FUNCTIONS OF BALLAST, SUBBALLAST, AND SUBGRADE

Ballast is the selected material placed on top of the track subgrade to support the track structure. Conventional ballast is a coarse-sized, noncohesive, granular material, that usually has a uniform gradation. This aggregate layer, tamped under and around the ties, has several important functions:

1. It limits tie movement by resisting vertical, lateral, and longitudinal forces from the train and the track.
2. It reduces the stresses from train loads that are applied to the subgrade of the roadbed and thus limits permanent settlement.
3. It provides immediate water drainage from the track structure.
4. It helps to alleviate frost problems.
5. It facilitates maintenance surfacing and lining operations.
6. It retards the growth of vegetation and resists the effects of fouling from surface-deposited materials.
7. It provides support for the ties and the necessary resilience to absorb the shock from dynamic loads.

Traditionally, angular, crushed, hard stones and rocks, uniformly graded to drain freely, free of dust and dirt, and not prone to cementing action have been considered good ballast materials. However, availability and economic considerations have often been the prime factors considered in the selection of ballast materials. Thus, a wide variety of materials—such as crushed granite, basalt, limestone, slag, and gravel—have been used for ballast in the United States and Canada.

Subballast is material that is used as a transition layer between the upper layer of large-particle good-quality ballast and the lower layer of fine-graded subgrade. The subballast used in most new construction, in addition to fulfilling some of the functions of the ballast (particularly nos. 2, 4, and 7 cited above), is intended to prevent the mutual penetration or intermixing of the subgrade and the ballast and to reduce frost penetration into the subgrade. Any free-draining sand or gravel materials can serve as a subballast as long as they meet the proper requirements of a filtering material.

The mechanical properties of ballast result mostly from its physical state. Physical state is defined by (a) the in-place density and (b) the index properties of the individual material particles, such as size, distribution, shape, angularity, and hardness. The in-place density of ballast is the result of some type of compaction process. Typically, the resulting initial density is created by maintenance tamping and the subsequent density changes result from train traffic and environmental factors. Experience has shown that tamping does not produce a high degree of compaction, and there is clearly little control of geometry when compaction is achieved by train traffic. Therefore, consideration is now being given to additional compaction during maintenance by using special machines or new techniques.

The need for more information on the subject of ballast compaction has resulted in a research project at the State University of New York at Buffalo sponsored by the FRA. In this study the mechanics of ballast compaction and the optimization of the maintenance process by using compaction to improve the ballast physical state and reduce traffic-induced track settlement are being investigated.

Subgrade is the layer of material on which the ballast and subballast layers rest; it has the following functions and requirements.

1. It must support, without appreciable permanent deformation, the maximum dynamic, traffic-induced stresses transmitted through the ballast.
2. It must resist the cyclic stresses without excessive cumulative volume or strength reductions.
3. It must be nonfrost susceptible and volumetrically stable during cycles of wetting and drying.
4. It must resist softening that could cause pumping and penetration into the ballast.

The subgrade is a very important component in the track structure and has frequently been the cause of track failure and the development of poor track. Unfortunately, in existing track, the subgrade is not involved in the maintenance operation and little can be done to alter its characteristics without major track reconstruction, i.e., removal and replacement of track, ballast, and subballast.

The present state of the art of track design as it concerns the ballast and the subgrade is mostly empirical, and the factors that control performance are poorly understood. Reliance on past experience can be very misleading, because not only is the experience at a particular site a complex and unknown function of many factors, but the controlling factors are often not even adequately documented. For example, to assess the reasons why a particular section of track is in the poor-track category, it is necessary to know (a) the characteristics of the ballast and the subgrade, (b) the maintenance history (including frequency and type of operation), (c) the environmental history, and (d) the traffic history. Usually, only the last item is readily available, although the second and third can sometimes be estimated from records. Necessary information of the characteristics of the ballasts and subgrades of existing track, however, is practically nonexistent. Even the classification of these materials is in doubt, not to mention their physical state. Often,

knowledge of the present conditions of a site based on a field examination is all that is possible, because past records are not normally available.

MECHANISMS OF PERMANENT DEFORMATION

The major causes of track settlement can be grouped into two general categories: (a) repeated loading from rail traffic and (b) environmental factors such as moisture changes, frost action, and mechanical and chemical weathering. In addition, the subgrade, including the foundation soil strata, can undergo settlement because of consolidation over a period of time. Although this category is also important and deserves consideration, this paper will focus on the effects of traffic loading and related phenomena only.

Permanent deformation of track structure results from four basic mechanisms of ballast and subgrade mechanical behavior. The first is volume reduction or densification caused by particle rearrangement under the cyclic shear straining produced by repeated trainloads. The second is inelastic recovery on unloading or stress removal and is a function of both stress history and stress state. The third is volume reduction caused by particle breakdown from train loading or environmental factors. The fourth is subgrade penetration into ballast voids that allow the ballast to sink into the subgrade. The first two apply to both ballast and subgrade, but the third applies mainly to ballast and the fourth to subgrade.

Normally, ballast is initially open graded, which facilitates maintenance operations and allows free drainage. In service, the ballast gradation changes as a result of (a) mechanical particle degradation during construction and maintenance work and under traffic loading, (b) chemical and weathering degradation from environmental changes, and (c) migration of fine particles. As the ballast degrades, it loses its open-graded characteristics and, in some cases, cementing may occur, which produces a layer of undesirable rigidity and reduces resiliency.

Traffic-induced stresses at the ballast-subgrade interface may be high enough relative to the strength of the subgrade soil that the soil is squeezed into the voids in the ballast. Under repeated cycles of loading, the amount of intermixing may be substantial, particularly with soft soil conditions. Water is trapped in depressions that develop under the rail seat, and both drainage and drying are impeded by the fines in the ballast. Thus, the soft conditions and ballast fouling are extended and the track settlement is self-perpetuating. In existing track, this problem occurs most frequently at rail joints. In new construction and in major rehabilitation work, this source of track settlement can be reduced by the use of a layer of subballast or a filter fabric placed over the subgrade.

Ballast fouling can also be caused by internal abrasion of the ballast particles or by surface infiltration of fines. Whatever the cause, the track-supporting capability of such ballast decreases when it is wet and the permanent settlement under load increases. When the fouled ballast is dried, its resiliency decreases. In either case, maintenance operations to correct surface and line are inhibited.

Frost heaving may occur in subgrades and ballasts when fine-grained material in the track is wet and then freezes. Soils display volume changes during freezing and thawing, and significant volume increases occur when ice lenses develop. Differences in volume changes in the subgrade soil over short distances along or across the track can cause rough track.

The tamping process used in track maintenance is generally believed to loosen the ballast under a tie and decrease the density state that had developed over time under traffic loading. Tamping also leaves the crib ballast very loose. Loose crib ballast is a disadvantage because it does not contribute significantly to tie lateral resistance and because it reduces the supporting capacity of the ballast under the tie by providing less lateral confinement than does dense crib ballast. For this reason, machines to recompact the crib and shoulder ballast after tamping are now being considered in the United States and Canada to speed up the process of traffic-induced densification and to provide higher lateral track stability immediately after maintenance.

Very little direct evidence is available to support many of these conclusions because in situ methods of measuring the physical state of ballast have been inadequate. However, new or refined methods have recently been developed to provide tools for the study of the behavior of ballast. A few examples are shown in Figures 1 to 6 to illustrate some of the methods and the resulting observations; a detailed evaluation of the techniques is given elsewhere (3).

A device that measures the resistance of individual ties to lateral force is shown in Figure 1. This type of test is the only one extensively used in the past that provides a measure of the physical state of ballast. However, it is only an indirect test of physical state, its primary function having been to assess lateral track stability. Typical results that relate lateral force to displacement are shown in Figure 2. Crib and shoulder compaction following tamping significantly increases tie lateral resistance.

A device that measures ballast stiffness by means of the vertical settlement of a small loaded plate is shown in Figure 3. The 12.7-cm (5-in) diameter plate can be seated anywhere on the crib or shoulder surface or on the tie-bearing area after the tie is carefully removed. The preliminary field results (see Figure 4) show that there is a significant increase in stiffness in the compacted crib near the rail and a lesser, but still noticeable, increase beneath the tie.

A newly developed method for the measurement of the in-place density of ballast is illustrated in Figure 5. The results of one set of tests (see Figure 6) show the density increase achieved by applying crib and shoulder compaction after tamping compared with only tamping the ballast.

ANALYTICAL TRACK MODELS

The principal function of a track model is to interrelate the components of the track structure so that their complex interactions in determining the net effect on the stresses, strains, and deformations of the system of the traffic loads is properly represented. Such a model provides the foundation for predicting track performance and, therefore, the technical and economic feasibility of track design and maintenance procedures. Analyses are complicated, however, by the fact that the physical states of the ballast and the subgrade, but especially the ballast, change with time. Because maintenance life is measured in years, these long-term effects must be considered. Considerable effort has been devoted to the development of track models that could realistically represent the actual behavior of a track system subjected to various loading conditions. However, more research is needed for several reasons: (a) the difficulty of handling the complexities inherent to each component of the track structure and their interactions under loads, (b) the lack of adequate understanding of the ballast and subgrade behavior to define the model

requirements, (c) the lack of field data on track performance for validating the models, and (d) the high computer costs of running the more elaborate of the models.

Because a railroad track is generally subjected to three-dimensional loads, i.e., loads in vertical, lateral, and longitudinal directions, various analytical models have been suggested for each of these components of the track response or for multidimensional representations. However, the vertical behavior of the track structure has received the greatest attention. The following is a brief summary of the existing models for vertical-response analysis of conventional railroad track.

Based on the theory of a continuous beam on an elastic foundation, Talbot's work (4) was a significant contribution to understanding the behavior of a railway track system under vehicle loading. The concept of "track foundation modulus" was introduced, and mathematical formulations were developed for calculation of the deflection and moment in the rail. Clarke (5, 6) has summarized this approach to present a basis for track design procedures. However, this theory does not include several important factors that are known to affect the stresses and deflections in railroad track, such as longitudinal loads from thermal stresses, a restoring moment proportional to the rotation of the rail and ties, the eccentricity of the vertical load on the rail head, or any track-dynamic effects. In addition, a rather significant limitation to the approach is that it does not adequately model the stress-strain behavior of the ballast and the subgrade.

Figure 1. Apparatus for determination of lateral resistance of individual ties.

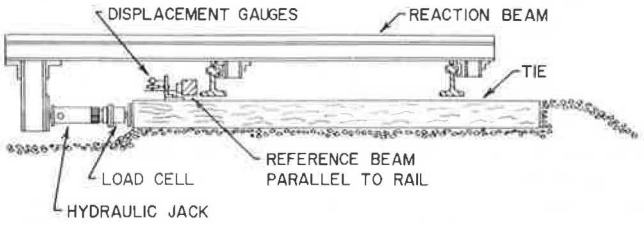

Figure 2. Effect on lateral resistance of crib and shoulder compaction after maintenance tamping: wooden tie in limestone ballast.

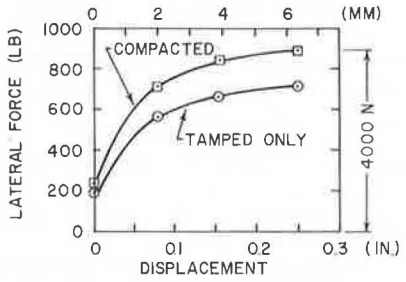

Figure 3. Apparatus for determination of ballast stiffness by plate-load method.

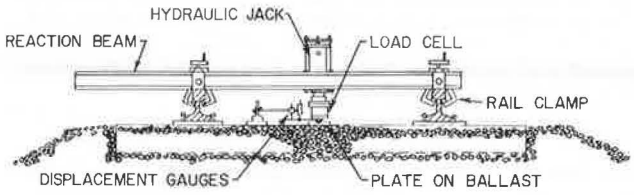

Figure 4. Effect on ballast bearing resistance of crib and shoulder compaction after maintenance tamping of limestone ballast.

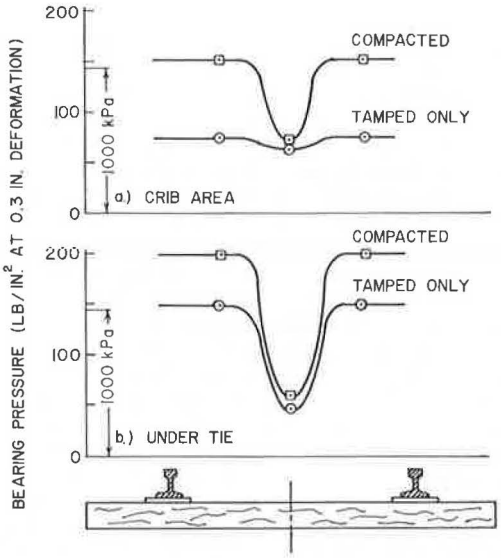

Figure 5. Apparatus for determination of ballast density by water-replacement method.

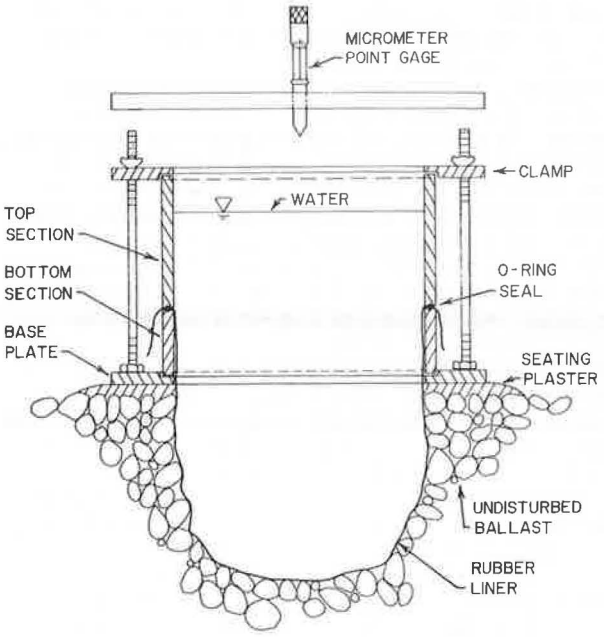

Figure 6. Effect on ballast density of crib and shoulder compaction after maintenance tamping of limestone ballast.

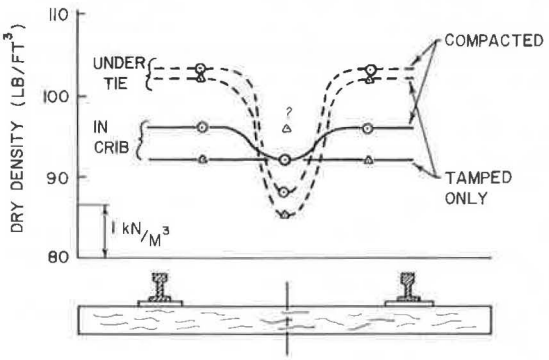

Meacham and others (7, 8) and Prause and others (9) have attempted to overcome some of the limitations of the earlier beam-on-elastic-foundation approaches by developing a theoretical method for the determination of the track-modulus value. In this method, each component of track structure is represented by a series of elastic springs, and the spring stiffnesses are computed by considering various track parameters (such as rail type, tie type, ballast depth, ballast type, subgrade type, and tie spacing).

The finite-beam-on-elastic-foundation approach is basically similar to the above theories, except that it considers the tie as a finite beam resting on an elastic (Winkler-type) foundation as the representation of the response of a tie resting on the ballast. The approach has been extensively studied by Hetenyi (10), and various analysis methods for the solution have been presented. For example, Barden (11) has considered a nonuniform foundation modulus, and Harrison and others (12) have included both a nonuniform beam section and a nonuniform foundation. An approximate analytical method was developed that makes assumptions about the distribution of wheel load over the rail and across the ties. The vertical stress distribution with depth in the ballast and subgrade layers under any given tie is then computed by using the Boussinesq theory. Ireland (13) has presented a design chart for ballast-subballast depth selection versus cohesive strength of subgrade soil by using this approach.

An approach has been developed at the Association of American Railroads that uses Burmister's multilayer theory for the ballast and subgrade and a structural model for the rail-tie interaction. The contact between a tie and the ballast is represented by a series of circular areas that have uniform pressure. The superstructure and the substructure models were then combined and extended to form the model termed MULTA (14). This is a three-dimensional model; however, the properties within any layer are constant and cannot be varied with horizontal position.

Finite-element methods have also been used for track-structure analysis. Lundgren and others (15) have developed a two-dimensional system by assuming plain-strain behavior of a longitudinal section of unit thickness along the vertical centerline of the rail. Svec and others (16) used a three-dimensional model that represents a detailed description of the physical system. The rail-tie system was added to the model as simple beams, and nonlinear mechanical properties of ballast, subballast, and subgrade were obtained from laboratory tests. One feature of the procedure was the representation of the ballast and subballast as no-tension materials. However, the model did not have clearly defined failure criteria.

Another finite-element model—ILLI-TRACK—has been developed at the University of Illinois (17). This is not a three-dimensional model but consists essentially of two two-dimensional models, one transverse and the other longitudinal, and uses the output from the longitudinal model as the input to the transverse model. This gives a three-dimensional effect at less computer cost than a three-dimensional model. Nonlinear mechanical properties for the materials were obtained in the laboratory from repeated-load triaxial tests. An incremental load technique was used to affect a solution. Explicit failure criteria were developed for the ballast, subballast, and subgrade material. However, the model does not prevent tension from being transferred across the rail base into the tie plate, and further study is needed to determine whether the combined two-dimensional models accurately represent three-dimensional physical conditions. Certainly, the three-dimensional qualities of track structure must be fully accounted for if the behavior of a track system is to be successfully predicted by using finite-element models.

The mathematical models developed for the prediction of track performance under dynamic loads have been limited almost entirely to recoverable deformations; thus, they do not adequately represent the factors involved in maintenance-life prediction. However, even the properties associated with recoverable deformation do not fully represent the stress-state-dependent behavior of ballast and soil under cyclic loads. Although there has recently been considerable study of the cyclic behavior of these materials, measures such as resilient modulus should be designated as cyclic-index properties rather than as behavioral properties, because they represent only a few special stress paths and cannot be used without a factor that compensates for the effect of stress path.

Currently, the approach to the prediction of permanent deformation of track caused by ballast and subgrade behavior is patterned after methods used in highway flexible-pavement design (18). An elastic track model is used to predict the stresses in the ballast and subgrade from traffic loads, and repeated-load triaxial tests are used to determine limiting the threshold stress and cumulative strain as a function of confining pressure and number of cycles of deviator stress. Repeated loads are started from a zero load, increased to some predetermined magnitude, and then decreased to zero, thus never putting the sample in extension in the axial direction. The process is repeated until either the desired number of cycles or a limiting permanent strain is reached. Track settlement is predicted by summing the inelastic strains from the triaxial tests for the stress conditions determined from the elastic model.

MEASURED AND PREDICTED RESPONSES

The nature of the recoverable deformations of ballast and subgrade, as well as the stresses and strains in these materials from traffic loading, have been predicted by using the various available track analytical models. These response parameters have also been determined experimentally on actual track structures. The resulting data have been used not only to study the track behavior, but also to evaluate the analytical models. However, the difficulty of measuring stresses and strains, particularly in ballast, has greatly restricted the amount of such data that has been obtained. The examples that follow will illustrate the general trends in both the analytical and the experimental studies.

Salem (19) has studied the vertical stress distributions in ballast and subgrade under statically loaded wooden ties in a series of laboratory tests that used various ballast depths, tie spacings, and types of ballast. Figure 7 (19) shows that chat, pit-run gravel, and crushed slag ballast produce nearly the same vertical pressure below the centerline of a single tie. Figure 8 (19) illustrates the average vertical pressure distribution when varying depths of ballast were used at a constant tie spacing. Figure 9 (19) illustrates the average vertical pressure distribution on the subgrade in a longitudinal direction parallel to the tie and below its centerline at a constant depth of ballast. These tests indicated that the depth of ballast needed to obtain a fairly uniform pressure on the subgrade equals the tie spacing minus 7.6 cm (3 in). A comparison of measured and calculated values also indicated that, although the shapes of the measured and the calculated curves are similar, the calculated pressures may be

considerably different than the measured data.

Analytical predictions of track responses have been made by using MULTA for a particular range of track parameters. This analysis assumed uniform properties under the tie, which is usually not the case, and the ballast was assumed to be much stiffer than the subgrade. The following general trends were observed (14):

1. The maximum bending moments at the center of the tie decrease as the ballast depth increases. However, the maximum rail-seat bending moments increase by a small amount (approximately 5 percent) when the ballast depth increases from 31 to 91 cm (12 to 36 in).
2. The vertical rail displacement and the rail bending moment decrease and the rail-seat load increases as the ballast depth increases.
3. The deviatoric and bulk stresses at the middepth of the ballast decrease rapidly as the ballast-layer thickness increases. However, this decrease is a result of stress attenuation with depth. Because the rail-seat load and the maximum pressure at the bottom of the tie increase as the ballast depth increases, at a common depth in the ballast, the stresses should actually increase as the thickness of the ballast layer increases.
4. The maximum vertical stress on the subgrade surface and the stresses in the subgrade decrease

Figure 7. Vertical pressure distribution below centerline of a single tie.

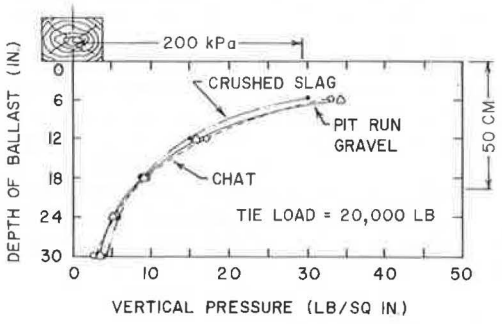

Figure 8. Average vertical pressure distribution on subgrade at different depths of ballast.

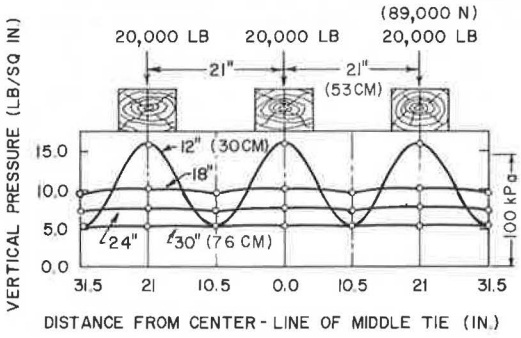

Figure 9. Average vertical pressure distribution below a single tie on subgrade at ballast depth of 45.7 cm.

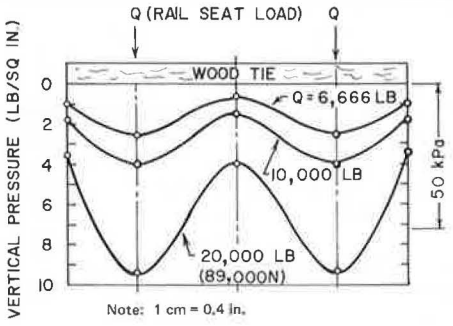

Figure 10. Typical gauge layout at FAST track.

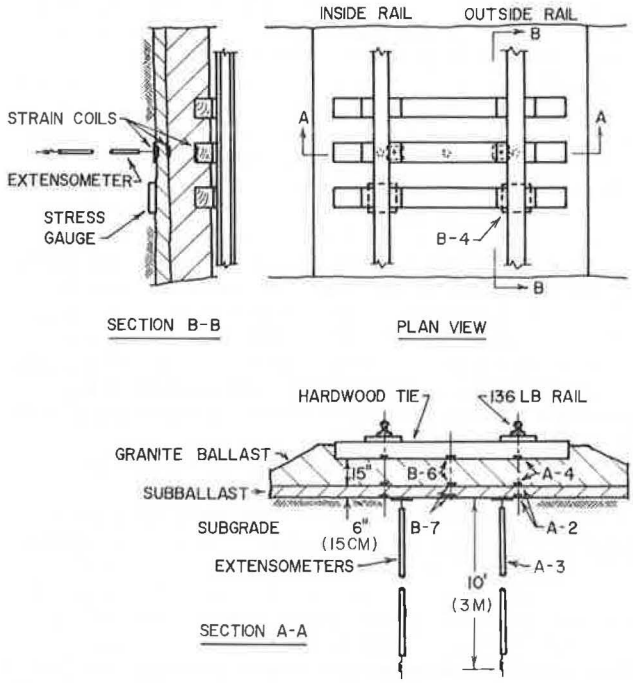

Figure 11. Dynamic response of inductance-coil instruments in FAST track section shown in Figure 10.

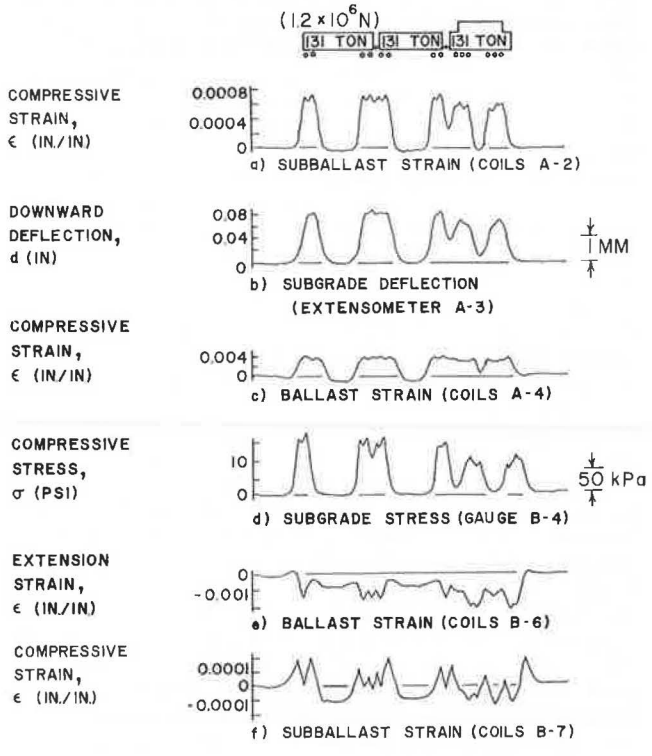

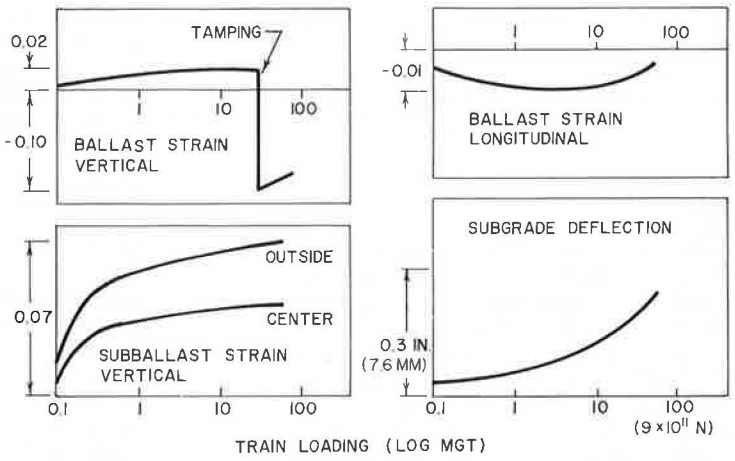

Figure 12. Cumulative substructure strain and displacement in FAST track section shown in Figure 10.

rapidly as the ballast-layer thickness increases. This trend is also largely a result of attenuation of stress with depth.

The most extensive track response measurement program undertaken to date is that being conducted at the FAST track. This program includes strains in the ballast and subballast, vertical stress at the subballast-subgrade interface, and vertical deformation of the subgrade surface relative to an anchor point approximately 305 cm (10 ft) below this surface. A typical layout is shown in Figure 10. The strain measurement method in particular is new and provides important data not previously available. This instrumentation is described in detail elsewhere (20).

A typical set of dynamic records is shown in Figure 11 and illustrates the elastic response when a three-car train passes slowly over the instrumented wooden tie section. The observations that can be made from these records include the following:

1. The permanent strain and deformation from one pass of the train is negligible compared with the elastic components.
2. The 119-metric ton (131-ton) hopper cars produce larger responses than does the 119-metric ton locomotive (because of the higher axle loads).
3. The variation in stress, strain, or deformation as each individual axle in a group passes over the gauge is small compared with the group average, indicating that the rail is distributing the axle loads over distances greater than the axle spacing.
4. The vertical strain in the ballast is mostly negative (extension) beneath the center of the tie at the centerline of the track. The extension and compression strains beneath this point in the subballast are approximately equal.
5. The subgrade deflection is always downward relative to the unloaded track position, and the subballast strains beneath the rail are essentially only compressive.
6. The ballast strains are extensional at the midpoint of the cars because of the spring-up of the rail. However, part of this extension could be a result of the lifting of the tie from the ballast because the top part of the strain gauge was attached to the tie rather than to the ballast surface.

Analytical models that directly predict permanent ballast strain and cumulative track settlement from traffic loading have not been developed. Also, very few experimental data are available from the field. The current project at FAST is providing important new information on this subject, however. Cumulative ballast and subballast strain and subgrade deflection have been measured as a function of total traffic load for a variety of track conditions. A typical set of results is shown in Figure 12 for one track section. Strain measurements of this type have not previously been available. The slopes of all of these curves decrease rapidly as the traffic increases but permanent subgrade settlement was still continuing to accumulate significantly even after 91 million gross metric tons (100 million gross tons) of loading.

CONCLUSIONS

A general understanding of the functions and behavior of ballast, subballast, and subgrade has been achieved. Analytical models exist for track structure that predict elastic response under train loading. A beginning has been made in obtaining needed field data on dynamic and permanent strains in the substructure. Field test methods are available to investigate the ballast physical state, and data are being obtained on operating track.

Continued development of analytical tools for the prediction of stress and strain (both elastic and inelastic) that are consistent with material behavior and track-structure boundary conditions is necessary. It is especially important to account for stress-state-dependent material behavior and the effects of the mechanisms that cause permanent deformation. Simultaneously, the collection of field data on track performance should be encouraged with emphasis on the behavior of ballasts and subgrades. The FAST track is currently the principal source of such information.

REFERENCES

1. E. J. Ward. Technology and Reviving the Railroads. Technology Review, July-Aug. 1976.
2. G. P. Raymond and O. Svec. Selection and Performance of Railroad Ballast. Paper presented at Symposium on Railroad Track Mechanics, Princeton Univ., NJ, April 21-23, 1975.
3. E. T. Selig, T. S. Yoo, and C. M. Panuccio. Mechanics of Ballast Compaction: Vol. 1—Field Methods for Ballast Physical-State Measurement. Transportation Systems Center, U.S. Department of Transportation, Cambridge, MA, Interim Rept., Nov. 1977.
4. A. N. Talbot. Stresses in Railroad Track. Repts. of Special Committee on Stress in Railroad Track, Proc., AREA, Vol. 19, 1918, pp. 873-1062; Vol.

21, 1920, pp. 645-814; Vol. 24, 1923, pp. 297-453; Vol. 26, 1925, pp. 1081-1245; Vol. 31, 1930, pp. 69-336; Vol. 35, 1934, pp. 66-308.
5. C. W. Clarke. Track Loading Fundamentals: 1. Railway Gazette, Vol. 106, No. 2, Jan. 11, 1957, pp. 45-48.
6. C. W. Clarke. Track Loading Fundamentals: 3. Railway Gazette, Vol. 106, No. 6, Feb. 8, 1957, pp. 157-160 and p. 163.
7. H. C. Meacham and others. Study of New Track-Structure Designs. Battelle Memorial Institute, Columbus, OH; U.S. Department of Transportation, Summary Rept., Aug. 20, 1968.
8. H. C. Meacham and others. Studies for Rail Vehicle Track Structures. Battelle Memorial Institute, Columbus, OH; Office of High Speed Ground Transportation, U.S. Department of Transportation, Rept. DOT-FR-9-0021, April 1970.
9. R. H. Prause and others. Assessment of Design Tools and Criteria for Urban Rail-Track Structure. Battelle Columbus Laboratories, OH; U.S. Department of Transportation, Final Rept. DOT-TSC-UMTA-74-5, April 1974.
10. M. Hetenyi. Beams on Elastic Foundations. Univ. of Michigan Press, Ann Arbor, 1946.
11. L. Barden. Distribution of Constant Pressure Under Foundations. Geotechnique, Vol. 13, No. 3, Sept. 1962, pp. 181-198.
12. H. B. Harrison. General Computer Analysis of Beams on Elastic Foundations. Proc., Institution of Civil Engineers, London, Vol. 55, Pt. 2, Sept. 1973, pp. 605-618.
13. H. O. Ireland. Railroad Subgrade Stresses. Proc., AREA, Bulletin 641, Jan.-Feb. 1973, pp. 382-386.
14. R. H. Prause and J. C. Kennedy. Parametric Study of Track Response and Performance. Battelle Columbus Laboratories, OH; U.S. Department of Transportation, Transportation Systems Center, Cambridge, MA, Sept. 1977.
15. J. R. Lundgren, G. C. Martin, and W. W. Hay. A Simulation Model of Ballast Support and the Modulus of Track Elasticity. Univ. of Illinois, Urbana-Champaign, Transportation Series, Vol. 4, Sept. 1970.
16. O. J. Svec, G. P. Raymond, K. Van Dalen, P. N. Gaskin, and K. R. Davies. Analytical and Experimental Investigation of a Rail Track Structure. Paper presented at 2nd Symposium on Applications of Solid Mechanics, McMaster Univ., Hamilton, Ont., June 1974.
17. Q. L. Robnett, M. R. Thompson, R. M. Knutson, and S. D. Tayabji. Development of a Structural Model and Materials Evaluation Procedure. Ballast and Foundation Materials Research Program, Univ. of Illinois, Urbana-Champaign; Federal Railroad Administration, Rept. DOT-FR-30038, May 1975.
18. D. L. Heath, M. J. Shenton, R. W. Sparrow, and J. M. Waters. Design of Conventional Rail Track Foundations. Proc., Institution of Civil Engineers, London, Vol. 51, Feb. 1972, pp. 251-268.
19. M. T. Salem. Vertical Pressure Distribution in the Ballast Section and on the Subgrade Beneath Statically Loaded Ties. Department of Civil Engineering, Univ. of Illinois, Urbana-Champaign, PhD thesis, 1966.
20. E. T. Selig. Soil Strain Measurement Using Inductance Coil Method. In Special Technical Publication 584: Performance Monitoring for Geotechnical Construction, ASTM, Aug. 1975, pp. 141-158.

Techniques for Evaluating Effects of Track and Vehicle Wear on Freight-Car Performance

C. Thomas Jones, ENSCO, Alexandria, Virginia
Donald E. Gray, Federal Railroad Administration

Track and vehicle wear affect the dynamic performance and therefore the economic performance of the railcar-track system. A multiphase test program has been designed to determine the relationship between the dynamic performance of freight vehicles and track condition, vehicle-component wear, and variations in track structure. The first part of this program has been completed, i.e., the development of test, instrumentation, and analysis techniques and the determination of their applications to a baseline dynamic-performance test. The test methodology involves dynamic testing of a high-travel car and a reference or low-travel car. Two test tracks at the Transportation Test Center were used, the facility for accelerated services testing track and sections of the railroad test track. The instrumentation for each test vehicle included precision accelerometers to measure accelerations on the car body, bolsters, and trucks and instrumented wheel sets to measure lateral and vertical forces on the wheels. The analysis of the acceleration data is based on the use of six degrees of freedom, or rigid-body modes, for each primary mass (car body and truck). Statistical processing of the computed modal data is used to determine the effects of track structure and condition on vehicle performance. Transmissibility between truck and car body is calculated to determine the effect of component wear on vehicle performance. Finally, statistical processing of wheel-rail forces is used to obtain lateral-to-vertical force ratios and lateral wheel forces as functions of the track section. The instrumentation and data-processing techniques designed for this program proved effective in evaluating freight-car dynamics. Evaluation of the effects of variations in track structure on vehicle dynamics led to the following conclusions: (a) track containing unsupported bonded joints produced the highest car-body accelerations; (b) curves greater than 4 degrees and discrete events such as turnouts produced high accelerations and wheel forces; and (c) variations in track and roadbed such as ballast-shoulder width and depth, spiking patterns, tie material, and rail anchor type had little if any effect on the dynamic response of the vehicle.

The dynamic performance of the railcar-track system has a direct effect on the economics of railroad operations in terms of lading damage and maintenance costs. This performance changes with accumulated use as a

result of degradation in the track structure and the vehicle components.

To establish a relationship between the dynamic performance of freight vehicles and the wear of track and components, a multiphase dynamic-performance test program (1) was designed as one part of phase 1 of the facility for accelerated services testing (FAST) program (2). The specific objectives of the dynamic performance test program are

1. To establish the relationship between ride performance and track condition,
2. To establish the relationship between ride performance and vehicle-component wear, and
3. To quantify the dynamic responses of freight vehicles to different track structures.

This paper provides a description of the test, instrumentation, and analysis techniques developed for the program. The results of the first in a series of dynamic performance tests are also presented.

TEST DESCRIPTION

The test methodology compares the dynamic performance of two freight vehicles that have traveled different distances. One car, designated the high-travel car, is operated at an accelerated service rate as a part of the FAST test train and the second car serves as a reference vehicle, or low-travel car, for comparative analysis. Two test tracks located at the Transportation Test Center are used, the FAST track and sections of the railroad test track (RTT). Tests are to be conducted in 80 000-km (50 000-mile) increments up to a maximum of 480 000 km (300 000 miles).

A baseline test was conducted in February 1977. The test consist included a locomotive, two 91-Mg (100-ton) hopper cars, and the Federal Railroad Administration T-5 data-acquisition car. The reference and the high-travel hopper cars were instrumented with precision servoaccelerometers. The reference vehicle was also equipped with instrumented wheel sets for measuring wheel-to-rail vertical and lateral forces. Signals from the instrumentation system were cabled to the T-5 data-acquisition car and recorded in digital form on magnetic tape. The test consist was operated at a constant 48-km/h (30-mph) speed over the 7.7-km (4.8-mile) FAST track, and data were recorded from both cars.

The FAST track has 22 separate sections, each of which has a different track structure and roadbed composition. Hence, operation of the test consist over this track provided data that could be used to quantify vehicle response to differing track and roadbed compositions. Second, the FAST track is subjected to accelerated service (approximately five times that experienced on a typical operating railroad). Thus, the baseline test provides an initial set of reference data for determining the effect of track degradation on ride performance.

Tests were conducted on a section of the RTT at speeds of 16, 32, 48, 64, and 80 km/h (10, 20, 30, 40, and 50 mph). The purpose of this phase of testing was to provide baseline data for determining the relationship between vehicle-component wear and ride performance. The RTT is subjected to relatively light traffic and, therefore, track variation with time has minimal effect. Hence, the subsequent tests will isolate the effects of vehicle-component wear on ride performance.

To correlate the data acquired during the dynamic performance tests with component wear and track degradation, measurements were made of pertinent car-truck wear surfaces and of the track geometry. These measurements will be repeated as travel is accumulated on both the car and track.

INSTRUMENTATION

The instrumentation developed for this test program consisted of

1. Servoaccelerometers,
2. A wheel-force-measurement system,
3. A speed and location system, and
4. A data-acquisition system.

Figure 1 is an overall system block diagram of the instrumentation.

Twenty force-balance servoaccelerometers were used to measure the accelerations on the car body, the bolsters, and the trucks of each test vehicle. Figure 2 shows the location and orientation of the accelerometers. Special mechanical isolators were used to filter out the high-amplitude, impulse-type accelerations that are potentially damaging to these precision instruments. An additional benefit derived from the isolation was that of maximizing the effective resolution of the acceleration measurement.

Two instrumented wheel sets built by the American Association of Railroads were used to measure wheel lateral and vertical forces on the reference car. Strain gauge bridges mounted on the wheel plate provided signals proportional to both lateral and vertical forces. The lateral signal is of a continuous nature, and the vertical signal consists of four outputs per wheel revolution.

The speed of the consist was obtained from an optical shaft encoder mounted on the T-5 data-acquisition vehicle. The encoder, which was mechanically driven by the car wheel, provides a pulse train output whose frequency is proportional to car speed.

The location of the test consist along the track was determined by a capacitive sensor mounted on the test vehicle. Metal targets were attached to the ties marking the beginning and end of each test section, and the passing of the consist over the targets generated a voltage pulse that was recorded on magnetic tape.

The primary elements of the T-5 data-acquisition system are a Raytheon 704 minicomputer, a 2032 bytes/cm (800 bytes/in) tape recorder, signal conditioning and filtering electronics, and an analog chart recorder.

The analog signals routed to the data-acquisition system are conditioned and filtered for compatability with the recording system. The conditioned signals are then converted to a 12-bit digital word and recorded on magnetic tape at a rate of 128 samples/s. For the purpose of visual analysis of data during testing and to ensure that the measurement and recording systems are functioning properly, selected channels of the digital data are passed through a digital-to-analog converter and the resultant time histories are displayed on a six-channel chart recorder.

DATA REDUCTION AND ANALYSIS TECHNIQUES

For the purpose of this study, the measured accelerations were reduced to accelerations with respect to a generalized coordinate system for both the car body and the truck. A right-hand Cartesian coordinate system was used that had its origin located at the geometric centroid. Accelerations with respect to the generalized coordinate system are referred to as modes. The modal representation of accelerations for each of the primary masses (car body and truck) offers two distinct advantages in the analysis of dynamic performance. First, the modes are conceptually easy to visualize,

Figure 1. Block diagram of overall system.

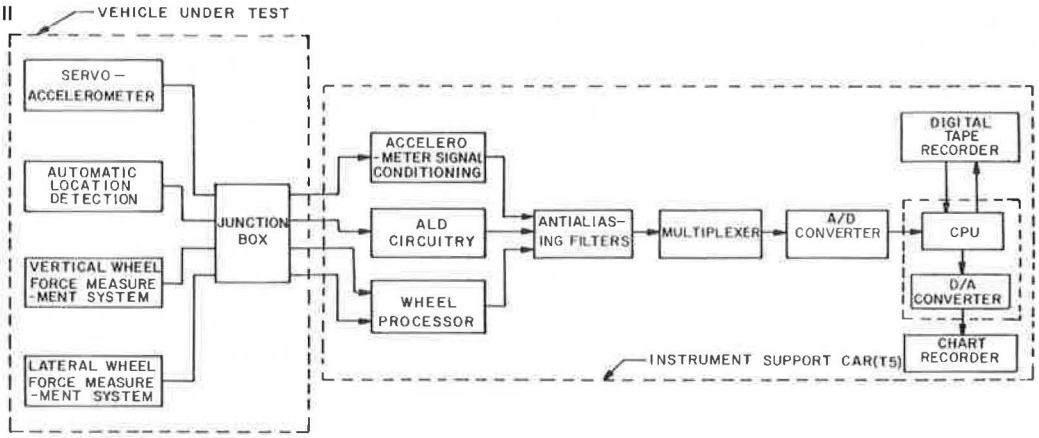

Figure 2. Locations and orientation of accelerometers.

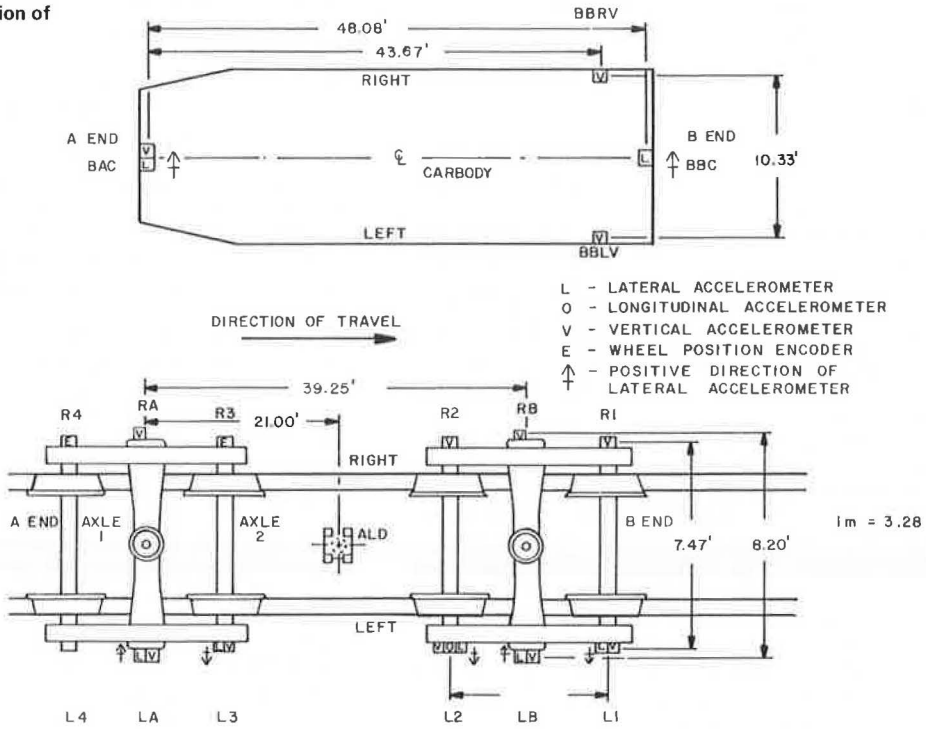

Figure 3. Car-body conventions and transducer locations.

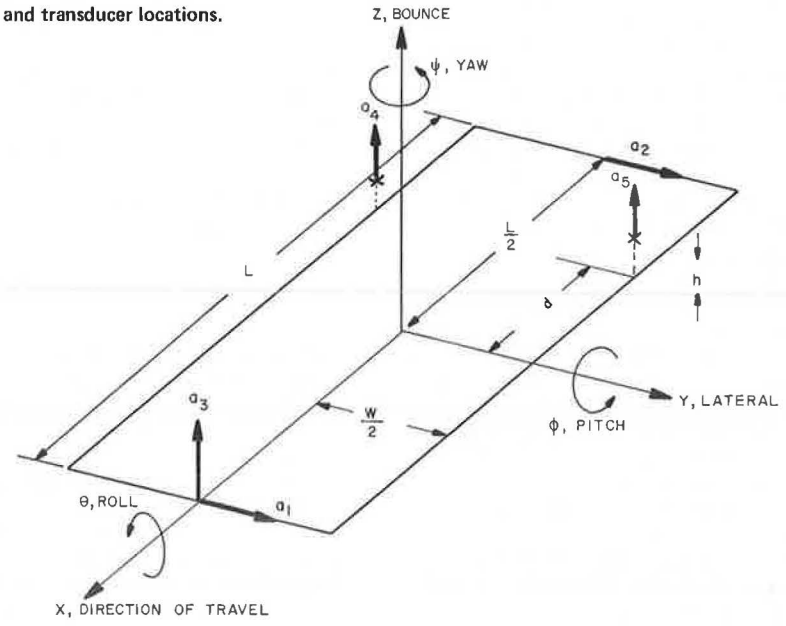

Figure 4. Truck conventions and transducer locations.

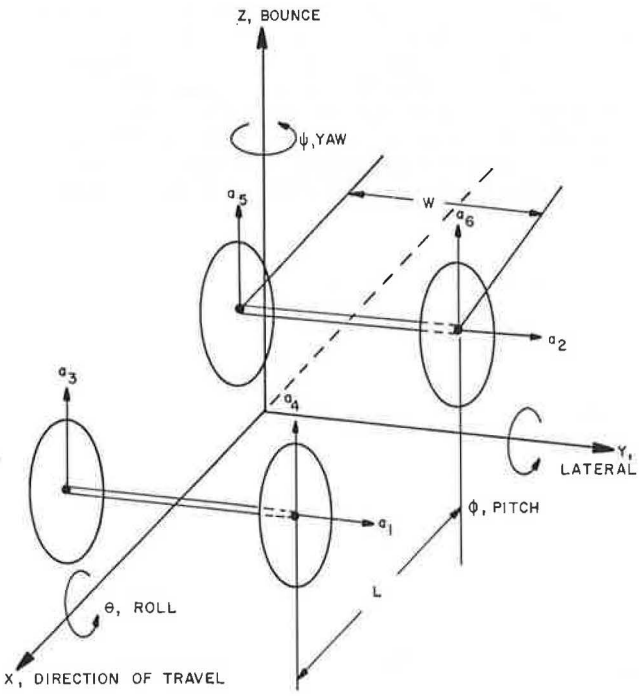

Figure 5. Truck twist mode.

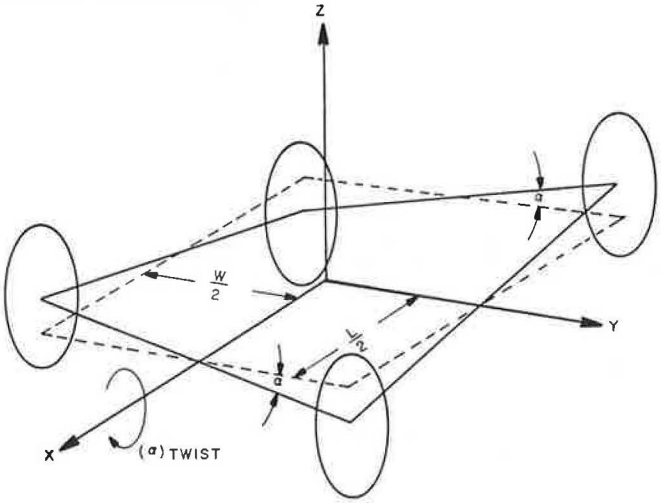

which facilitates subsequent analysis. Second, by assuming that the selected modes account for most of the acceleration experienced by the car body and the truck, a linear combination of modal accelerations can be used to determine the acceleration level at any point on the car body.

The car-body accelerations were assumed to be made up of six modes that correspond to the six rigid-body degrees of freedom. Three of these modes are the linear accelerations along the axes of the Cartesian coordinate system. The remaining three modes are the angular accelerations about each of the three principal axes. The modes are referred to as longitudinal, lateral, bounce, roll, pitch, and yaw and denoted by $\ddot{x}$, $\ddot{y}$, $\ddot{z}$, $\ddot{\phi}$, and $\ddot{\psi}$ respectively (see Figure 3). The double dot above each symbol denotes a double differentiation with respect to time.

Longitudinal acceleration ($\ddot{x}$) is primarily influenced by train handling and is not considered in this study. The remaining modes are to be determined by measurement of the five accelerations indicated by boldface arrows labeled a_i (i = 1, 2, 3, 4, 5) in Figure 3. Note that a_4 and a_5 lie a distance h above the plane of the other measurements. If these measurements are written in terms of their modal components,

$$a_1 = \ddot{y} + (L/2)\ddot{\psi} \tag{1}$$

$$a_2 = \ddot{y} - (L/2)\ddot{\psi} \tag{2}$$

$$a_3 = \ddot{z} - (L/2)\ddot{\phi} \tag{3}$$

$$a_4 = \ddot{z} + d\ddot{\phi} - (W/2)\ddot{\theta} \tag{4}$$

$$a_5 = \ddot{z} + d\ddot{\phi} + (W/2)\ddot{\theta} \tag{5}$$

and, if

$$F \equiv 2d + L \tag{6}$$

then, by solving for the modes, one obtains

$$\ddot{y} = (a_1 + a_2)/2 \tag{7}$$

$$\ddot{z} = [2da_3 + (L/2)(a_4 + a_5)]/F \tag{8}$$

$$\ddot{\theta} = (a_5 - a_4)/W \tag{9}$$

$$\ddot{\phi} = (a_4 + a_5 - 2a_3)/F \tag{10}$$

$$\ddot{\psi} = (a_1 - a_2)/L \tag{11}$$

The definitions and determination of the truck modes were similar to those used for the car body with the addition of the twist mode. As before, a right-hand Cartesian coordinate system was used that had its origin at the geometric center of the truck in the plane of the axles as shown in Figure 4. These modes are directly analogous to those of the car body and are given the same names and symbols. Also shown in Figure 4 are the locations of accelerations measured on the truck denoted a_i (i = 1, 2, ..., 6).

The trucks consist primarily of two axles and two side frames that behave as rigid bodies within the truck system. These subcomponents can displace angularly with respect to one another, which results in an asymmetric mode referred to as twist. The twist angle (α) is a function of the distance along the x axis as shown in Figure 5 and is expressed in units of radians per unit length. If the small-angle approximation ($\sin \alpha = \alpha$) is made and the convention that twist and roll have opposite signs is remembered, one can write the measured accelerations in terms of the truck modes as

$$a_1 = \ddot{y} + (L/2)\ddot{\psi} \tag{12}$$

$$a_2 = \ddot{y} - (L/2)\ddot{\psi} \tag{13}$$

$$a_3 = \ddot{z} - (W/2)\ddot{\theta} - (L/2)\ddot{\phi} + (WL/4)\ddot{\alpha} \tag{14}$$

$$a_4 = \ddot{z} + (W/2)\ddot{\theta} - (L/2)\ddot{\phi} - (WL/4)\ddot{\alpha} \tag{15}$$

$$a_5 = \ddot{z} - (W/2)\ddot{\theta} + (L/2)\ddot{\phi} - (WL/4)\ddot{\alpha} \tag{16}$$

$$a_6 = \ddot{z} + (W/2)\ddot{\theta} + (L/2)\ddot{\phi} + (WL/4)\ddot{\alpha} \tag{17}$$

This system of equations can be solved for the truck modes, which gives

$$\ddot{y} = (a_1 + a_2)/2 \tag{18}$$

$$\ddot{z} = (a_3 + a_4 + a_5 + a_6)/4 \tag{19}$$

$$\ddot{\theta} = (a_6 - a_5 + a_4 - a_3)/2W \tag{20}$$

$$\ddot{\phi} = (a_6 + a_5 - a_4 - a_3)/2L \quad (21)$$

$$\ddot{\psi} = (a_1 - a_2)/L \quad (22)$$

$$\ddot{\alpha} = (a_6 - a_5 - a_4 + a_3)/WL \quad (23)$$

Based on equations 7 through 11 for the car body and equations 18 through 23 for the truck, the individual measured acceleration can be transformed into 11 mode-acceleration time series. The mode-acceleration time series are then processed by using standard statistical techniques to provide root-mean-square (RMS) values, 95th and 99th percentile levels, histograms, and probability densities. The RMS values of the modes were derived for each of the 22 sections of the FAST track. This technique provides data that can be used to quantify the effect of track and roadbed composition on the dynamic performance of the truck and the car body. Data

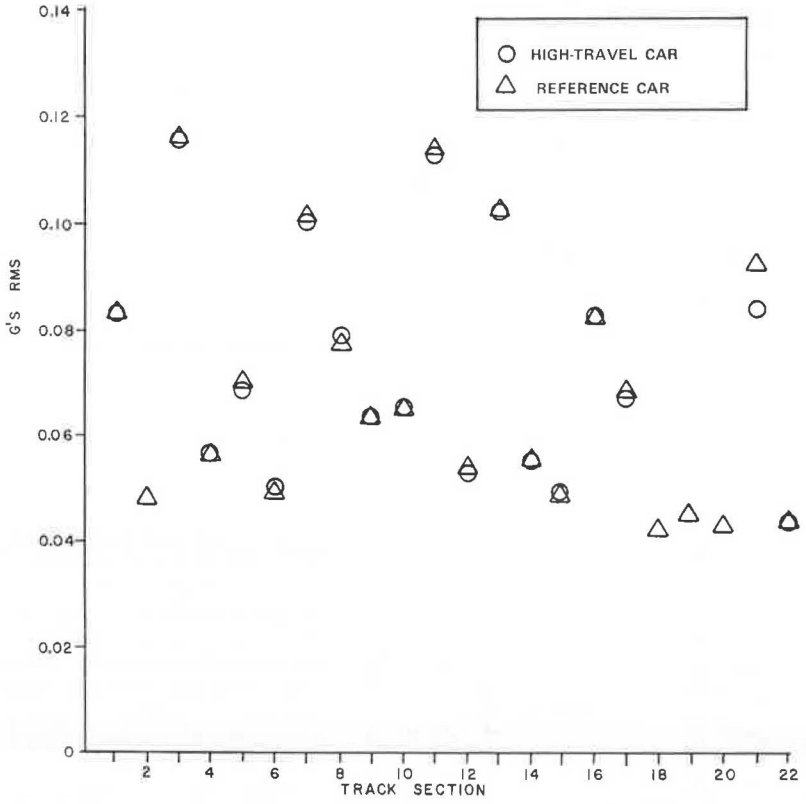

Figure 6. Relationship between truck vertical-mode acceleration and track section.

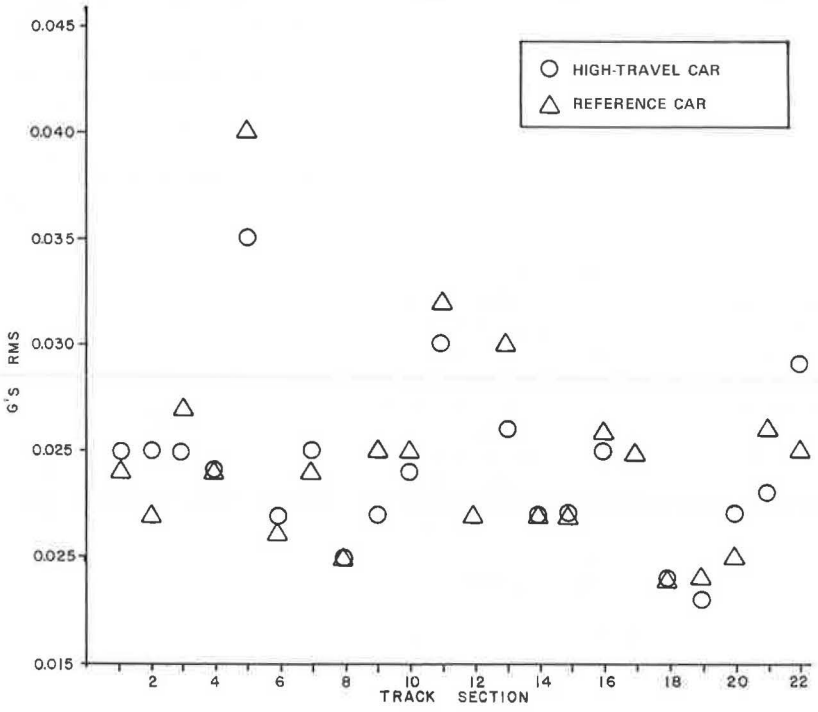

Figure 7. Relationship between car-body vertical-mode acceleration and track section.

presented in this manner will also be used in future tests to determine the effects of track degradation on vehicle performance.

To assess the effect of component wear on the ride performance of freight vehicles, the transmissibility between truck and car-body modes was determined. The transmissibility can be thought of as a characteristic of the freight car system that is independent of the track condition over which the car is operated. The changes in transmissibility characteristics with accumulated travel can, therefore, be directly attributed to changes in the freight-car components.

The transmissibility or gain was formed in the frequency domain by using power spectral densities (PSDs). The mode-acceleration time series were first transformed to a Fourier representation by using a fast Fourier transform. Then the PSD of a given modal acceleration was generated by multiplying the Fourier transform by its complex conjugate. The power associated with each frequency increment of a selected car-body mode was then divided by the power associated with the corresponding frequency increment of a selected truck mode. The result is the spectral distribution of the mean-square gain between the two selected modes.

The primary parameter used in the analysis of wheel-force data was the lateral-to-vertical (L:V) force ratio. This ratio is an important safety index that is used to determine the potential of rail rollover and wheel-flange climb. As discussed above, the lateral wheel forces were measured and recorded continuously, but the vertical forces were measured accurately only four times per revolution. Thus, to construct a continuous L:V time series, the four vertical measurements were averaged over each wheel revolution. The continuous lateral-force time series were then divided by the average vertical force for each wheel revolution. Statistical processing similar to that used for the acceleration modes gave the L:V ratios and lateral wheel forces as functions of track section.

RESULTS AND CONCLUSIONS

The instrumentation and data processing techniques developed for this test program proved highly successful for the evaluation of the dynamic performance of freight vehicles. The use of RMS modal accelerations yielded clear concise results that correlated well with physical phenomena.

A plot of modal acceleration versus track section is shown in Figure 6. The vertical-mode accelerations are shown for both the high-travel and the reference cars. This figure indicates that there is considerable variation in the truck vertical-mode acceleration from one track section to the next but that the accelerations of both trucks are nearly identical. This second observation was anticipated because the accelerometers are mounted on the journal box adapters and, in essence, are directly coupled to the rail. This is an important observation because it implies that the modal acceleration of the truck can be used as an index of track condition.

Car-body vertical-mode accelerations are plotted against track section in Figure 7. Again, variations in modal accelerations are shown for different track sections. As opposed to the truck modes, however, the car-body accelerations of the reference and the high-travel cars exhibited some differences. This was anticipated because car-body modal accelerations are a function of both track geometry and suspension components and the components may differ from car to car. By comparing Figures 6 and 7, one finds attenuation factors of between 2:1 and 5:1 between truck and car-body modes.

Conclusions related to the objective of quantifying the dynamic response of freight vehicles to different track structures are as follows. Variations in track structures (such as ballast-shoulder width and depth, spiking patterns, tie material, and rail anchors) had little if any effect on truck and car-body accelerations or wheel forces. In contrast, curves greater than 4 degrees and discrete events (such as turnouts) had a marked effect on vehicle dynamics. The highest car-body accelerations were those experienced on section 5 of the FAST track, which contains unsupported bonded joints. Because truck modal accelerations were moderate to low over this same section of track, it can be theorized that this particular track structure excites a resonance in the vehicle suspension system.

In summary, the techniques that were developed for this program proved effective in evaluating the dynamic performance of freight vehicles and for determining the effects of variations in track structure on that performance. The use of these techniques in subsequent phases of the test program will provide the necessary input for the evaluation of track and component wear as it affects vehicle dynamic performance.

ACKNOWLEDGMENT

The work described in this paper was sponsored by the Federal Railroad Administration, Office of Freight Systems. We would like to express our appreciation to the FAST program personnel and the ENSCO personnel whose cooperation and long hours of hard work produced a successful test program and made this paper possible.

REFERENCES

1. Dynamic Hopper-Car Test Results. ENSCO, Alexandria, VA, Bid Rept., June 1977.
2. Facility for Accelerated Service Testing: The First Experiment. Association of American Railroads Technical Center, Chicago, Nov. 1, 1976.

Part 2
Electrification

Effects of Energy-Cost Variation on Feasibility of Electrifying the Cincinnati-Atlanta Main Line of the Southern Railway System

K. L. Lawson, Bechtel do Brasil Construcoes, Sao Paulo
J. H. Wujek, Bechtel, San Francisco
K. J. Ingram,* University Computing Company, San Francisco

A study completed in 1975 considered the economics of electrifying the Cincinnati-Atlanta main line of the Southern Railway System. The differential cash flow of electric operation versus diesel operation, computed over the interval 1975-2002, yielded a 6.0 percent rate of return for electrification. This paper summarizes a study that applied plausible variations in energy prices to the operating scenarios used in the 1975 study. Two time intervals were chosen for analysis, taking a 2-year construction period for electrical facilities, followed by 26 years of operation. The first interval, 1975 through 2002, is identical to that of the initial study. For this interval, if the price of diesel fuel is taken as its maximum and dollar inflation is ignored, the rate of return for electrification ranges from 9.8 to 6.1 percent, depending on the price of electrical energy; if an annual dollar inflation of 10 percent is included, the corresponding rates are 20 and 15 percent. If the price of diesel fuel is taken as its minimum and dollar inflation is ignored, the rate of return for electrification is less than 35 percent; if an annual dollar inflation of 10 percent is included, the rate of return is less than 10 percent. The second interval was 1983 through 2010. For this interval, if the price of diesel fuel is taken as its maximum and dollar inflation is ignored, the rate of return for electrification ranges from 13 to 9.2 percent, again depending on the price of electrical energy; if an annual dollar inflation of 10 percent is included, the range of rates is 23 to 19 percent. If the price of diesel fuel is taken as is its minimum and inflation is ignored, the rate of return for electrification is less than 5 percent; if an annual inflation of 10 percent is included, the rate of return ranges from 7 to 10 percent.

In a 1975 study by the Electro-Motive Division (EMD) of the General Motors Corporation the costs were compared of diesel versus electric locomotive operations on the 782-km (486-mile) Cincinnati-Atlanta line of the Southern Railway System (1). That study took initial energy prices as

1. 0.33 cents/MJ (1.2 cents/kWh) for electrical energy and
2. 7.92 cents/L (30 cents/gal) for diesel fuel,

used these prices for the 1975 base, and applied to them an annual inflation rate of 1.5 percent. In the study summarized in this paper, these prices have been taken as variables. And precisely because energy prices appear to be the most unpredictable costs and because these costs dominate the cash flow, this study has focused on the effects they produce.

All other capital costs, maintenance costs, operational parameters, and traffic projections used here are identical to the EMD figures. The capital costs (in 1975 dollars) used in the EMD study and retained in this one are summarized below (1 kW = 1.341 hp and 1 km = 0.62 mile).

Item	Cost
Diesel locomotive (2237-kW unit), $	425 000
Electric locomotive [4474-kW (diesel equivalent) unit], $	750 000
Main line catenary and substations, $/track-km	39 248
Yard catenary and substations, $/track-km	19 624
Communication and signal alterations (entire line, site-specific), $	31 398 000
Clearance costs (entire line, site-specific), $	4 000 000

Several comments on this table are appropriate. The $4 million associated with clearance is an average of $5114/route-km ($8230/route-mile). Because much of the territory is mountainous, some of these costs could also be accrued for diesel operations because of higher or wider cars (or both) and loads. However, in this study, these costs are assigned to the electric case only.

The maintenance costs (in 1975 dollars) used in the EMD study and retained in this one are summarized below.

Item	Cost
Diesel locomotive maintenance, $/year + $/km	19 332 + 0.062 14
Electric locomotive maintenance, $/year + $/km	5865 + 0.062 14
Annual catenary and substation maintenance, $/track-km	546

[Locomotive maintenance costs are more often stated as entirely variable, i.e., cost per kilometer. Converting to this convention and using the locomotive annual utilization figures given below, one obtains 17.4 cents/km (27.8 cents/mile) for diesel and 9.32 cents/km (14.9 cents/mile) for electric. This is a ratio of 1.87, slightly lower than the range of 2 to 3 commonly argued in the industry. An independent (confidential) study in 1970 computed a ratio of 2.6 based on suggested maintenance, but without field experience.]

The operational parameters used in the EMD study and retained in this one are summarized below (1 metric ton = 1.1023 short tons).

Item	Value
Traffic base (1975), gross metric tons	36 288 000
Annual traffic growth, %	3.3
Diesel locomotive annual avg use, km	173 904
Electric locomotive annual avg use, km	193 960
Availability: diesel locomotive, %	90
Availability: electric locomotive, %	95

In this table, the traffic base is averaged over the four operating districts between Cincinnati and Atlanta; the variation between districts is less than 14 percent. In the estimate of annual traffic growth, no allowance has been made for capacity saturation of single-track territory. From 1975 to 2010, traffic will increase by a factor of 3.1. If it is assumed that the same loading assignments will be maintained, this corresponds to an

increase from 10 to 31 daily trains in each direction. Not shown above, but also retained from the EMD study, were the electrical efficiencies of

1. 80 percent for catenary transmission and
2. 95 for substation conversion.

Locomotive efficiencies are inherent to the loading ratings assigned in the EMD study. The relative performance of the two locomotive types under overload condition is not explicitly stated or provided for in the EMD report. Also, no attempt was made to optimize locomotive use or otherwise improve operational strategies in either study.

METHOD

The method used in this study of computing the rate of return is identical with that used in the EMD study. The annual cash flow for diesel and electric operations are computed separately and then summed. In the analysis, the costs associated with electric operation are taken (arbitrarily) as negative quantities and the costs associated with diesel operation are taken as positive. The resultant summed cash flow is thus a differential cost. A positive sign for the sum indicates a saving brought about by electrification. Conversely, a negative sign indicates a net saving in diesel relative to electric operations. The rate of return is then computed for a 28-year interval. A computer program is used to find an equivalent interest rate for capital such that the net cash flow is zero for the (28-year) investment cycle. This interest rate is then the rate of return on the operation. Note that this definition does not take into account investment opportunities, borrowing considerations, or combinations of these factors.

Two major intervals were analyzed:

1. Case 1, which uses the interval 1975-2002 (this is the same time span used in the EMD work and differs only in energy pricing), and
2. Case 2, which uses the interval 1983-2010 (this updates the older study and reflects the lead times associated with financing, engineering, and constructing a project of this magnitude).

ENERGY PRICES

Because energy-price projections are fundamental to this study, it is important that the best estimates available be used in the calculations. Discussions were held with individuals who have had experience in projecting energy prices, and a survey of the literature was made. There was general agreement that a recent report published by the Federal Energy Administration (FEA) provides an authoritative basis for future energy price estimates (2).

The FEA report lists energy prices projected for a variety of international and domestic events. These prices were established from predictions of supply and demand for three price levels of imported oil (in 1975 constant dollars): (a) \$50.29/m^3 (\$8/barrel), (b) \$81.71/m^3 (\$13/barrel), and (c) \$100.57/m^3 (\$16/barrel). Twelve scenarios were reported, 10 for 1985 and 1 each for 1980 and 1990.

Escalation in prices is due to political, social, and technological factors manifested in the international economy. The differences in pricing therefore reflect the interaction of many complex forces. Although it recognizes the limitations and difficulties inherent in such forecasting, the FEA study does establish plausible and consistent energy prices.

By using the data and formulas given in the FEA report, maximum (MAX) and minimum (MIN) energy prices were developed. These prices take into account differences for delivery. For the present study, two delivery regions are of interest: east south central (ESC), which includes all of Kentucky and Tennessee, and south Atlantic (SA), which includes all of Georgia.

The 1985 delivery energy costs developed are summarized below (1 cent/L = 3.86 cents/gal and 1 mill/MJ = 3.6 mills/kWh).

Energy Source	Price in 1975 Constant Dollars	
	Maximum	Minimum
Electrical, mills/MJ	8.39	6.06
Diesel fuel, cents/L	11.89	7.13

Although the prices given above are reported to three or four significant figures, this was done only to show calculated differences between assumptions and does not imply this precision in estimation. Prices are stated in constant (1975) dollars; therefore, dollar inflation was included in the analysis.

In the table above, note that the lowest price for electrical energy is 6.06 mills/MJ (21.8 mills/kWh); this is a 1985 price, expressed in constant 1975 dollars. Compared with the 1975 price of 3.32 mills/MJ (12 mills/kWh) used in the EMD study, this is an 82 percent increase, equivalent to a 6.15 percent average annual rate from 1975 to 1985. The maximum 1985 electrical-energy price of 8.39 mills/MJ (30.2 mills/kWh) is 152 percent of the EMD (1975) figure. This is equivalent to an annual 1975 to 1985 increase of 9.7 percent.

The MAX and MIN 1985 diesel fuel prices are 11.89 and 7.13 cents/L (45 and 27 cents/gal) respectively. Compared with the 1975 price [7.93 cents/L (30 cents/gal)] used in the EMD study, the corresponding (1975 to 1985) annual rates are 4.1 percent and minus 1.1 percent.

The table above gives prices for 1985 only. For the present study, projections to the year 2010 were needed. These extensions were developed from statements and data in the FEA reports and other sources (3). For a constant-dollar economy, the consensus expectation is that

1. Diesel-fuel prices will increase an average of 3 percent annually after 1985 and
2. Electrical-energy prices will remain relatively constant after 1985.

As before, dollar inflation was included in the subsequent analysis.

The FEA estimates and these post-1985 projections are shown in Figures 1 and 2; the historical prices are added for reference. The prices shown between 1975 and 1985 were interpolated by assuming a constant annual rate of change over the interval.

In Figures 1 and 2, note that the 1975 prices differ from those used in the EMD study. In particular, these plots show

1. Diesel fuel at 8.98 cents/L (34 cents/gal) [versus the EMD study price of 7.93 cents/L (30 cents/gal)] and
2. Electrical energy at 4.43 to 6.09 mills/MJ (16 to 22 mills/kWh) (versus the EMD study price of 3.32 mills/kWh).

In Figure 2, electrical-energy prices are shown as the U.S. average from 1965 to 1972. From 1972 to 1975, the range of prices reflects the variance of negotiated rates. For comparison, the industrial rate in the

Cincinnati-northern Kentucky area was in the range of 4.99 to 5.54 mills/MJ (18 to 20 mills/kWh).

Throughout this report, the electrical-energy prices used are industrial rates. However, railroad rates may be greater than these industrial rates because of the poor load-factor characteristics of railroads and the relatively poor power factor of the AC traction system. The unbalance produced by single-phase loading of a three-phase power supply may also incur a penalty.

The prices shown in Figures 1 and 2 were the basis for the calculations of cases 1 and 2.

RESULTS

Case 1

The case 1 inputs, except for energy costs, are identical to those used in the EMD study. Energy costs are as shown in Figures 1 and 2 for the operating interval 1977-2002.

The rate of return for electrification versus the annual inflation rate is shown in Figure 3. For the combination of diesel fuel prices at MIN and electrical energy prices at MAX, electrification costs exceed diesel costs for each year of operation (1977-2002); therefore, this combination of prices does not appear in Figure 3.

Case 2

Case 2 was developed to test the economic feasibility of a realistic start of construction. The 1985-2010 prices shown in Figures 1 and 2 are used in this case.

Figure 4 shows the sensitivity of rate of return to inflation for combinations of energy prices in the same manner as Figure 3.

The post-1985 diesel-fuel prices shown in Figure 1 reflect an annual increase of 3 percent, with electrical-

Figure 1. Diesel-fuel prices.

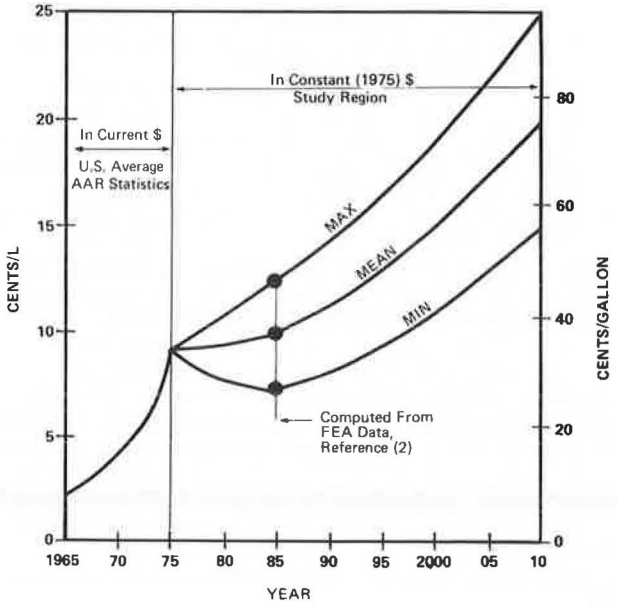

Figure 2. Electrical-energy prices.

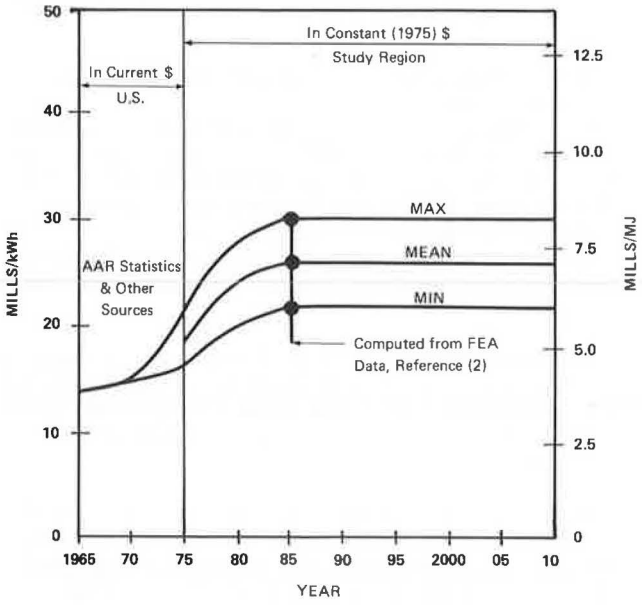

Figure 3. Rate of return for electrification at different energy price combinations: 1977-2002 operations.

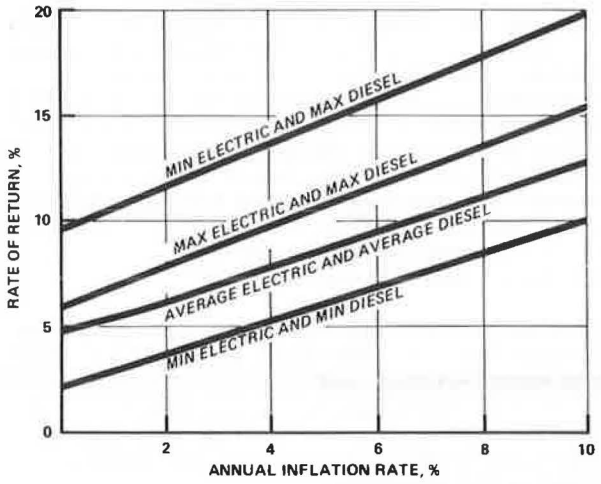

Figure 4. Rate of return for electrification at different energy price combinations: 1985-2010 operations.

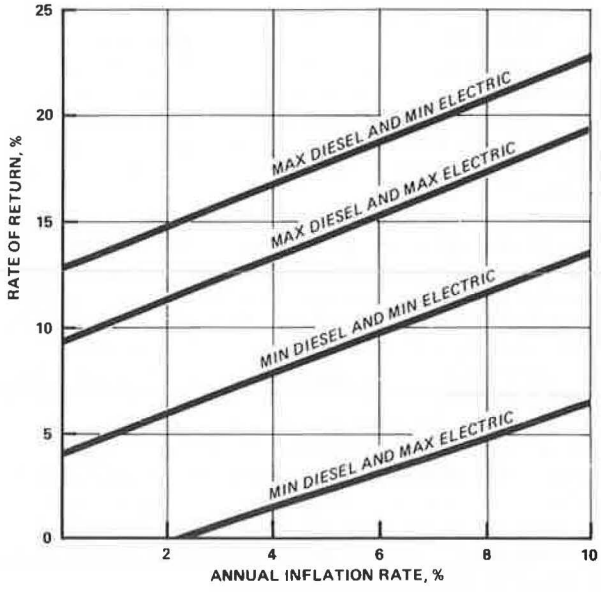

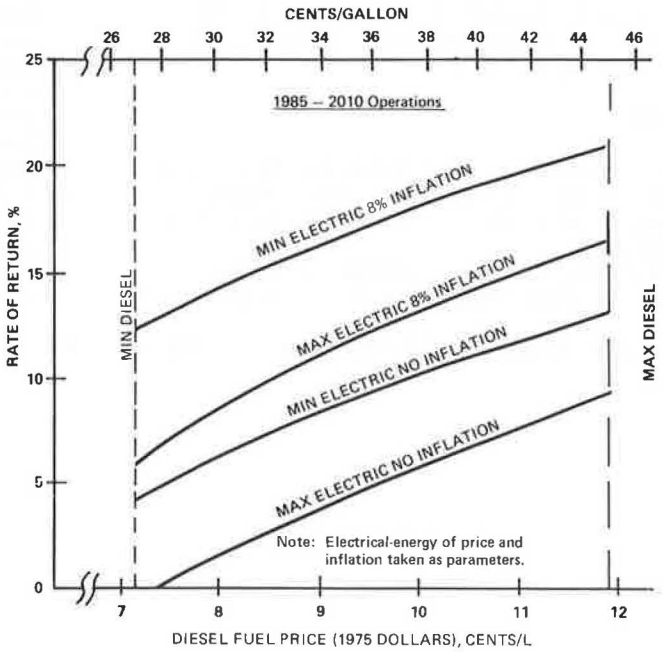

Figure 5. Rate of return for electrification as a function of base year (1985) and diesel-fuel price: 1985-2010 operations.

energy prices stable. By using the MAX and MIN electric prices as parameters, rates of return were computed as a function of base year (1985) diesel-fuel price. The results are shown in Figure 5 without dollar inflation and for an annual inflation of 8 percent.

DISCUSSION OF RESULTS

The analyses (cases 1 and 2) are based on projections from FEA estimates that have been checked against other sources. Not all of these sources are independent of the FEA figures. The converse is also true. However, the projections through 1990 are believed to be the best estimates currently available, notwithstanding the vagaries of forecasting.

The costs used in the study are for conventional energy sources. Certain exotic technologies (e.g., solar energy, geothermal energy, and synthetic fuels) may be expected to contribute in the future. However, these sources are expected to contribute no more than 1 percent to the U.S. energy pool through 1990. Given the long lead times that will be required to perfect these technologies and the time required to construct significant capacity, this conclusion appears valid. Production of oil from shale is included in some of the FEA scenarios (2) and is not considered an exotic technology in the present context.

Beyond 1990, the impact of new technologies is even more difficult to assess. However, given the energy prices developed in this study and the fundamental economic laws of supply and demand, marked decreases in electrical-energy costs do not appear likely. Rather, a general stabilization of prices is indicated, due in large measure to saturation of technology and the mix of primary energy sources used to produce power. As a separate check of electrical prices used in this study, it is useful to compute an absolute ceiling.

A recent study has established the maximum costs of electricity for a 1982 New England scenario (4). With 10 percent annual inflation, energy costs in 1982 are projected to be

1. Nuclear—13.38 mills/MJ (48.3 mills/kWh),
2. Coal (without scrubbers)—17.56 mills/MJ (63.4 mills/kWh), and
3. Coal (with scrubbers)—20.89 mills/MJ (75.4 mills/kWh).

Recent increases in uranium prices will contribute an estimated 2.77 mills/MJ (10 mills/kWh) to the 1982 nuclear price, which means that this price is then 16.15 mills/MJ (58.3 mills/kWh) [i.e., 8.28 mills/MJ (29.9 mills/kWh)] in 1975 dollars.

However, New England power is typically 0.14 to 0.55 mills/MJ (0.5 to 2 mills/kWh) less costly than Cincinnati-Atlanta power (2). The ceiling (regional) price is thus 8.86 mills/MJ (32 mills/kWh) for the area of interest. This is in excellent agreement with the 8.37 mills/MJ (30.2 mills/kWh) used in this study. Thus, nuclear power may, in fact, serve as a ceiling.

The corresponding price ceiling for post-1985 synthetic fuels can be projected from current estimates. On an energy-equivalent basis, the 1976 price of synthetics, if sufficient production capacity were available, would be \$151/m^3 to \$170/m^3 (\$24/barrel to \$27/barrel) (5). This is (approximately) a factor of two greater than the current price of imported oil. The 1985 price estimate (energy equivalent) ranges from 98 to 178 percent of the maximum price of domestic offshore oil (6). Moreover, the construction and operation of plants in sufficient quantity to supply a significant fraction of U.S. energy needs is not likely before the year 2000. These considerations tend to support the oil-price projections shown in Figure 1.

For both case 1 and case 2, dollar inflation produces a (nearly) linear increase in rate of return. These are shown as linear functions in Figures 3 and 4. The departure from linearity is less than 5 percent over the range of the independent variable.

Because both relative and absolute energy prices dominate the cash flow, significant escalations in future prices should initiate further study.

ACKNOWLEDGMENTS

We wish to thank several individuals for their cooperation and assistance in the work leading to this paper: from the Southern Railway System—Stanley Crane and W. W. Simpson; from the Electro-Motive Division of the General Motors Corporation—H. W. Barber and M. E.

Turek; and from Bechtel—G. F. Mader, W. Dunlop, L. F. Eriksen, S. D. Ritchie, and S. E. Wong. The study was funded by Bechtel.

REFERENCES

1. Comparison of Electric and Diesel Locomotives on the Southern Railway System. Electro-Motive Division, General Motors Corporation, La Grange, IL, Feb. 1975.
2. National Energy Outlook. Federal Energy Administration, Feb. 1976, pp. F-5, G-2 to G-25, and others.
3. Evaluation of World Energy Developments and Their Economic Significance. Sherman H. Clark Associates, Menlo Park, CA, Vol. 4, Aug. 1975.
4. Study of Economics of Power Generation in the New England Area. Bechtel Power Corporation, San Francisco, May 1975.
5. What About New Energy Sources? Conoco, Continental Oil Company, House Publ., Vol. 7, No. 2, 1976.
6. B. Rubin and others. A Rationale for Setting Priorities for New Energy Technology Research and Development. Lawrence Livermore Laboratory, Univ. of California, Rept. UCRL-51511, Jan. 4, 1974, p. 50.

Mr. Ingram was with Bechtel when this research was performed.